

1-1-1990

A spectroscopic study of phase transitions in polymers/

Nicholas Matthew Reynolds
University of Massachusetts Amherst

Follow this and additional works at: https://scholarworks.umass.edu/dissertations_1

Recommended Citation

Reynolds, Nicholas Matthew, "A spectroscopic study of phase transitions in polymers/" (1990). *Doctoral Dissertations 1896 - February 2014*. 774.
https://scholarworks.umass.edu/dissertations_1/774

This Open Access Dissertation is brought to you for free and open access by ScholarWorks@UMass Amherst. It has been accepted for inclusion in Doctoral Dissertations 1896 - February 2014 by an authorized administrator of ScholarWorks@UMass Amherst. For more information, please contact scholarworks@library.umass.edu.

UMASS/AMHERST



312066007712923

A SPECTROSCOPIC STUDY OF PHASE TRANSITIONS IN POLYMERS

A Dissertation Presented

By

NICHOLAS MATTHEW REYNOLDS

Submitted to the Graduate School of the
University of Massachusetts in partial fulfillment
of the requirements for the degree of

DOCTOR OF PHILOSOPHY

May 1990

Department of Polymer Science and Engineering

© Copyright by Nicholas M. Reynolds 1990

All Rights Reserved

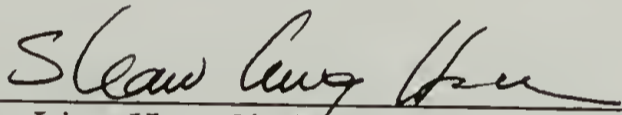
A SPECTROSCOPIC STUDY OF PHASE TRANSITIONS IN POLYMERS

A Dissertation Presented

by

NICHOLAS MATTHEW REYNOLDS

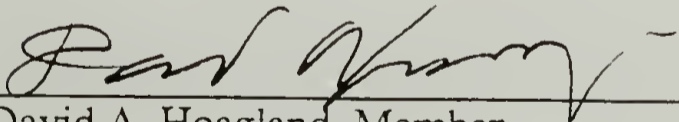
Approved as to style and content by:



Shaw Ling Hsu, Chairman of Committee



Richard S. Stein, Member



David A. Hoagland, Member



William J. MacKnight, Department Head
Polymer Science and Engineering

ACKNOWLEDGEMENTS

I would like to acknowledge the guidance and encouragement provided to me by my advisor, Professor Shaw Ling Hsu, throughout the course of this research. I am grateful to him for the opportunity to work on several interesting projects. I would also like to express thanks to the other members of my committee, Professor Richard S. Stein, and Professor David A. Hoagland, for their many helpful suggestions.

I wish to thank many members of our research group for the great deal of help I have received during this research. In particular I express appreciation to Prof. Kap Jin Kim, Cun Feng Fan, Drs. Chih Chang, Dave Waldman, Steve Pollack, and Han Sup Lee for many helpful scientific discussions and much experimental assistance. For help with the final preparation of this thesis I want to thank Katherine Antolin and Norbert Egger. I also wish to express great appreciation to Scott Nietzsche and John Savage for a great many fascinating discussions on a wide variety of scientific and often nonscientific subjects. Finally I want to thank my family for their support and encouragement .

ABSTRACT

A SPECTROSCOPIC STUDY OF PHASE TRANSITIONS IN POLYMERS

MAY 1990

NICHOLAS MATTHEW REYNOLDS, B.S., PURDUE UNIVERSITY

Ph.D., UNIVERSITY OF MASSACHUSETTS

Directed by: Professor Shaw Ling Hsu

In this study three examples of solid-solid phase transitions in polymers have been investigated with vibrational spectroscopy. This technique has been employed to monitor the changes in chain conformation and segmental orientation which occur during phase transitions induced by heating, drawing, and application of an electric field.

The effects of a high strength electric field on the microstructure of piezoelectric copolymers of vinylidene fluoride and trifluoroethylene has been studied. Their structure may be altered by annealing, orientation, and the application of an electric field. The application of an electric field is found to produce changes in dipolar orientation and also changes in chain conformation, and these are measured by infrared spectroscopy below and above the Curie transition temperature. Electrical poling behavior is examined for two copolymer compositions which show substantial differences in structure and Curie temperature, and infrared analysis provides a means to determine the differences in dipole orientation and chain conformation distribution for these two copolymers. A comparison is made with previous poling studies of PVDF homopolymer, in order to determine the effect of the TrFE unit on the electrical behavior.

The orientation and microstructure of highly oriented blends of PVDF and PMMA has been studied. Infrared spectroscopy is employed to determine the content of α and β phases of PVDF for two highly drawn blends and also for PVDF homopolymer. The

effects of annealing on the phase content and segmental orientation are measured. Highly drawn PVDF samples are used for determination of the transition dipole moment directions of selected vibrational bands .

The microstructure of different phases of syndiotactic polystyrene has also been studied. The presence of two crystalline phases including a helical structure in a solution cast film, and an all trans conformation upon annealing or drawing is shown. An irreversible transition to the all trans phase is observed to occur very rapidly near 200°C. Spectral features which are sensitive to specific conformations and packing order are identified. Upon annealing or extrusion, bands appear which are associated with long trans sequences.

A normal coordinate analysis is performed for the all trans conformation of syndiotactic polystyrene using nonredundant coordinates and force constants for the phenyl ring. Force constants for the chain have been obtained from studies of saturated hydrocarbons. Assignment of the infrared and Raman bands and their polarization characteristics is made upon comparison of the calculated results with the observed spectra obtained from coextruded films. Bands which involve coupling between the ring and backbone vibrations are found to correlate well with the observed bands which are associated with the trans conformation. Annealing the coextruded films increases the overall segmental orientation as the crystallinity increases. The theoretical modulus of a single chain has been calculated from the dispersion curve of the longitudinal acoustic branch near the Brillouin zone center.

The kinetics of the irreversible phase transition in syndiotactic polystyrene has been measured as a function of temperature and annealing history, in order to determine the effect of thermal history on the transition behavior. The transition appears to be highly cooperative occurring over a very narrow temperature range, and the transformation behavior has been modeled as one of nucleation and growth.

TABLE OF CONTENTS

	<u>Page</u>
ACKNOWLEDGEMENT.	iv
ABSTRACT.	v
LIST OF TABLES.	ix
LIST OF FIGURES.	x
Chapter	
I. INTRODUCTION.	1
Overview of Dissertation	1
Piezoelectric Polymers	4
Copolymers of PVDF with Trifluoroethylene	6
Blends of PVDF and Poly(methyl methacrylate)	9
Microstructure of Syndiotactic Polystyrene	10
References	12
II. ELECTRICAL FIELD INDUCED STRUCTURAL CHANGES IN PVDF-TrFE COPOLYMERS	15
Introduction	15
Experimental	17
Results and Discussion.	20
Band Assignments.	30
Poling Hysteresis	39
Irreversible Structural Change	46
Effect of Copolymer Composition	56
Conclusions	61
References	63
III. INFRARED STUDIES OF HIGHLY ORIENTED PVDF AND BLENDS WITH PMMA	65
Introduction	65
Experimental	67
Results and Discussion	69
Calculation of Transition Dipole Moments for PVDF	81
Microstructure of PVDF/PMMA Blends	82
Conclusions	85
References	86

IV.	A SPECTROSCOPIC STUDY OF SYNDIOTACTIC POLYSTYRENE	88
	Introduction	88
	Experimental	89
	Results and Discussion	90
	Conclusions	100
	References.	101
V.	A NORMAL VIBRATIONAL ANALYSIS OF SYNDIOTACTIC POLYSTYRENE.	102
	Introduction	102
	Structure and Force Field	106
	Results and Discussion	131
	Conformation Sensitive Bands	155
	Calculation of Theoretical Modulus.	157
	Conclusions	160
	References	162
VI.	A SPECTROSCOPIC STUDY OF PHASE TRANSITION KINETICS IN SYNDIOTACTIC POLYSTYRENE	164
	Introduction.	164
	Experimental	166
	Results and Discussion	167
	Conclusions.	180
	References.	182
VII.	RECOMMENDATIONS FOR FUTURE WORK	183
	Results and Recommendations.	183
	Copolymers of PVDF and TrFE.	183
	Blends of PVDF and PMMA.	186
	Microstructure of Syndiotactic Polystyrene.	187
	References.	190

LIST OF TABLES

	<u>Page</u>
2.1 Characteristics of vibrational bands chosen for analysis.	31
3.1 Calculated transition dipole moment directions for melt drawn PVDF.	80
5.1 Raman scattering activities for C_{2v} symmetry.	107
5.2 Structural parameters for all trans syndiotactic polystyrene	110
5.3 Definition of internal coordinates for syndiotactic polystyrene.	111
5.4 Definition of symmetry coordinates for syndiotactic polystyrene.	116
5.5 Force constants for syndiotactic polystyrene.	119
5.6 Observed and calculated frequencies (in cm^{-1}) and potential energy distribution of sPS.	122

LIST OF FIGURES

		<u>Page</u>
1.1	DSC Scan for a 70 mole% PVDF - 30 mole% TrFE Copolymer.	7
1.2	Variation in the melting temperature and Curie temperature with copolymer composition for PVDF- TrFE Copolymers. (from ref. 12).	8
2.1	Schematic drawing of experimental geometry for poling.	19
2.2	Infrared spectra of 75/25 PVDF/TrFE film as a function of temperature; (1600-400 cm^{-1}); (top) 125°C spectrum; (bottom) room temperature spectrum.	21
2.3	Infrared spectra of 75/25 PVDF/TrFE film before and after annealing at 130°C for 2 hours; (a) 1500-1000 cm^{-1} region; (b) 1000-400 cm^{-1} region; (···) annealed sample; (-) as cast film.	23
2.4	Infrared spectra of 75/25 PVDF/TrFE film as a function of electric field; (top) $E = 2.2$ MV/cm; (bottom) $E = 0.0$ MV/cm.	26
2.5.	Polarized infrared spectra of 75/25 PVDF/TrFE film at a draw ratio of 1.6; (1600-400 cm^{-1}); (top) perpendicular polarization; (bottom) parallel polarization.	28
2.6	Infrared data in the 1000-700 cm^{-1} region of 75/25 PVDF/TrFE films; (a) (···) annealed; (-) as cast; (b) oriented sample with draw ratio 1.6; (-) perpendicular polarization; (···) parallel polarization; (c) electric field applied, (···) $E = 2.2$ MV/cm; (-) 0.0 MV/cm; (d) (top) 110 K; (bottom) room temperature.	34
2.7	Intensity change of the 850 cm^{-1} band as a function of electric field and temperature; (a) 20°; (b) 75°; (c) 94°; (d) 125°C.	40
2.8	Intensity change of the 883 cm^{-1} band as a function of electric field and temperature; (a) 20°; (b) 75°; (c) 94°; (d) 125°C.	42
2.9	Intensity change as function of electric field for three poling cycles at room temperature; (a) 850 cm^{-1} ; (b) 883 cm^{-1}	44
2.10	Intensity change of the 612 cm^{-1} band as a function of electric field and temperature; (a) 94°; (b) 125°C.	45
2.11	Infrared spectra of 75/25 PVDF/TrFE obtained before and during the application of an electric field as a function of temperature; (950-550 cm^{-1}); (-) 0.0 MV/cm; (···) 1.0 MV/cm; (a) 20°C; (b) 125°C.	47

2.12	Infrared spectra of 75/25 PVDF/TrFE as a function of electric field. Spectra are obtained in the depolarized state; (-) 0.0 MV/cm; (····) 2.2 MV/cm; (a) 1500-1000 cm^{-1} ; (b) 1000-400 cm^{-1}	51
2.13	Parallel polarized infrared spectra of 75/25 VDF/TrFE copolymer film drawn to a draw ratio of 5, and annealed at 135°C; (—) before poling; (- - -) after depoling.	54
2.14	Hysteresis in the 850 cm^{-1} band intensity for VDF-TrFE copolymers containing 75% and 52% VDF.	58
3.1	Schematic diagram illustrating the preparation of highly oriented melt drawn films. (from ref. 20).	68
3.2	Polarized infrared spectra of drawn PVDF film; (a) 1500-1000 cm^{-1} region; (b) 1000-400 cm^{-1} region; (····) perpendicular polarization; (—) parallel polarization.	70
3.3	Polarized infrared spectra of 80% PVDF/ 20% PMMA blend; (a) 1800-1000 cm^{-1} region; (b) 1000-400 cm^{-1} region; (····) perpendicular polarization; (—) parallel polarization.	73
3.4	Polarized infrared spectra of 50% PVDF/ 50% PMMA blend; (a) 3100-2800 cm^{-1} region; (b) 1800-1000 cm^{-1} region; (c) 1000-400 cm^{-1} region; (····) perpendicular polarization; (—) parallel polarization; (bottom) as drawn; (top) after annealing at 100° C.	76
4.1	Infrared spectra of (a) atactic, (b) isotactic, and (c) syndiotactic polystyrene.	91
4.2	Infrared spectra of sPS (a) as cast, (b) after annealing at 295°C for 0.5 hour, and (c) coextruded at 100°C to a draw ratio of 4; inset region (1) as cast, (2) at liquid nitrogen temperature, (3) annealed at 200°C for 1 hour, and (4) annealed at 200°C and measured at liquid nitrogen temperature.	93
4.3	Infrared spectra of sPS at various temperatures; (a) 25°C, (b) 111°C, (c) 185°C, (d) 212°C, and (e) 238°C.	95
5.1	Schematic diagram of the sample orientation relative to the incident radiation for different scattering geometries.	105
5.2	Schematic structure of sPS showing internal coordinates.	108
5.3	Schematic structure of sPS showing the indexing of atoms used for defining the internal coordinates.	109
5.4	Definition of some of the nonredundant symmetry coordinates for the phenyl ring.	115

5.5	Infrared spectra of sPS (a) solution cast film, (b) after annealing at 295°C for 0.5 hours, and (c) coextruded at 100°C to a draw ratio of 4; inset region (1) cast film, (2) at liquid nitrogen temperature, (3) annealed at 200°C for 1 hour, and (4) annealed at 200°C and measured at liquid nitrogen temperature.	132
5.6	Polarized infrared spectra of coextruded sPS before and after annealing at 200°C. (3100 - 2800 cm ⁻¹) Perpendicular polarization (—); parallel polarization (-----).	134
5.7	Polarized infrared spectra of coextruded sPS before and after annealing at 200°C. (1700 - 1000 cm ⁻¹) Perpendicular polarization (—); parallel polarization (-----).	136
5.8	Polarized infrared spectra of coextruded sPS before and after annealing at 200°C. (1000 - 500 cm ⁻¹) Perpendicular polarization (—); parallel polarization (-----).	138
5.9	Polarized Raman spectra (scattering geometry A) of coextruded sPS after annealing at 210°C for 3 hours. (1700 - 1100 cm ⁻¹).	140
5.10	Polarized Raman spectra (scattering geometry A) of coextruded sPS after annealing at 210°C for 3 hours. (1100 - 900 cm ⁻¹).	142
5.11	Polarized Raman spectra (scattering geometry A) of coextruded sPS after annealing at 210°C for 3 hours. (900 - 100 cm ⁻¹).	144
5.12	Polarized Raman spectra (scattering geometry B) of coextruded sPS after annealing at 210°C for 3 hours. (1700 - 1100 cm ⁻¹).	146
5.13	Polarized Raman spectra (scattering geometry B) of coextruded sPS after annealing at 210°C for 3 hours. (1100 - 900 cm ⁻¹).	148
5.14	Polarized Raman spectra (scattering geometry B) of coextruded sPS after annealing at 210°C for 3 hours. (900 - 100 cm ⁻¹).	150
5.15	Dispersion curve of the longitudinal acoustic branch.	158
6.1	Schematic diagram of different conformations of syndiotactic polystyrene. (from ref. 7).	168
6.2	Integrated intensity of the 1222 cm ⁻¹ trans band with time at various temperatures for a sample annealed at 150°C.	169
6.3	Integrated intensity of the 1222 cm ⁻¹ band measured at equilibrium at various temperatures for a sample annealed at 150°C.	170
6.4	Integrated intensities at 191°C as a function of time for a sample annealed at 170°C; (a) 1222 cm ⁻¹ ; (b) 943 and 934 cm ⁻¹	171

6.5	Integrated intensity of the 1222 cm^{-1} band with time at 191°C for samples annealed at 120°C, 150°C, and 170°C.	173
6.6	Trans crystal phase content measured at equilibrium as a function of temperature for samples annealed at 150°C.	174
6.7	DSC scans of samples annealed at 150°C and 170°C.	175
6.8	Avrami plot of the 1222 cm^{-1} band intensity as a function of time for a sample annealed at 170°C.	178

CHAPTER I

INTRODUCTION

Overview of Dissertation

Polymers are extremely complex materials and are frequently observed to undergo various phase transitions due to the effects of heat treatment, stretching, or the application of electric fields. During these transitions significant changes may occur in the crystal structure, chain conformation, and in the segmental orientation. Study of these changes provides insight into the mechanism of structural transformations, as well as in the development of high mechanical and electrical properties. The goal of this study is to gain a better understanding of phase transition behavior in several semi-crystalline polymer systems.

In this study, phase transition behavior is examined in three polymer systems: copolymers of vinylidene fluoride and trifluoroethylene, highly drawn blends of poly(vinylidene fluoride) and poly(methyl methacrylate), and syndiotactic polystyrene. Vibrational spectroscopy is the primary technique employed. This technique is sensitive to localized order and chain conformation, providing information which is complementary to the large scale order information given by diffraction techniques. Vibrational spectroscopy is also highly sensitive to both segmental and dipolar orientation, the latter not easily determined by other methods.

This dissertation is divided into seven chapters. Following a general introduction given in the first chapter, the second chapter deals with the effects of a high strength electric field on the microstructure of piezoelectric copolymers of vinylidene fluoride (PVDF) and trifluoroethylene (TrFE). These copolymers exhibit greater electrical activity than PVDF homopolymer. The structure and electrical activity of these materials is highly dependent

upon the annealing history and orientation. The application of a high strength electric field can also change the chain conformation and crystal structure significantly. Copolymers of PVDF and TrFE undergo a ferroelectric to paraelectric (Curie) phase transition upon heating at which the ordered polar structure is lost. The presence of an electric field (poling) produces changes in dipolar orientation and also changes in chain conformation. These effects are measured spectroscopically for two copolymer compositions at temperatures both below and above the Curie transition temperature. A comparison will also be made with previous poling studies of PVDF homopolymer, in order to determine the effect of the TrFE unit on the electrical behavior. The primary goal is to better elucidate the mechanism of polarization reversal in these materials. This mechanism is unknown, although knowledge of it is important in order to gain an understanding of the molecular origin of piezoelectricity in polymers.

Chapter III involves studies of highly oriented PVDF and blends of PVDF with poly(methyl methacrylate) (PMMA). These two polymers are miscible over a wide composition range. PVDF is observed to exist in several crystal phases and the presence of PMMA is known to influence the relative amounts of each phase. Infrared spectroscopy is employed to determine the phase content for two highly drawn blends and also for PVDF. The effects of annealing on the PVDF structure and segmental orientation will also be measured. Polarized data obtained from PVDF films with nearly perfect segmental orientation will be used for determination of the transition dipole moment directions of selected α phase bands. This information is useful as it complements the vibrational assignments determined from previous normal coordinate analyses.

Chapter IV concerns the microstructure of syndiotactic polystyrene (sPS). This highly crystalline polymer, which is observed to possess a melting temperature of 270°C, exhibits a number of crystalline phases including a helical structure found in a solution cast film, and an all trans conformation formed upon annealing. The transition to the all trans phase is irreversible and occurs rapidly by annealing near 200°C or upon drawing. The

primary goal is to identify spectral features of each structure and to locate bands which are sensitive to specific conformations and packing order.

In order to elucidate the ill defined vibrational assignments of sPS, a normal coordinate analysis of the trans conformation is presented in Chapter V. This analysis makes use of nonredundant symmetry coordinates and force constants for the phenyl ring. This is done in order to remove the problem of cyclic redundancies, which increases the number of internal coordinates and force constants used, such that the eigenvalue solution may not be unique. Force constants for the chain will be transferred from studies of saturated hydrocarbons and polymers of such backbone. Assignment of the infrared and Raman bands to specific symmetry species will be made upon comparison of the calculated results with the observed spectra. Another goal is to determine the amount of coupling between the ring and backbone vibrations, and to correlate bands highly coupled bands with those associated with the trans conformation. A value for the theoretical modulus will be calculated from the slope of the dispersion curve of the longitudinal acoustic branch near the Brillouin zone center.

The kinetics of the irreversible phase transition in syndiotactic polystyrene is studied in Chapter VI. Kinetics will be measured as a function of temperature and annealing history, in order to determine the effect of the thermal history on the transition behavior. The enthalpy of transition and the degree of crystallinity will be measured by thermal analysis. The transition is found to occur over a very narrow temperature range, and a nucleation and growth model will be applied to interpret the transition behavior.

Piezoelectric Polymers

Ferroelectric and piezoelectric polymers are a subject of great interest today.

Piezoelectricity involves a coupling of the mechanical and electrical properties, such that upon application of an electric field, a stress is induced in a material. The converse effect may occur as well. It is generally observed in materials which exhibit a non-centrosymmetric crystal structure. There are two general types of piezoelectrics: displacive and order-disorder.¹ Low molecular weight inorganic crystals such as quartz or LiNbO_3 are of the displacive type, in which polarization is induced as ions of opposite charge are displaced relative to one another upon strain. Piezoelectric polymers are of the order-disorder type, in which polarization is produced by the individual ordering of dipoles.¹ Piezoelectric materials are often also ferroelectric, meaning that they have a permanent dipole moment which can be reoriented by an electric field. Ferroelectrics exhibit a Curie transition temperature, above which polarization is lost due to thermal motion.

Polymers which exhibit piezoelectricity are of significant interest. Although these materials exhibit lower piezoelectric activity than ceramic ferroelectrics such as quartz, they can be processed easily and are light weight and flexible.² Polymers such as poly(γ -benzyl-glutamate)³, copolymers of vinylidene cyanide with vinyl acetate⁴ and methyl methacrylate⁵, as well as the odd nylons⁶ are known to be piezoelectric. Piezoelectricity is usually considered to be solely a crystalline property, although it is also observed in several amorphous copolymers.^{4,5} Poly(vinylidene fluoride) (PVDF) has received much attention as it contains polar and nonpolar crystal phases (α , β , δ , and γ) which control the piezoelectric activity. The α phase, formed at low degree of supercooling, is not electrically active. This structure contains polar chains which are packed antiparallel, so that although the individual chains contain a dipole moment, the crystal lattice has no net dipole.⁷ The β phase (fully trans planar zigzag conformation) shows the greatest piezoelectric activity. It is generally produced by low temperature drawing and subsequent

annealing.⁷ The relative amounts of each phase can be altered by the application of a high strength electric field,⁷ and several studies have been reported on the structural change induced by poling and its field strength and temperature dependences.⁸⁻¹¹

Copolymers of PVDF with Trifluoroethylene

Copolymers of PVDF with trifluoroethylene (TrFE) are of interest as the addition of TrFE produces a trans structure similar to the β phase of PVDF. Thus the copolymers may exhibit greater piezoelectric activity than PVDF homopolymer.¹² The addition of TrFE creates disorder along the chain and produces the same effect as increasing the number of head-to-head defects in PVDF, which is to stabilize the trans conformation.¹³ In these materials a Curie phase transition is observed upon heating in which the planar trans ferroelectric phase containing ordered dipoles undergoes a solid-solid phase transition to a paraelectric phase with conformational disorder and loss of dipole orientation.¹⁴⁻¹⁶ It is believed that the Curie transition temperature for PVDF lies above its melting temperature, and that the presence of TrFE lowers the transition temperature sufficiently that it may be observed.^{7,13} A DSC scan showing this enthalpic transition along with the melting transition is given in Figure 1.1. The effect of TrFE on the copolymer chain conformation causes the Curie temperature and melting point to be highly dependent on the TrFE content, and the variation of these transition temperatures with composition is demonstrated in Figure 1.2.

Poling with a high strength electric field has been shown to increase the content of the extended trans phase.^{15,16} Using vibrational spectroscopy, it is possible to observe this conformational transformation as well as to determine the degree of dipole orientation. It is of interest to compare the electric field induced structural change of the copolymers to that of PVDF, and to assess the effect of the Curie phase transition on the poling behavior.

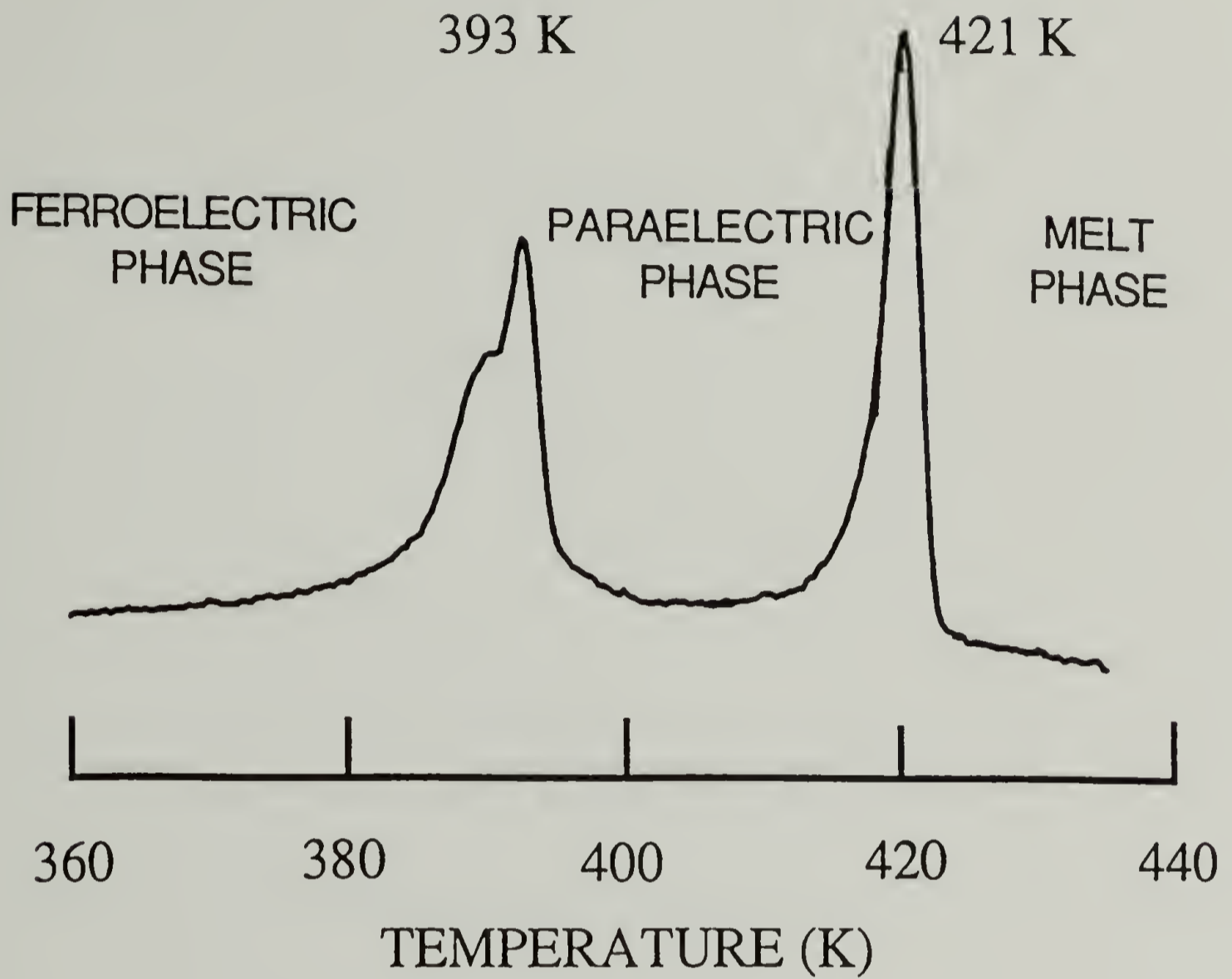


FIGURE 1.1. DSC Scan for a 70 mole% PVDF - 30 mole% TrFE Copolymer.

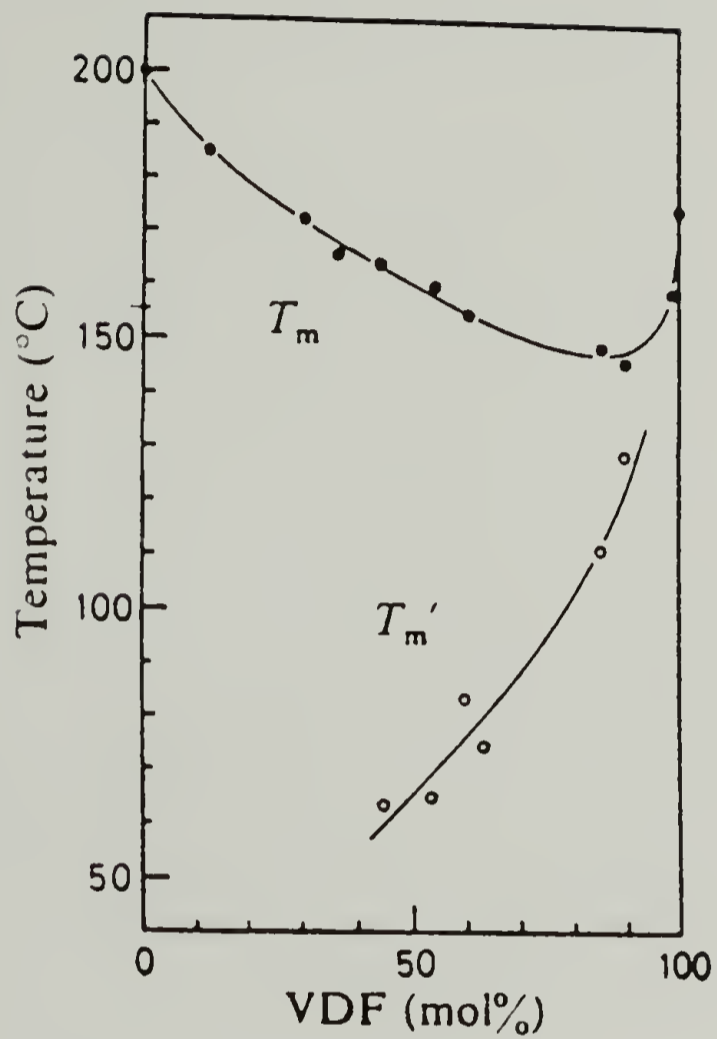


FIGURE 1.2 Variation in the melting temperature and Curie temperature with copolymer composition for PVDF- TrFE Copolymers. (from ref. 12)

Blends of PVDF and PMMA

Blends of PVDF with poly(methyl methacrylate) (PMMA) are miscible in the molten phase.¹⁷⁻²⁶ The occurrence of a single glass transition temperature and the negative interaction parameter, determined from melting point depression, are evidence for compatibility.¹⁸ It is known that the relative amounts of the α and β phases of PVDF, and the size and orientation of different crystallites all vary significantly with the blend composition and crystallization conditions.²⁷⁻²⁹

Pure β phase PVDF, however, is difficult to obtain unless the samples are crystallized under unusual conditions, such as under high pressure, on external substrates, in the presence of a high strength electrical field, or annealed under tension.^{7,30} Previously it has been demonstrated that the β phase of PVDF can be successfully obtained when crystallized in a high longitudinal flow gradient.^{29,31-33} For blends of PVDF with PMMA, the β phase content is increased under these conditions.²⁹ This is thought to occur because PMMA lowers the crystallization temperature, such that the β phase crystallizes more readily.²⁸ Most likely, blending affects both the nucleation and growth processes. It has also been suggested that since the trans conformation is the most energetically stable for PMMA, it may more efficiently interact with the trans conformation of PVDF and therefore stabilize the β crystal phase in these blends.³⁴ From infrared spectroscopy the α and β phase content and the segmental orientation may be quantitatively determined. With samples of known orientation, the transition moment angles of various vibrational modes may also be determined. Such information has been previously unavailable and is useful in assessing the validity of assignments determined from normal coordinate analyses of PVDF.^{35,36}

Microstructure of syndiotactic polystyrene

Syndiotactic polystyrene (sPS) has become a subject of great interest.³⁷⁻⁴⁵ Only quite recently has the synthesis been developed to produce polymer with greater than 98% syndiotactic content.^{37,38,43} This material has several interesting physical characteristics: 1. A melting temperature of approximately 270°C; 2. A variety of chain conformations including a fully trans planar zigzag backbone in addition to a helical conformation observed for solution cast films; and 3. The presence of a solid-solid phase transition at ~193°C involving changes in both chain conformation and packing.^{37,39-43} Because of its inherent backbone stiffness and strong intermolecular interactions, the macroscopic properties such as modulus and strength and their insensitivity to temperature are expected to exceed most polymers.

The structure of sPS is complex, and is still largely unknown. Diffraction and spectroscopic studies have revealed that this polymer exists in a helical conformation upon casting from dilute solution and can easily transform to the all trans conformation upon annealing or drawing.^{39,41,42,46,47} The differences in the infrared and Raman spectra observed for different forms of sPS are striking. From the spectra obtained from samples of different tacticity, and from previous vibrational analyses of isotactic and atactic PS,⁴⁸⁻⁵⁰ preliminary analyses have been carried out for sPS.^{44,47} However the exact band assignments for sPS are still ill defined, and must be understood in order to understand the conformational order and packing changes which occur during the phase transition between the helical and trans conformations. In this study a normal vibrational analysis is performed for the all trans conformation using nonredundant coordinates and force constants for the phenyl ring in order to assign features in the infrared and Raman spectra which are sensitive to conformation. Use of these nonredundant coordinates removes the cyclic redundancies of the phenyl ring which can lead to a nonunique solution for the

vibrational modes. Knowledge of the infrared and Raman assignments is necessary for the vibrational spectra to be employed for analysis of the microstructure and phase transition.

The irreversible phase transition between the helical and trans structures upon heating is observed to occur over a very narrow temperature range, which is unusual for polymers. The enthalpy and kinetics of the transition are measured and a nucleation and growth model will be applied in order to explain the transition behavior. The effects of annealing temperature on the formation of the trans state will also be studied.

References

1. Lines, M. E.; Glass, A. M. *Principles and Applications of Ferroelectrics and Related Materials*; Clarendon Press: Oxford, 1977, p 103.
2. Lovinger, A. J. *Science* **1983**, 220, 1116.
3. Date, M.; Takashita, S.; Fukada, E. *J. Polym. Sci., Part A-2* **1970**, 8, 61.
4. Miyata, S.; Yoshikawa, M.; Tasaka, S.; Ko, M. *Polymer J.* **1980**, 12, 857.
5. Maruyama, Y.; Sung, J. Y.; Inoue, Y.; Chujo, R.; Tasaka, S.; Miyata, S. *Polymer* **1987**, 28, 1087.
6. Litt, M. H.; Hsu, C.; Basu, P. *J. Appl. Phys.* **1977**, 48, 2208.
7. Lovinger, A. J.; *Developments in Crystalline Polymers*; Bassett, D.C., Ed.; Applied Science Publishers: Essex, UK, 1982; p 195.
8. Davis, G. T.; McKinney, J. E.; Broadhurst, M. G.; Roth, S. C. *J. Appl. Phys.* **1978**, 49, 4998.
9. Lu, F. J.; Waldman, D. A.; Hsu, S. L. *J. Polym. Sci., Polym. Phys. Ed.* **1984**, 22, 827.
10. Lu, F. J.; Hsu, S.L. *Polymer* **1984**, 25, 1247.
11. Hsu, S. L.; Lu, F. J.; Waldman, D. A.; Muthukumar, M. *Macromolecules* **1985**, 18, 2583.
12. Yagi, T.; Tatemoto, M.; Sako, J. *Polymer J.* **1980**, 12, 209.
13. Lovinger, A. J.; Davis, D. D.; Cais, R. E.; Kometani, J. M. *Polymer* **1987**, 28, 617.
14. Tashiro, K.; Takano, K.; Kobayashi, M.; Chatani, Y.; Tadokoro, H. *Polymer* **1981**, 22, 1312.
15. Lovinger, A. J.; Davis, G. T.; Broadhurst, M. G. *Macromolecules* **1982**, 15, 323.
16. Davis, G. T.; Furukawa, T.; Lovinger, A. J.; Broadhurst, M. G. *Macromolecules* **1982**, 15, 329.
17. Noland, J. S.; Hsu, N. N. C.; Saxon, R.; Schmitt, J. M. *Adv. Chem. Ser.* **1971**, 99, 15.
18. Nishi, T.; Wang, T. T. *Macromolecules* **1975**, 8, 909.
19. Paul, D. R.; Altamirano, J. O. *Adv. Chem. Ser.* **1975**, 142, 371.
20. Coleman, M. M.; Zarian, J.; Varnell, D. F.; Painter, P. C. *J. Polym. Sci., Polym. Lett. Ed.* **1977**, 15, 745.

21. Hourston, D. J.; Hughes, J. D. *Polymer* **1977**, 18, 1175.
22. Paul, D. R. Barlow, J. W., Bernstein, R. E.; Wahrmund, D. R. *Polym. Eng. Sci.* **1978**, 18, 1225.
23. Roerdink, E.; Challa, G. *Polymer* **1978**, 19, 173.
24. Roerdink, E.; Challa, G. *Polymer* **1980**, 21, 509.
25. Wendorff, J. H. *J. Polym. Sci., Polym. Lett. Ed.* **1980**, 18, 439.
26. Morra, B. S.; Stein, R. S. *J. Polym. Sci., Polym. Phys. Ed.* **1982**, 20, 2243.
27. Morra, B. S.; Stein, R. S. *J. Polym. Sci., Polym. Phys. Ed.* **1982**, 20, 2261.
28. Léonard, C; Halary, J. L.; Monnerie, L.; Broussoux, D; Servet, B.; Micheron, F. *Polym. Comm.* **1983**, 24, 110.
29. Yang, D.; Thomas. E. L. *J. Mat. Sci. Lett.* **1987**, 6, 593.
30. Lu, F. J.; Hsu, S. L. *Macromolecules* **1986**, 19, 326.
31. Gohil, R. M.; Petermann, J. *Polymer* **1981**, 22, 1612.
32. Yang, D. C.; Thomas, E. L. *J. Mat. Sci.* **1984**, 3, 929.
33. Hausler, E.; Kaufmann, W.; Petermann, J.; Stein, L. *Ferroelectrics* **1984**, 60, 45.
34. Léonard, C.; Halary, J. L.; Monnerie, L. *Macromolecules* **1988**, 21, 2988.
35. Kobayashi, M.; Tashiro, K; Tadokoro, H. *Macromolecules* **1975**, 8, 158.
36. Tashiro, K.; Itoh, Y.; Kobayashi, M.; Tadokoro, H. *Macromolecules* **1985**, 18, 2600.
37. Ishihara, N.; Seimiya, T.; Kuramoto, M.; Uoi, M. *Macromolecules* **1986**, 19, 2464.
38. Zambelli, A.; Longo. P.; Pellicchia, C.; Grassi, A. *Macromolecules* **1987**, 20, 2035.
39. Kobayashi, M.; Nakaoki, T.; Uoi, M. *Polym. Prep., Jpn.* **1988**, 37, E432.
40. Greis, O.; Asano. T.; Xu, J.; Petermann, J. Z. *Kristallogr.* **1988**, 182, 58.
41. Immirizi, A.; de Candia, F.; Iannelli, P.; Zambelli, A. *Makromol. Chem. Rapid Commun.* **1988**, 9, 761.
42. Vittoria, V.; de Candia, F.; Iannelli, P.; Immirizi, A. *Makromol. Chem. Rapid Commun.* **1988**, 9, 765.
43. Ishihara, N.; Kuramoto, M.; Uoi, M. *Macromolecules* **1988**, 21, 3356.

44. Conti, G; Santoro, E.; Resconi, L.; Zerbi, G. *Mikrochim. Acta* **1988**, 1, 297.
45. Nyquist, R. A. *Appl. Spectrosc.* **1989**, 43, 440.
46. Petermann, J. private communication.
47. Reynolds, N. M.; Savage, J. D.; Hsu, S. L. *Macromolecules* **1989**, 22, 2867.
48. Painter, P. C.; Koenig, J. L. *J. Polym. Sci., Polym. Phys. Ed.* **1977**, 15, 1885.
49. Snyder, R. W.; Painter, P. C. *Polymer* **1981**, 22, 1633.
50. Liang, C. Y.; Krimm, S. *J. Polym. Sci.* **1958**, 27, 241.

CHAPTER II

ELECTRICAL FIELD INDUCED STRUCTURAL CHANGES IN PVDF-TrFE COPOLYMERS

Introduction

Ferroelectric and piezoelectric polymers are of great interest today. They exhibit lower piezoelectric activity than ceramic ferroelectrics such as quartz or LiNbO_3 , but are light weight, inexpensive and easily processed.¹ Polymers such as poly(γ -benzyl-glutamate)², copolymers of vinylidene cyanide with vinyl acetate³ and methyl methacrylate⁴, as well as the odd nylons⁵ are known to be piezoelectric. Poly(vinylidene fluoride) (PVDF) has received much attention as it contains polar and nonpolar crystal phases which control the piezoelectric activity. The relative amounts of each phase can be altered by the application of a high strength electric field,⁶ and studies have been reported on the structural change induced by poling and its field strength and temperature dependences.⁷⁻¹⁰

The interest of this study is focused on PVDF and its copolymers with trifluoroethylene (TrFE). These copolymers have been the subject of much study since the addition of trifluoroethylene produces a trans structure similar to the β phase of PVDF and exhibiting greater piezoelectric activity.¹¹ In these materials a Curie phase transition is observed in which the planar trans ferroelectric phase containing ordered dipoles undergoes a solid-solid phase transition to a paraelectric phase with conformational disorder and loss of dipole orientation.¹²⁻¹⁴

The application of a high strength electric field is known to raise the Curie temperature^{14,15} and is frequently employed to increase piezoelectric activity. Previous x-ray analyses have been carried out to determine structural changes occurring at the Curie transition and the effects of poling.¹³⁻¹⁷ Several theories have been proposed for the

mechanism by which chain dipoles couple to the field and produce conformational change,¹⁸⁻²⁰ however this mechanism is still uncertain.

This study focuses on the microstructural change occurring in VDF/TrFE copolymers due to an applied electric field. Such information is important in order to gain an understanding of the mechanism of piezoelectricity in these materials. Vibrational spectroscopy is our primary structural characterization technique, however the vibrational assignments for this material are unclear. Therefore we have examined the effects of annealing, low temperature, orientation, and electric field application in order to clarify these assignments. In the infrared spectra of these materials there are absorptions representative of specific conformations which provide information about structural changes in the presence of an electric field. These vibrations show substantial intensity changes at the Curie transition and are monitored as a function of field strength and temperature. A cyclic electric field is applied to observe reversible structural changes due to dipole orientation under the field, as well as irreversible conformation and molecular packing changes. Such information will complement earlier x-ray and spectroscopic studies.^{13-15,21,22} Poling behavior is compared with that of PVDF and is related to the microstructural disorder present in the copolymer structure due to the presence of TrFE units.

Experimental

Samples used in this study are a 75 mole% VDF - 25 mole% TrFE copolymer provided by Pennwalt Corporation in the form of 9 μm uniaxially oriented films. In order to remove the effects of prior poling treatments, the films used in our experiment were annealed for two hours at 130°C. The Curie temperature for this composition is broad and depends on the experimental parameters. The onset of transition in our DSC scans starts at 116°C.

It is difficult to obtain infrared data for the 9 μm films for quantitative analysis since many bands show high absorbance values. Therefore a 2% solution was prepared by dissolving pellets of the 75/25 copolymer in acetone. Films were cast in aluminum pans and annealed or drawn at room temperature to a maximum draw ratio of five. An annealing experiment was carried out by placing the unoriented cast film in a sample holder placed in a 130°C oven. The thickness of cast films was obtained by measurement of the integrated intensity of the CH stretching region and by comparison of this intensity with that of a film cast of known average thickness from a 2 wt.% solution.

In order to observe in situ structural changes produced by the electric field, as described in previous studies, gold-palladium electrodes were sputter coated directly onto the as received copolymer films or onto polished KBr windows.⁸⁻¹⁰ A Polaron SEM sputter coater was employed operating at a voltage of 2.2 kV and a current of 15 mA with a four to five minute coating time. The electrodes were thick enough to conduct electricity, yet thin enough to allow transmittance of the infrared beam. The sample was held in a clamp and placed in a heating cell for high temperature poling experiments. The temperature was maintained to within 1°C of the setting temperature. A high voltage power supply was used to generate fields up to 2.2 MV/cm. A schematic diagram illustrating the experimental poling setup is found in Figure 2.1. Infrared spectra were obtained with both IBM IR32 and Nicolet 60SXB FTIR spectrometers. To obtain spectra with high signal-to-

noise ratio, 500 scans were collected at a resolution of 2 cm^{-1} . In general, electric fields were applied for ten minutes before spectra were obtained.

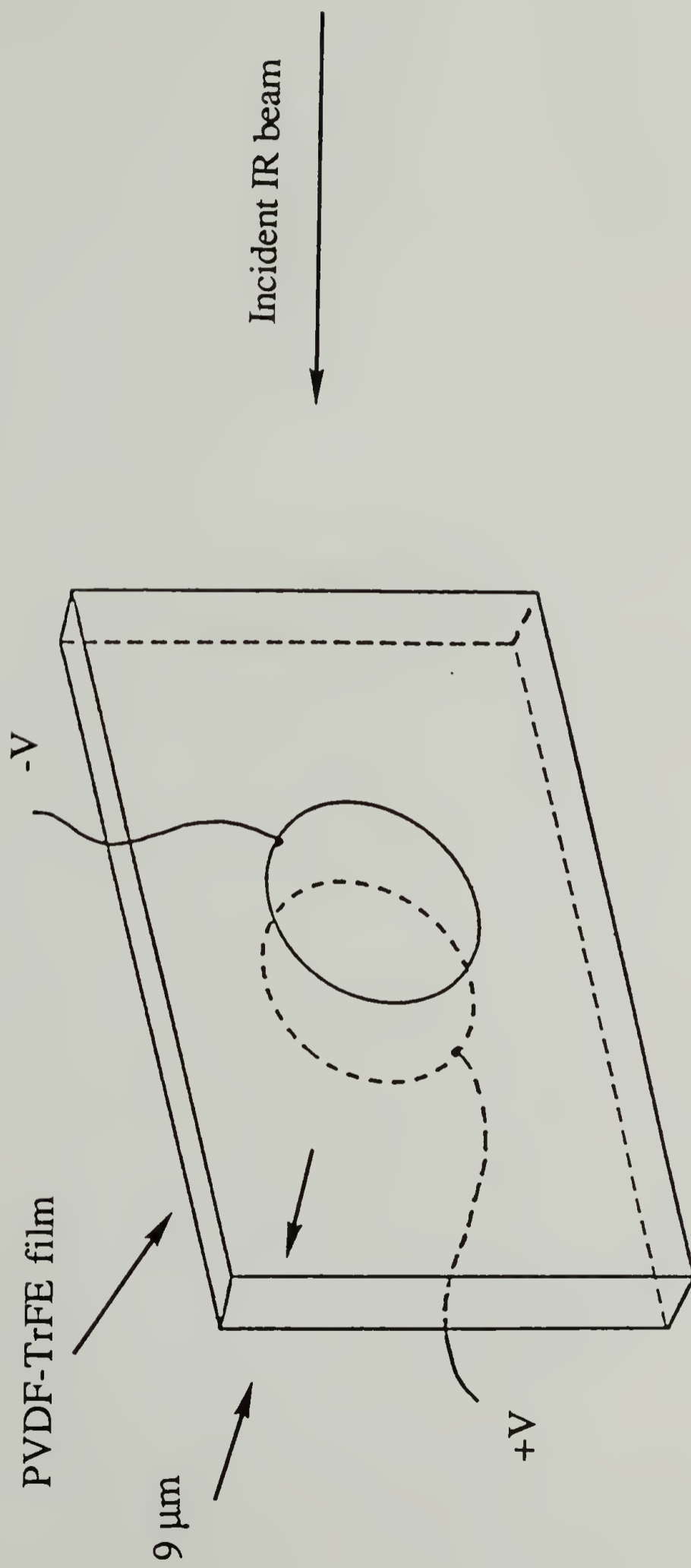


FIGURE 2.1 Schematic drawing of experimental geometry for poling.

Results and Discussion

Unlike PVDF, the chain conformation and packing are not well understood for PVDF-TrFE copolymers. It is generally agreed however that the electrically active crystalline phase has a nearly planar zigzag chain conformation and packing similar to the β phase found for PVDF.^{11,12} It has been suggested that the TrFE units may be excluded from the β form crystalline unit cell.²⁰ However, x-ray and DSC studies suggest both subunits of the copolymer can be incorporated into the unit cell.^{11,24} It is uncertain what structure is present above the Curie transition, for this polymer, approximately 116°C. It is generally agreed that this chain conformation is a statistical distribution involving TT, TG, TG', T₃G and T₃G' rotational isomers.^{12,15} However recent studies suggest that the paraelectric phase exists in a TGTG' conformation similar to the α phase of PVDF with some trans isomers remaining.^{25,26} The available x-ray data suggest that chains are packed in a hexagonal array.^{11,12}

The participation of the β phase of PVDF in the piezoelectric effect is well established.⁶ Transformation between the various phases has also been characterized for PVDF,⁶⁻¹⁰ however relatively little information is available for the copolymer of PVDF and TrFE. The main objective of this spectroscopic study is to characterize the conformation of the various phases of a PVDF-TrFE copolymer and to determine how the chain segments in these phases respond to an applied electric field. The principal advantage of vibrational spectroscopy when compared to other physical techniques is its ability measure localized chain orientation, packing, and conformation. In addition, the large dipoles of the chain couple strongly to the applied field, thus the spectroscopic technique is sensitive to the small structural subunits change induced by an electric field. In Figures 2.2 through 2.5 are shown the infrared spectra of the copolymer as a function of temperature, annealing treatment, electric field application, and orientation. Spectral changes arise from either a change in the chain conformation or from the orientation of the transition dipoles.

FIGURE 2.2 Infrared spectra of 75/25 PVDF/TrFE film as a function of temperature; (1600-400 cm^{-1}); (top) 125°C spectrum; (bottom) room temperature spectrum.

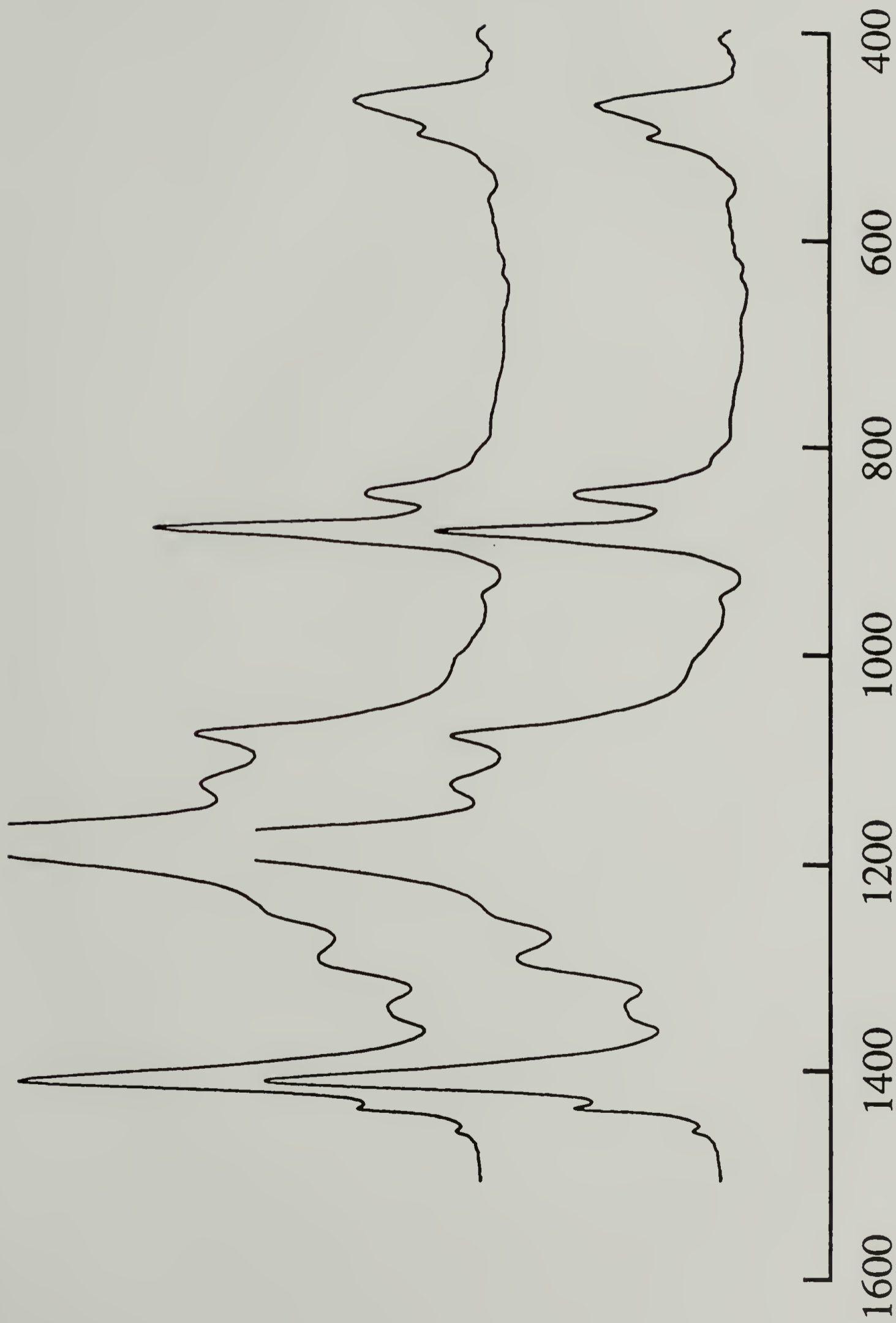
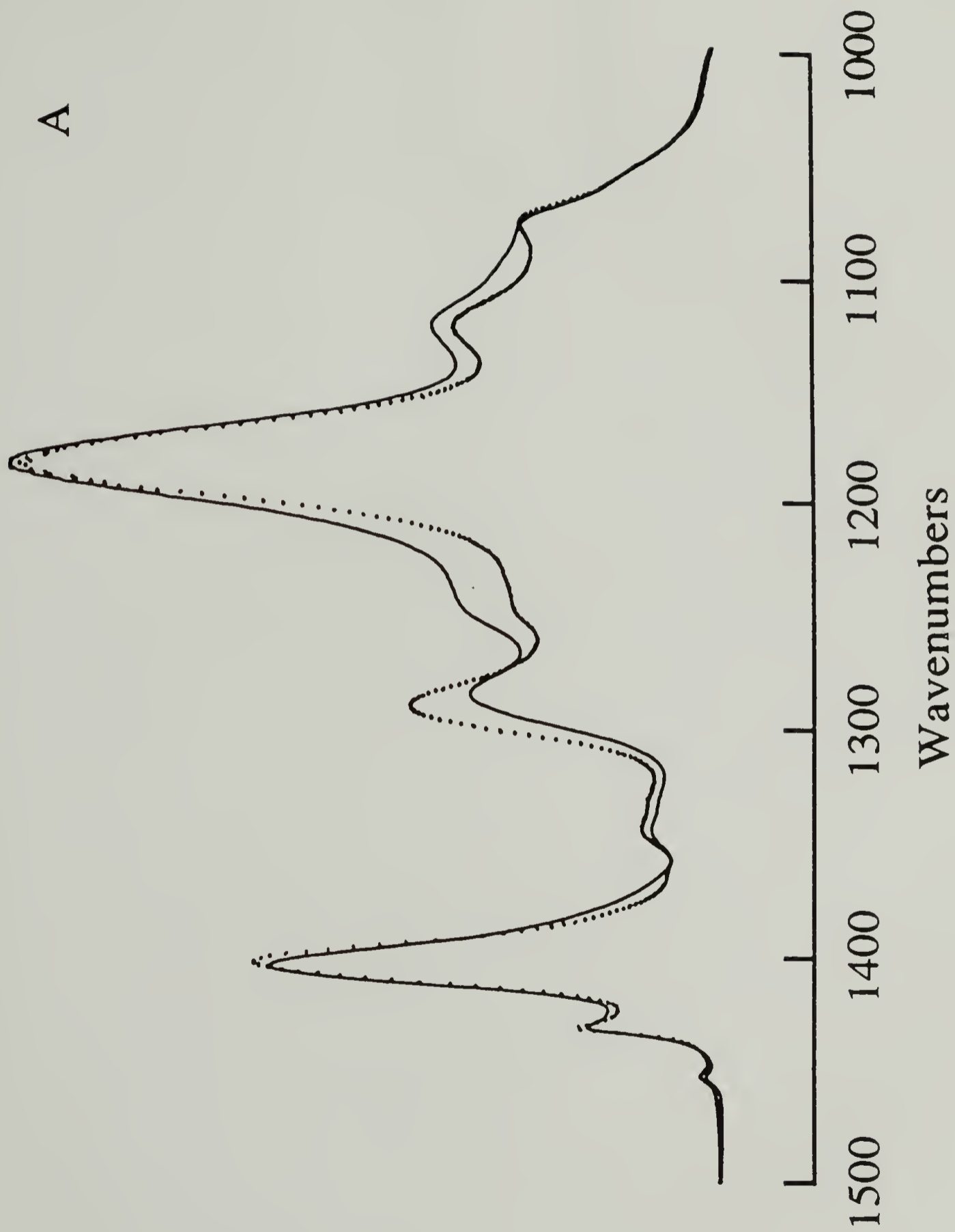


FIGURE 2.3 Infrared spectra of 75/25 PVDF/TrFE film before and after annealing at 130°C for 2 hours; (a) 1500-1000 cm^{-1} region; (b) 1000-400 cm^{-1} region; (....) annealed sample; (-) as cast film.



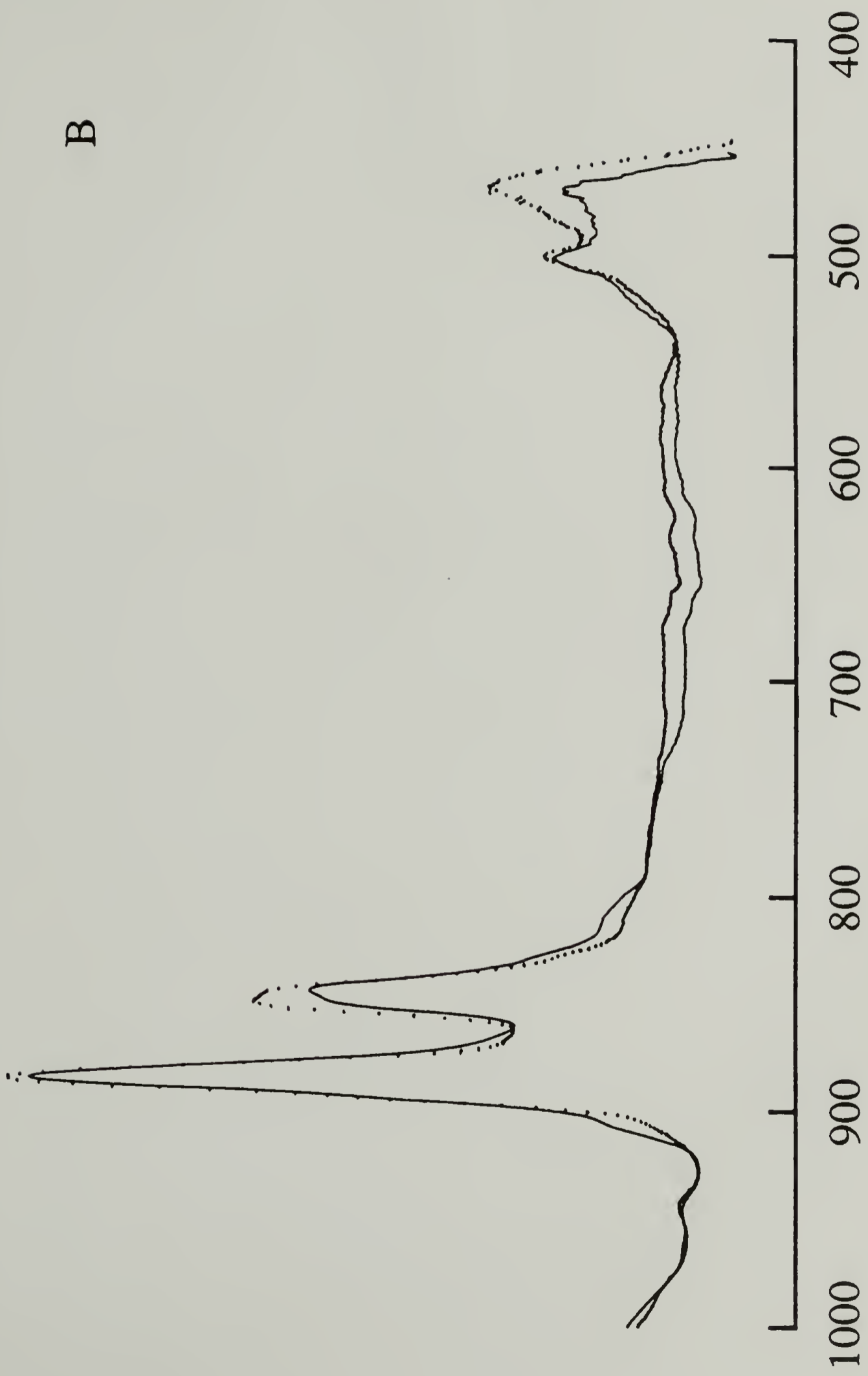
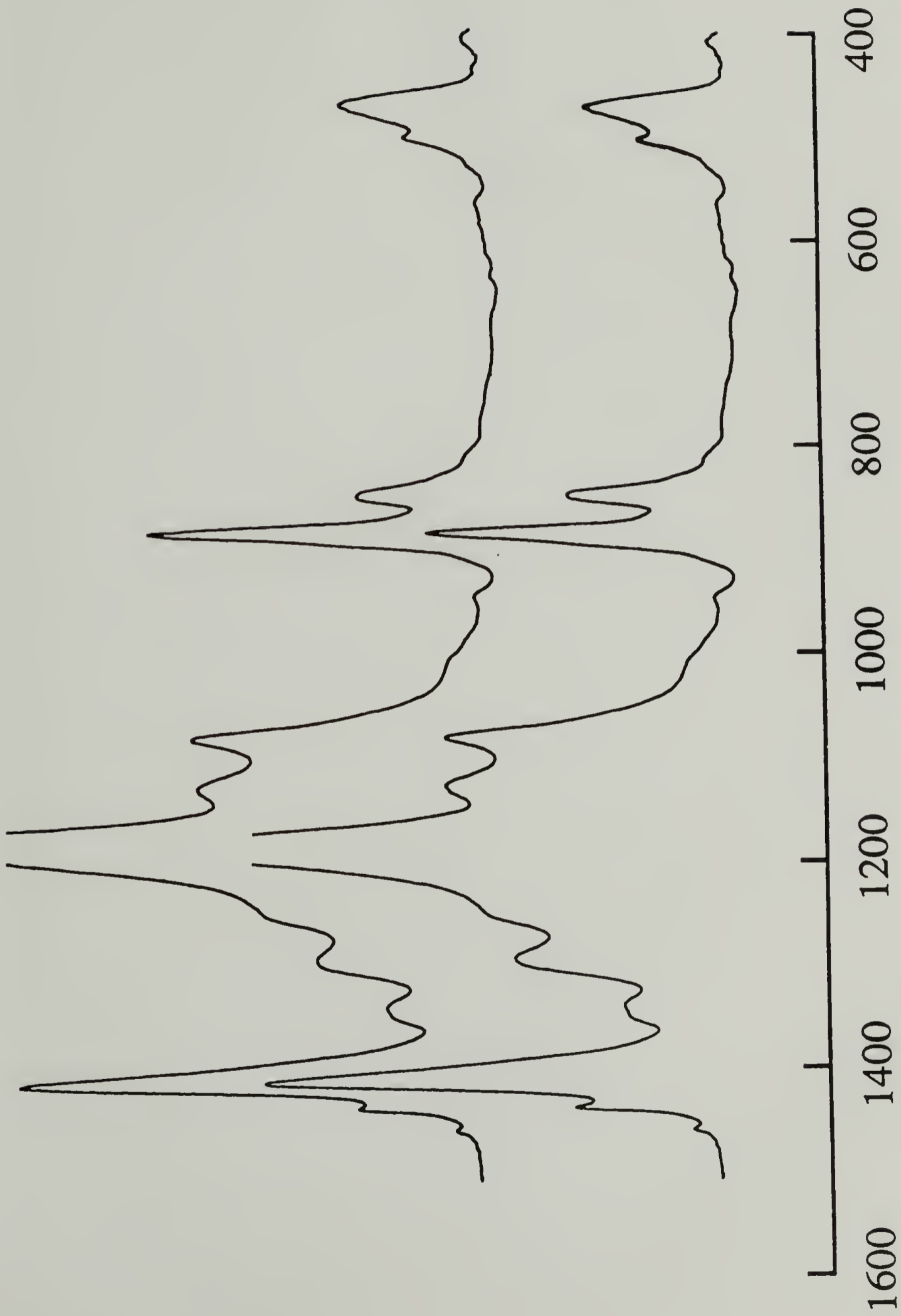
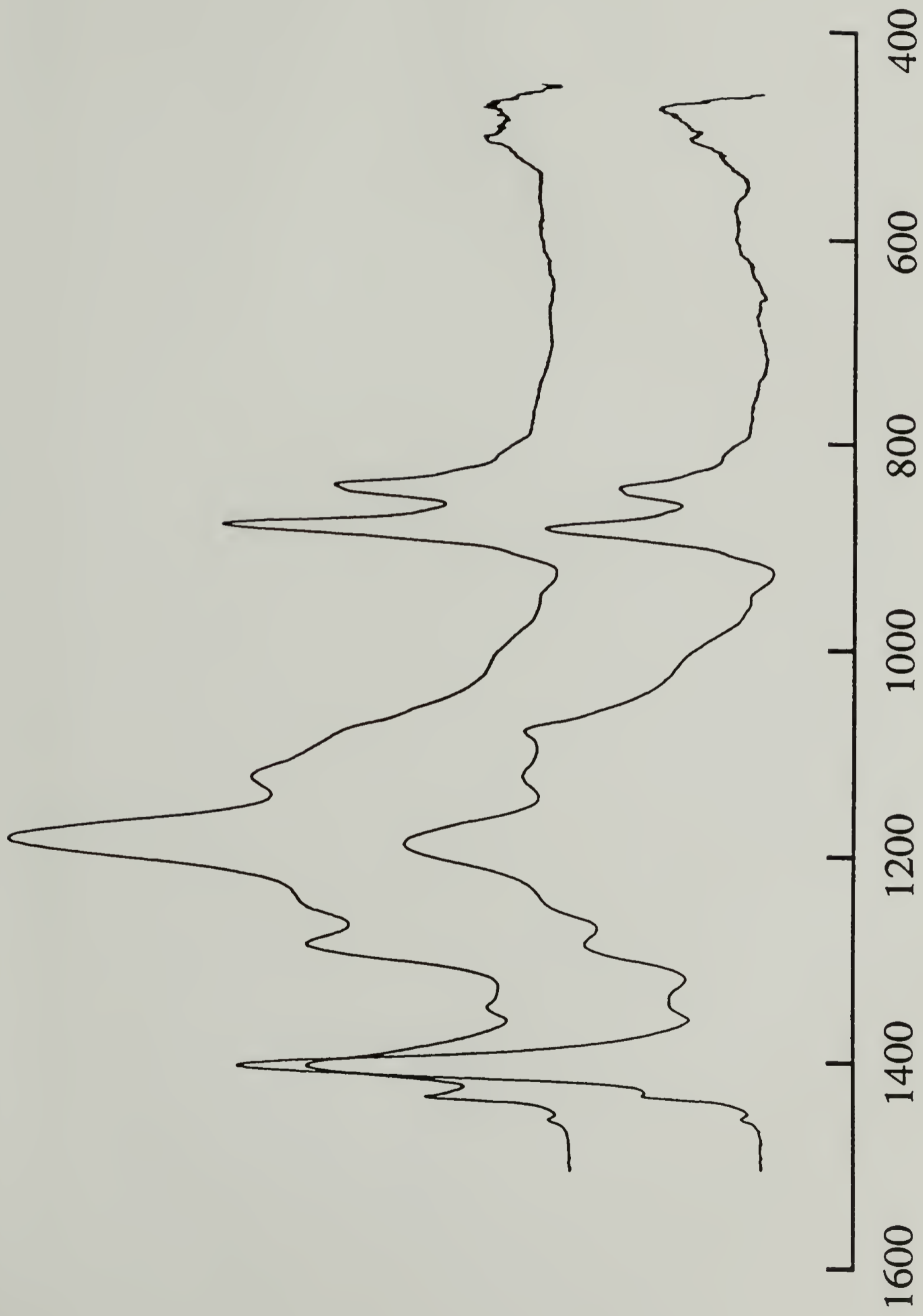


FIGURE 2.4 Infrared spectra of 75/25 PVDF/TrFE film as a function of electric field; (top) $E = 2.2 \text{ MV/cm}$; (bottom) $E = 0.0 \text{ MV/cm}$.



Wavenumbers

FIGURE 2.5. Polarized infrared spectra of 75/25 PVDF/TrFE film at a draw ratio of 1.6; (1600-400 cm^{-1}); (top) perpendicular polarization; (bottom) parallel polarization.



In an earlier experiment, the response of the electrically active or nonactive phases in PVDF to an external field was directly interpretable from the intensity changes in the infrared spectra.⁸⁻¹⁰ Unlike PVDF, nearly all the bands in PVDF-TrFE copolymers change in frequency or intensity as a function of electric field strength and polarity. However, for the same field strength and measurement temperature the changes observed for the copolymer are much smaller than those observed for PVDF.¹⁰ The rather insignificant intensity changes can be interpreted as weaker coupling to the applied field as a result of the inherently smaller effective dipole of the copolymer chain, since for each TrFE unit the CF₂ dipole is partially compensated by a CFH unit. However the fact that nearly all the observed infrared active vibrations are sensitive to the applied field suggests that the β chain conformation is indeed the most favorable one due to the stabilizing factor of the TrFE units.

Band Assignments

In order to have a more detailed interpretation of the field induced structural changes, band assignments need to be more certain. In comparison to what is known about polyethylene or normal alkanes, there has been only limited normal vibrational analysis for the fluorinated polymers due to the unclear chain structure and ill defined force field. Analysis of vibrational spectra has been carried out for poly(tetrafluoroethylene)²⁷⁻³¹ and for PVDF.³²⁻³⁶ These studies have proven to be enormously useful for selection of the vibrations employed to interpret the molecular structure changes giving rise to the piezoelectric effect for PVDF.

Since such normal vibrational analysis is unavailable for the copolymer, our understanding of the vibrational spectra associated with PVDF-TrFE copolymers is far from complete. Due to the large mass of the fluorine atom, most infrared active vibrations for the copolymer are concentrated in a rather narrow region, 1500 to 400 cm⁻¹. Virtually

all the vibrations are coupled delocalized vibrations involving many atoms making exact band assignments difficult. Clearly the more complete the vibrational analysis, the more detailed is our explanation for the molecular mechanism of field induced structural change.

Several vibrational bands for the copolymer have been assigned to specific conformations by Tashiro et al.,^{12,16,17,26} and these assignments will be employed in this study. These bands exhibit changes as a function of temperature, field strength or orientation and therefore are used in this study to interpret the response of a PVDF-TrFE copolymer to an external electric field. The assignments and polarizations of the selected bands are listed in Table 2.1.

Table 2.1 Characteristics of vibrational bands chosen for analysis

<u>Frequency</u> (cm ⁻¹)	<u>Polarization</u>	<u>Assignment</u>	<u>Conformation</u>
3014	⊥	v _a (CH ₂)	-
2977	⊥	v _s (CH ₂)	-
1290	⊥	v _s (CF ₂) δ(CCC)	T _m (m>4)
883	⊥	r(CH ₂) v _a (CF ₂) r(CF ₂)	T
850	⊥	v _a (CF ₂)	T _m (m>3)
802	⊥	r(CH ₂)	TG
612		δ(CF ₂) δ(CCC)	TG

The 1290, 883, 850 (doublet), 802 and 612 cm^{-1} bands exhibited the most interesting and interpretable changes. One of our original candidates, the 507 cm^{-1} band, may correspond to the 510 cm^{-1} CF_2 bending band observed for trans sequences associated with either the β or γ phases of PVDF. However, Davis et al. have observed a band at this position for P(TrFE)¹⁴, making it difficult to employ for structural interpretation.

As seen in Table 2.1, the 1290 cm^{-1} band has been assigned to the symmetric CF_2 stretching vibration coupled to the backbone stretching and bending vibrations.^{35,36} It is assigned to sequences of four or more VDF units corresponding to trans isomer sequences four or more units long and is therefore characteristic of the extended chain or β structure.^{12,16,17} It may be seen in Figure 2.2 that this band is absent in the high temperature paraelectric phase. It should have a perpendicular polarization as observed in the oriented film spectrum shown in Figure 2.5.

The 883, 850 (doublet), and 612 cm^{-1} bands, assigned to CH_2 rocking and CF_2 asymmetric stretching, CF_2 symmetric stretching, and CF_2 bending coupled to skeletal bending, respectively, are useful for structural characterization.^{26,34-36} Although not used extensively in this study, the 802 cm^{-1} band assigned to the CF_2 symmetric stretching vibration is extremely strong in the Raman spectrum of these copolymers.^{25,26} The dichroic ratios of these bands measured for the highly oriented films are all consistent with the expected polarization characteristics. It should be emphasized that these vibrations are characteristic of conformations of PVDF sequences. Strictly speaking, it is not possible to directly interpret the overall chain conformation, however it is concluded that the molecular response of the comonomers cannot be separated. The two bands near 850 cm^{-1} , similar to the 1290 cm^{-1} band, are characteristic of long sequences of at least three trans isomers.^{12,16,17} In contrast, the bands at 802 and 612 cm^{-1} are characteristic of gauche conformers.^{12,16,25,26} The relative amount of chain conformations in this study are based on the relative intensity of the different bands. We cannot easily quantify the degree of

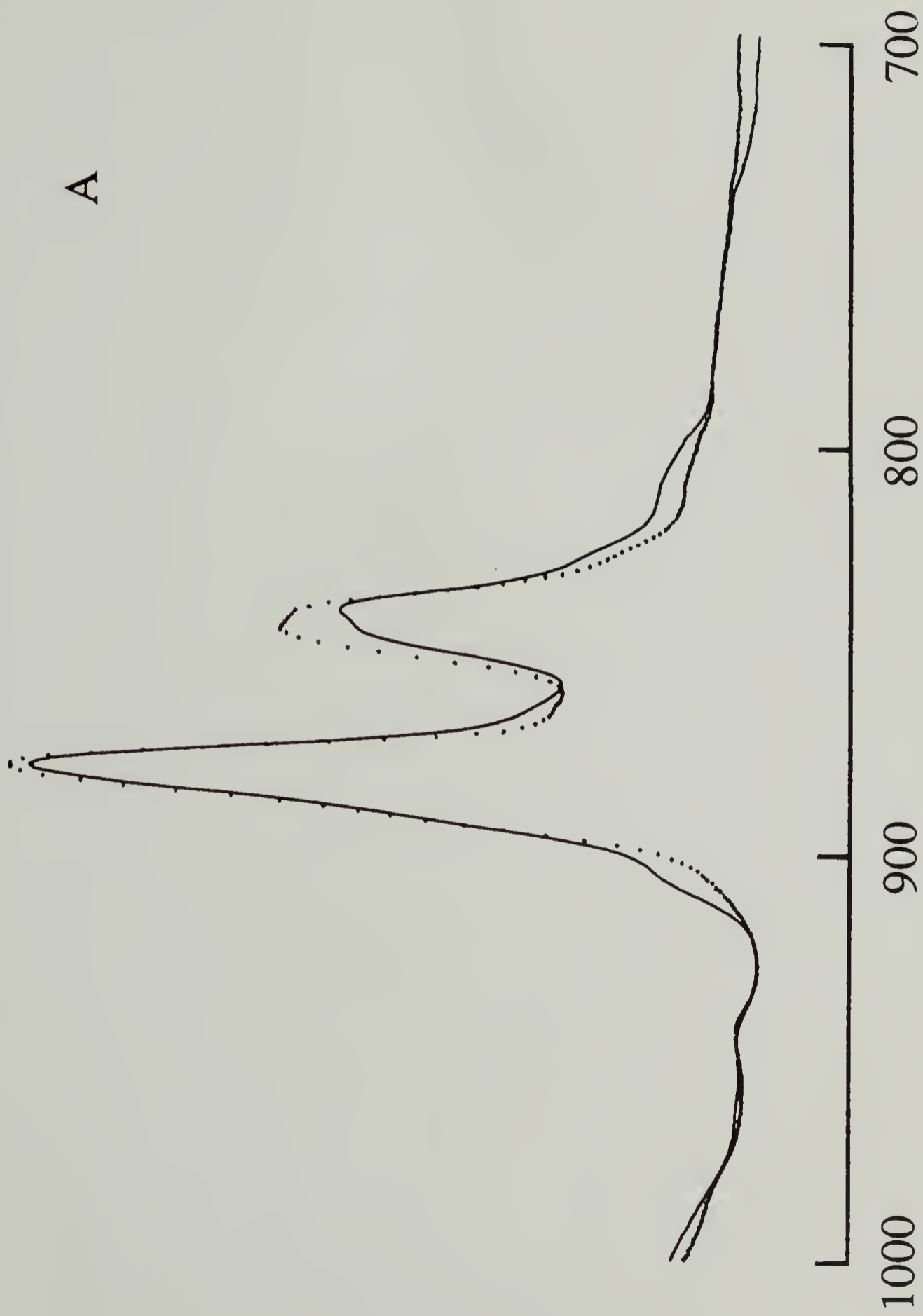
conformation change as the intrinsic absorption coefficients of each vibration are unknown. In previous studies, these coefficients have been assumed to be equivalent.¹⁷

There has been some controversy regarding the assignments of the bands listed above. Originally, the assignments of the 880 cm^{-1} and 840 cm^{-1} bands for PVDF were unclear.³⁴ In a recent poling experiment and normal vibrational analysis, the new assignments are consistent with polarized Raman studies on rolled PVDF films, with the 880 cm^{-1} band assigned to the CH_2 rocking, CF_2 asymmetric stretching, and CF_2 rocking vibrations, while the 840 cm^{-1} band is assigned to the CF_2 symmetric stretching mode.³⁵ It will be shown that these new assignments are consistent with the present copolymer poling experiment.

The clearly resolved doublet observed for the copolymer needs a more detailed analysis. In an earlier study it was concluded that the 842 and 850 cm^{-1} bands observed in PVDF at liquid nitrogen temperature are associated with crystal field splitting.⁹ The 850 cm^{-1} doublet for the copolymer is somewhat complicated by the fact that PTrFE exhibits a relatively weak and broad peak at 851 cm^{-1} .¹⁴ The 850 cm^{-1} region is summarized for various experiments in Figure 2.6. The relative intensity of the doublet can differ significantly as a function of annealing, electric field strength and polarity, or sample orientation. The two components at 844 and 849 cm^{-1} when measured at 110 K are found to be polarized perpendicular to the draw direction, as expected. We believe these two components are related to the ordered regions in the copolymer, and may also be related to the crystal field splitting found for PVDF. We came to this conclusion because of the enhanced splitting observed for the copolymer film at low temperature in Figure 2.6d. Generally speaking, vibrations sensitive to the magnitude and specificity of non-bonded intermolecular interactions are sensitive to temperature as these two components are.

Further evidence for this assignment is obtained by preparing a solution cast film which contains both crystalline and amorphous regions. Based on previous energy calculations, it is known that the trans conformation of the β unit cell is more stable.¹⁶

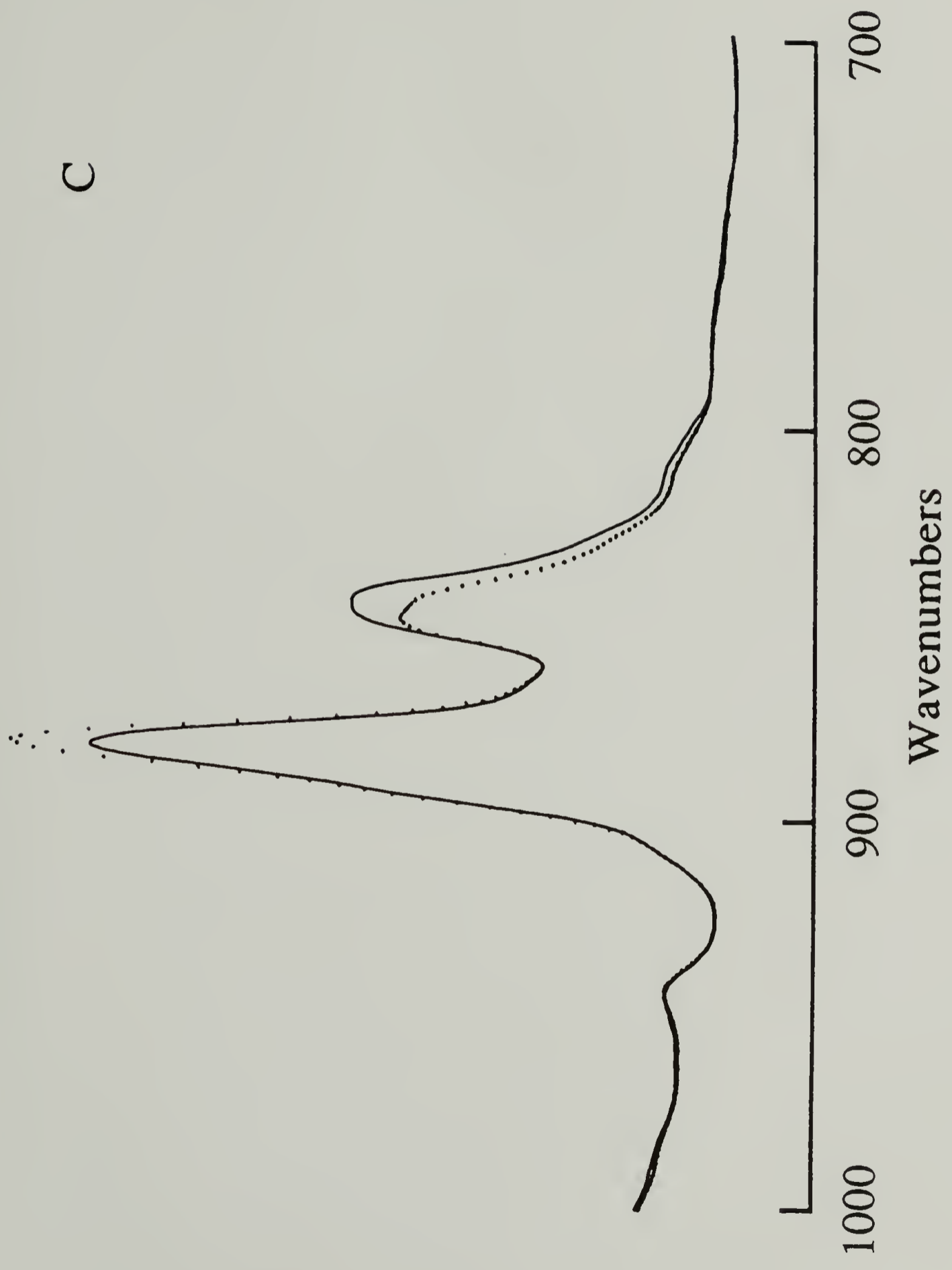
FIGURE 2.6 Infrared data in the 1000-700 cm^{-1} region of 75/25 PVDF/TrFE films; (a) (····) annealed; (-) as cast; (b) oriented sample with draw ratio 1.6; (-) perpendicular polarization; (····) parallel polarization; (c) electric field applied, (····) $E = 2.2 \text{ MV/cm}$; (-) 0.0 MV/cm ; (d) (top) 110 K; (bottom) room temperature.

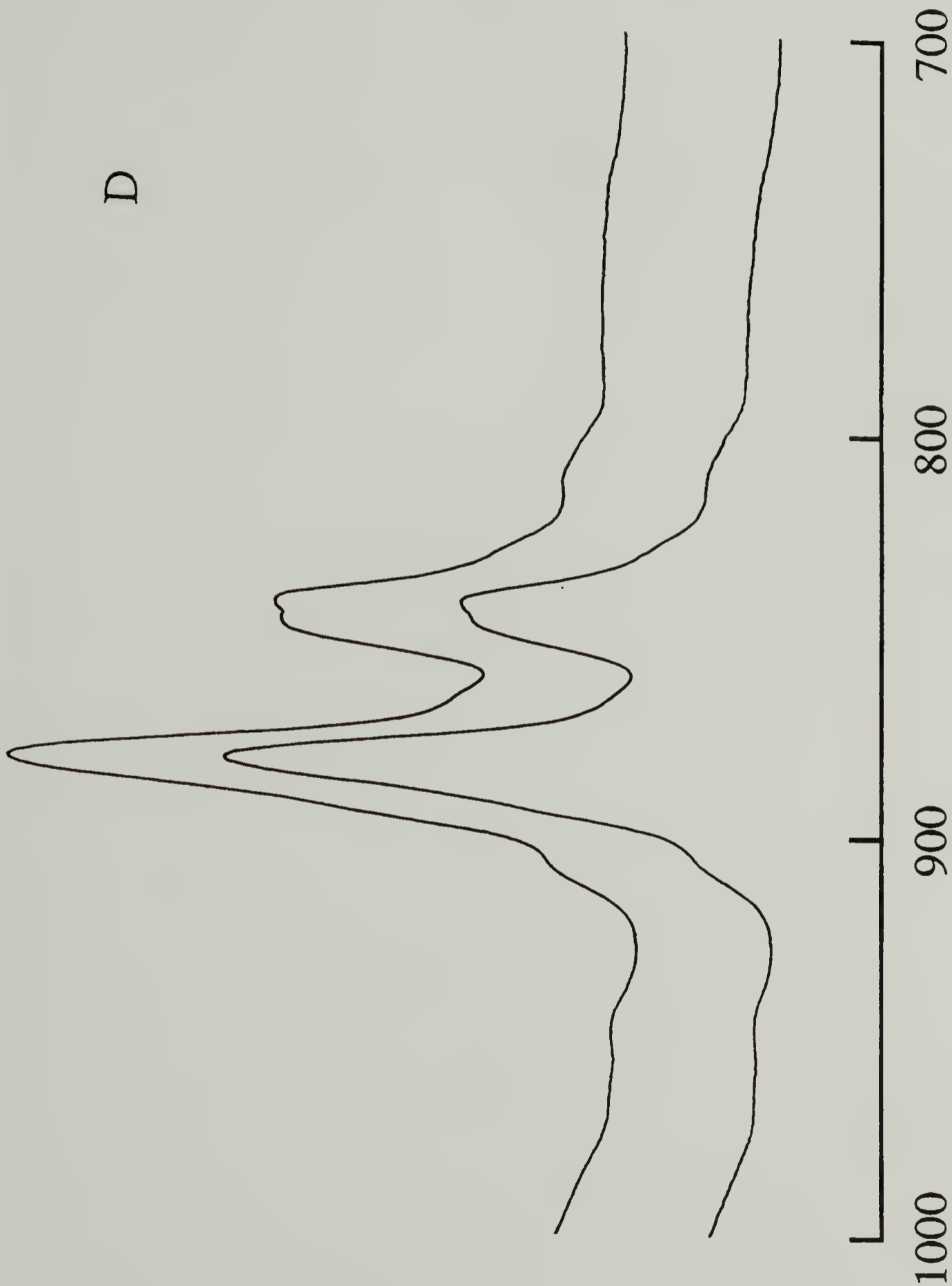


A

Wavenumbers







D

Wavenumbers

Therefore for annealed samples, bands assigned to trans chain conformations or unit cells are seen to rise in intensity while features assigned to gauche structures weaken in intensity. For the PVDF-TrFE copolymer, annealing significantly enhanced the splitting of the doublet in the 850 cm^{-1} region, with an inversion in the relative intensities of the two components, as seen in Figure 2.6a.

Poling Hysteresis

The infrared spectra obtained for the copolymer film in the presence of a cyclic electric field differ significantly as a function of field strength and polarity. Spectral changes measured in the presence of the field are indicative of the conformation and/or chain orientation changes taking place. It should be emphasized that variations in infrared intensity and frequency due to conformation and packing changes must be separated from those due to dipole orientation change relative to the polarization of the incident electric field in order to understand the field induced microstructural change.

The bands listed in Table 2.1 follow the applied electric field quite closely. The 850 cm^{-1} band intensity change with field strength at different temperatures is shown in Figure 2.7. As the electric field is increased, the large CF_2 dipoles have a tendency to align in the field direction, parallel to the propagation direction of the IR beam in the experimental geometry. Thus vibrational modes with transition dipole moment along the CF_2 dipoles show decreased absorbance as the field is increased. Bands assigned to modes with transition moment normal to the CF_2 dipole direction, such as the CF_2 asymmetric stretch, should show an intensity increase with field. Although the two components near 850 cm^{-1} are both perpendicularly polarized, they show different degrees of intensity change in the presence of the electric field as shown in Figure 2.6c. This observation is consistent with the assignment that these two bands are associated with the vibrations of the unit cell and have transition dipole moments at an angle with respect to each other. The 883 cm^{-1} and

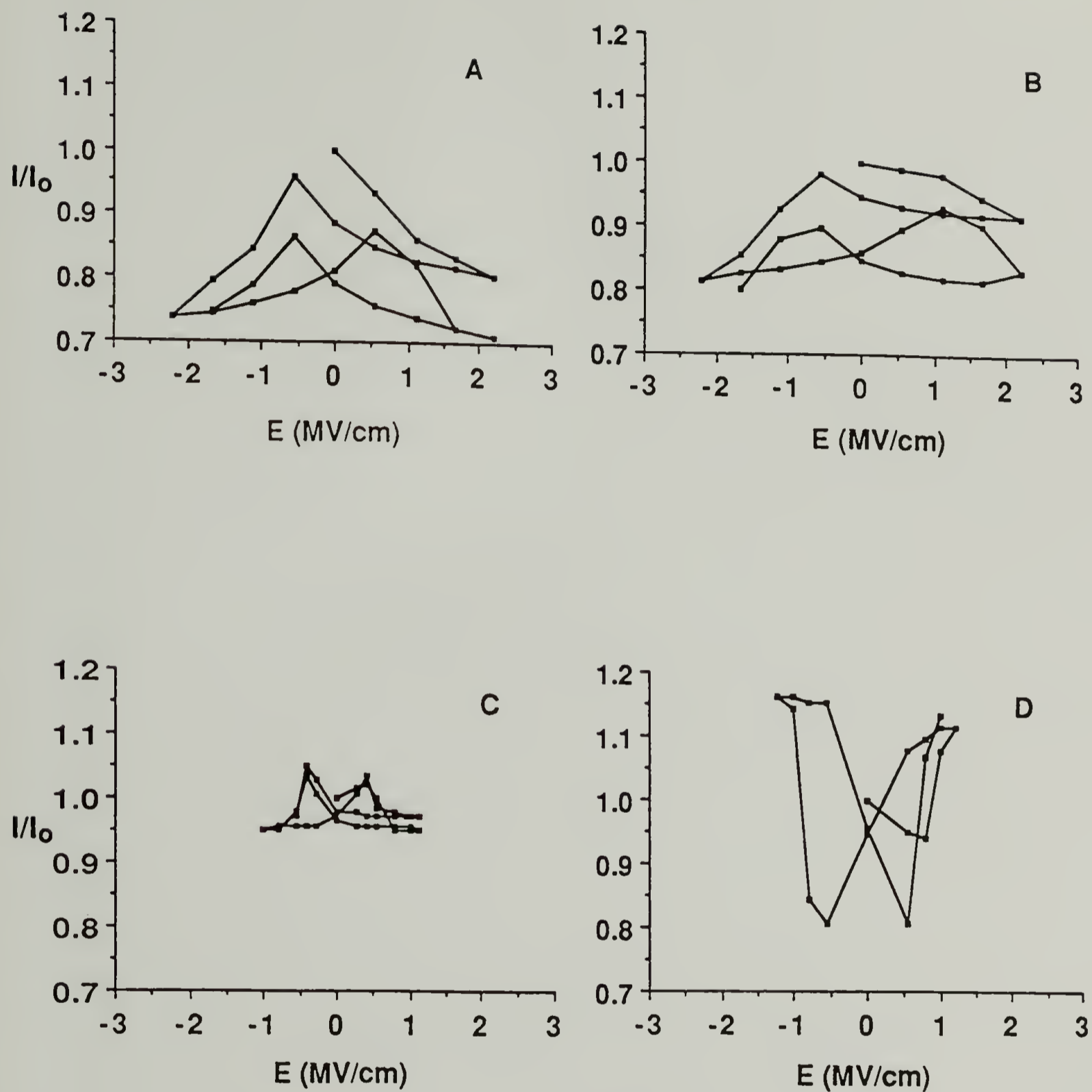


FIGURE 2.7 Intensity change of the 850 cm⁻¹ band as a function of electric field and temperature; (a) 20°; (b) 75°; (c) 94°; (d) 125°C.

850 cm^{-1} bands both exhibit perpendicular polarization. However, as seen from Figure 2.6c, upon poling the 883 cm^{-1} band increases in intensity, while the 850 cm^{-1} band weakens in intensity. The polarization and electric field induced behavior of the 883 cm^{-1} band and the two components of the 850 cm^{-1} band demonstrate that the crystalline units are aligned in the drawing direction and the molecular chains are rotated by the electric field.

Similar to the behavior observed for the 850 cm^{-1} bands, the plot of intensity change with field strength for the 883 cm^{-1} band shown in Figure 2.8 also demonstrates the dipole reorientation following a cyclic field. These observations support the idea that the trans sequences for the copolymer, as for the β phase in PVDF, are the molecular units which give rise to the piezoelectric effect. For PVDF the piezoelectric effect is directly associated with the effective dipole moment for the β unit cell containing two nearly planar zigzag chains. In earlier studies, no evidence was found of coupling to the applied electric field for the α phase, unless the applied field exceeded 2 MV/cm. For the copolymer, virtually all bands follow the changing electric field closely, with the exception of the doublet in the 1350 cm^{-1} region. However it is difficult to conclude that different phases exist and how each would react to the field.

As the electric field strength is reduced back to zero, the infrared band intensity weakens but does not return to its initial value. A negative field must be applied to obtain the initial band intensity. This field, termed the coercive field, should effectively remove the remnant polarization induced by the applied electric field.⁴⁰ This intensity versus electric field plot forms a hysteresis curve and from it permanent structural modifications due to molecular packing and conformation change may be separated from the reversible orientation of dipoles. Thus it is possible to describe structural changes in terms of the volume fraction of different phases only if the residual chain orientation is considered. This can be accomplished by applying the coercive field and measuring the spectrum in the

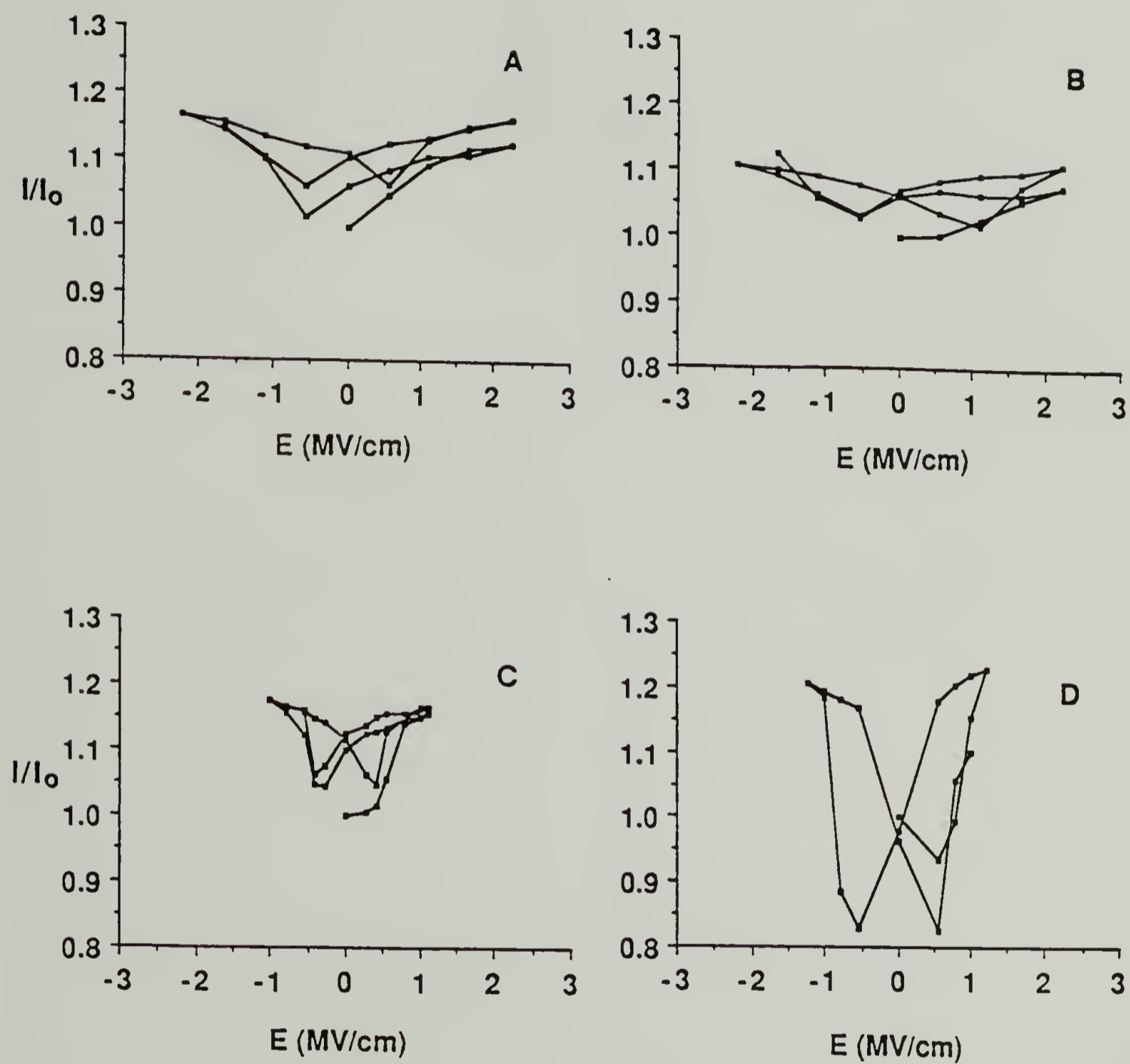


FIGURE 2.8 Intensity change of the 883 cm^{-1} band as a function of electric field and temperature; (a) 20° ; (b) 75° ; (c) 94° ; (d) 125°C .

depolarized state. This technique has been applied to PVDF to monitor the reduction in the volume fraction of the α phase with varying field strength and temperature.^{8,10}

In a previous study on PVDF, the hysteresis cycles did not differ substantially. Over three cycles, changes larger than the signal to noise ratio were not observed unless experiments were carried out at high temperatures. However, a more recent study suggests that the intensity of the trans band increases steadily as a function of cycles.⁴¹ Hysteresis curves for the copolymer show a large change during the first poling cycle, although subsequent cycles are identical, and this can be seen from Figure 2.9.

For the copolymer, the hysteresis curves change significantly as a function of temperature as shown in Figures 2.7 and 2.8. In Figure 2.8 curves at 20°C and 75°C are quite similar, but at 94°C intensity change is observed at a much lower field strength, and at 125°C the intensity change increases dramatically. At this temperature, which is above the 116°C Curie temperature, the 883 cm^{-1} band intensity initially decreases with field strength, then increases as the field strength rises. Upon lowering the field back to zero, the intensity returns very nearly to its initial value. This behavior is in contrast to that seen at 94°C, which is below the Curie transition, where an irreversible intensity increase occurs during the first half cycle.

Similar hysteresis behavior is seen in Figure 2.10 for the 612 cm^{-1} band, which although extremely weak at room temperature shows appreciable intensity at 94°C. As mentioned above, this band is assigned to a TG conformation for a 55/45 copolymer.¹² The fractional intensity change with field is larger than that of the 883 cm^{-1} band, with both bands exhibiting sharp intensity changes at the same field strength. Thus it appears that dipoles in a TG conformation couple to the field as efficiently as those in the trans state, with dipoles in both conformations following the field together.

A considerable amount of structural disordering occurs at the Curie transition. This disordering is thought to be primarily conformational, however dielectric results suggest that thermally activated rotational motions of chain segments in the crystal also play a

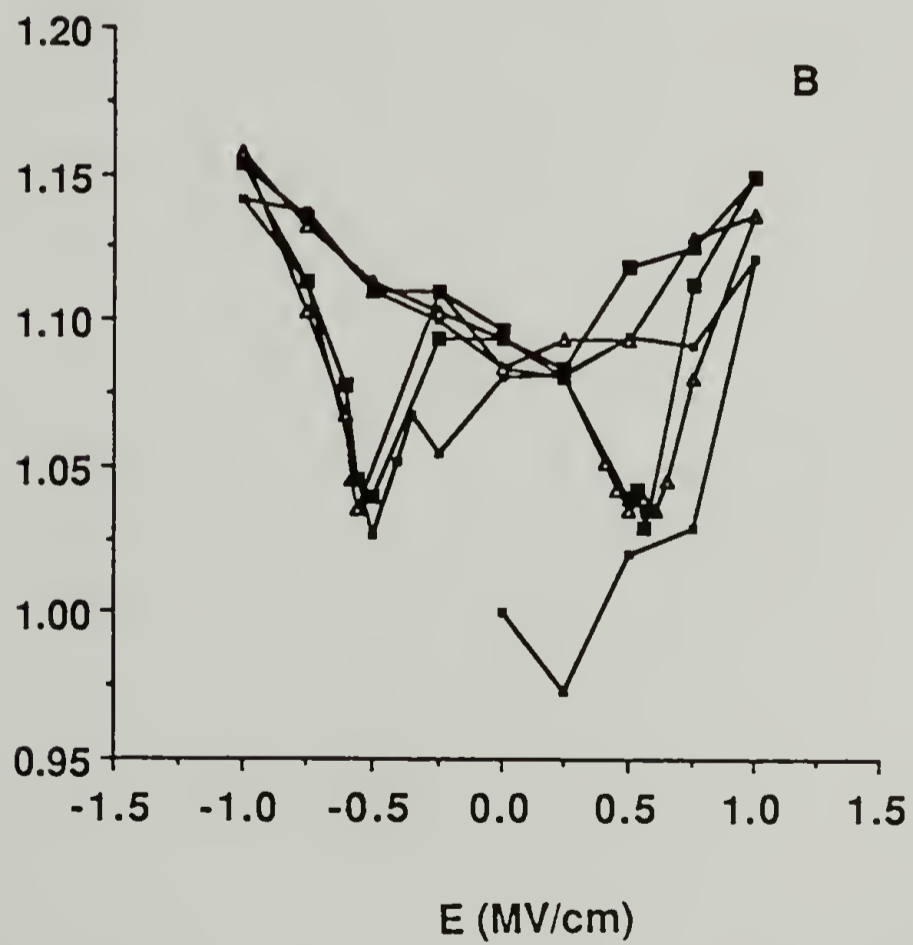
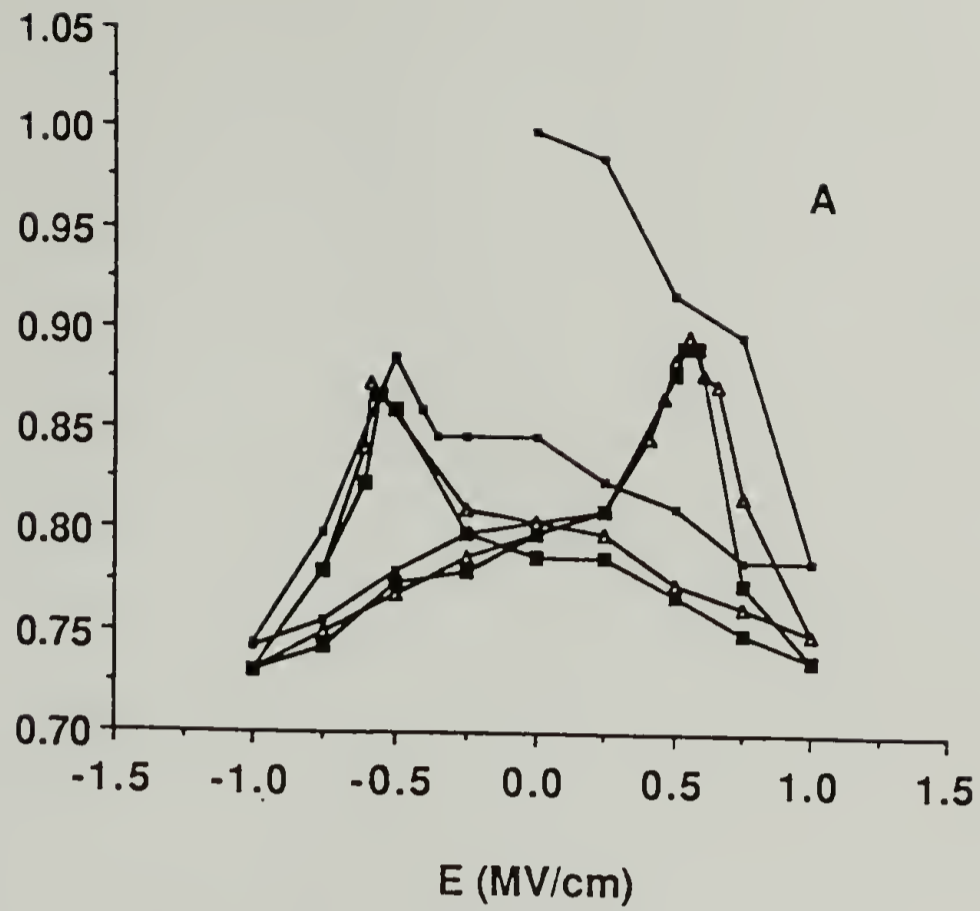


FIGURE 2.9 Intensity change as function of electric field for three poling cycles at room temperature; (a) 850 cm⁻¹; (b) 883 cm⁻¹.

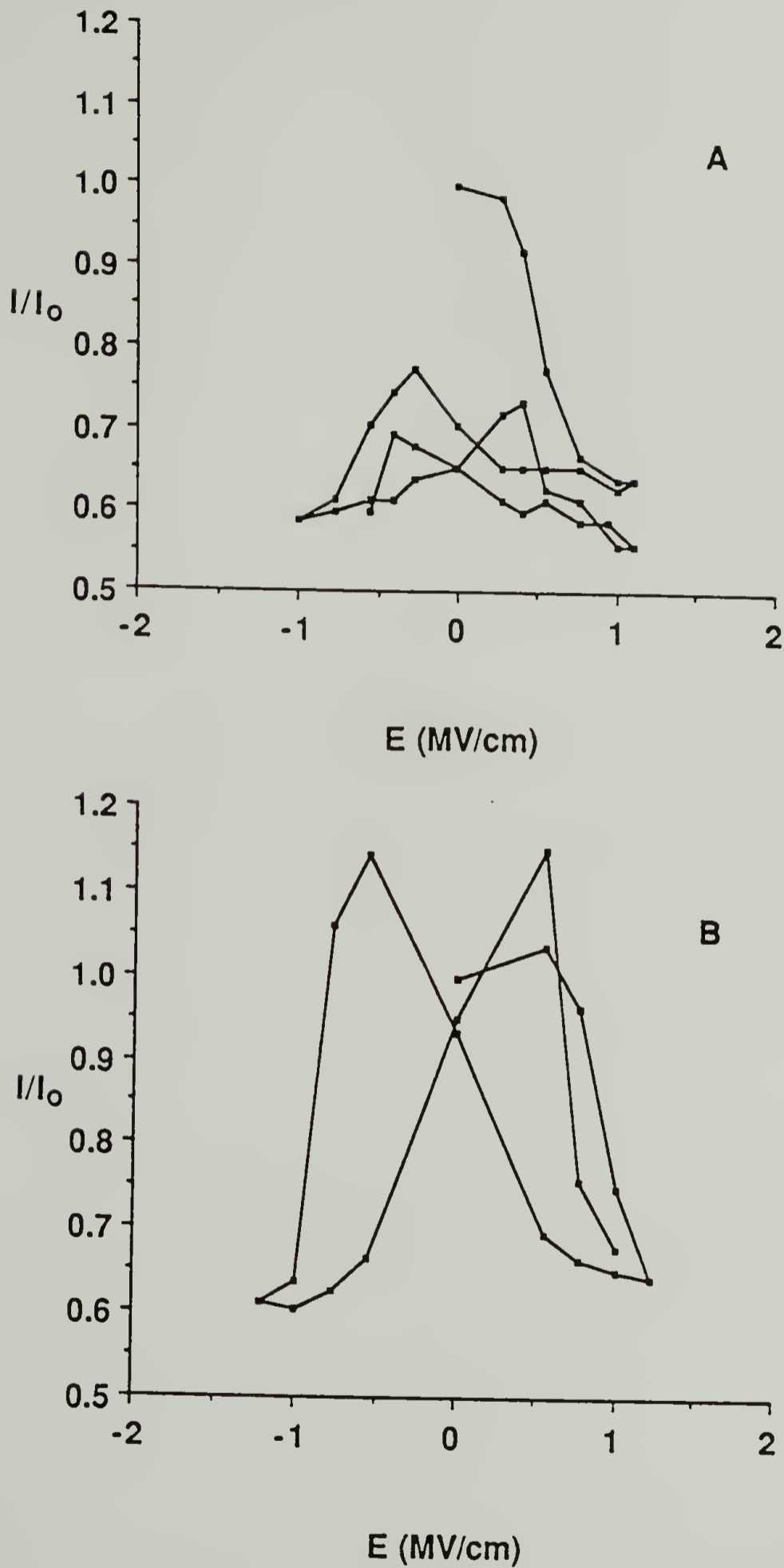


FIGURE 2.10 Intensity change of the 612 cm⁻¹ band as a function of electric field and temperature; (a) 94°; (b) 125°C.

role.¹⁴ Lattice spacings for a 72 mole% copolymer increase linearly with temperature in both the low and high temperature phases.^{14,16,17} The lattice expansion and increased chain mobility found at high temperature allow greater rotational freedom of the chains¹⁶ and reduce intermolecular dipole-dipole interactions.

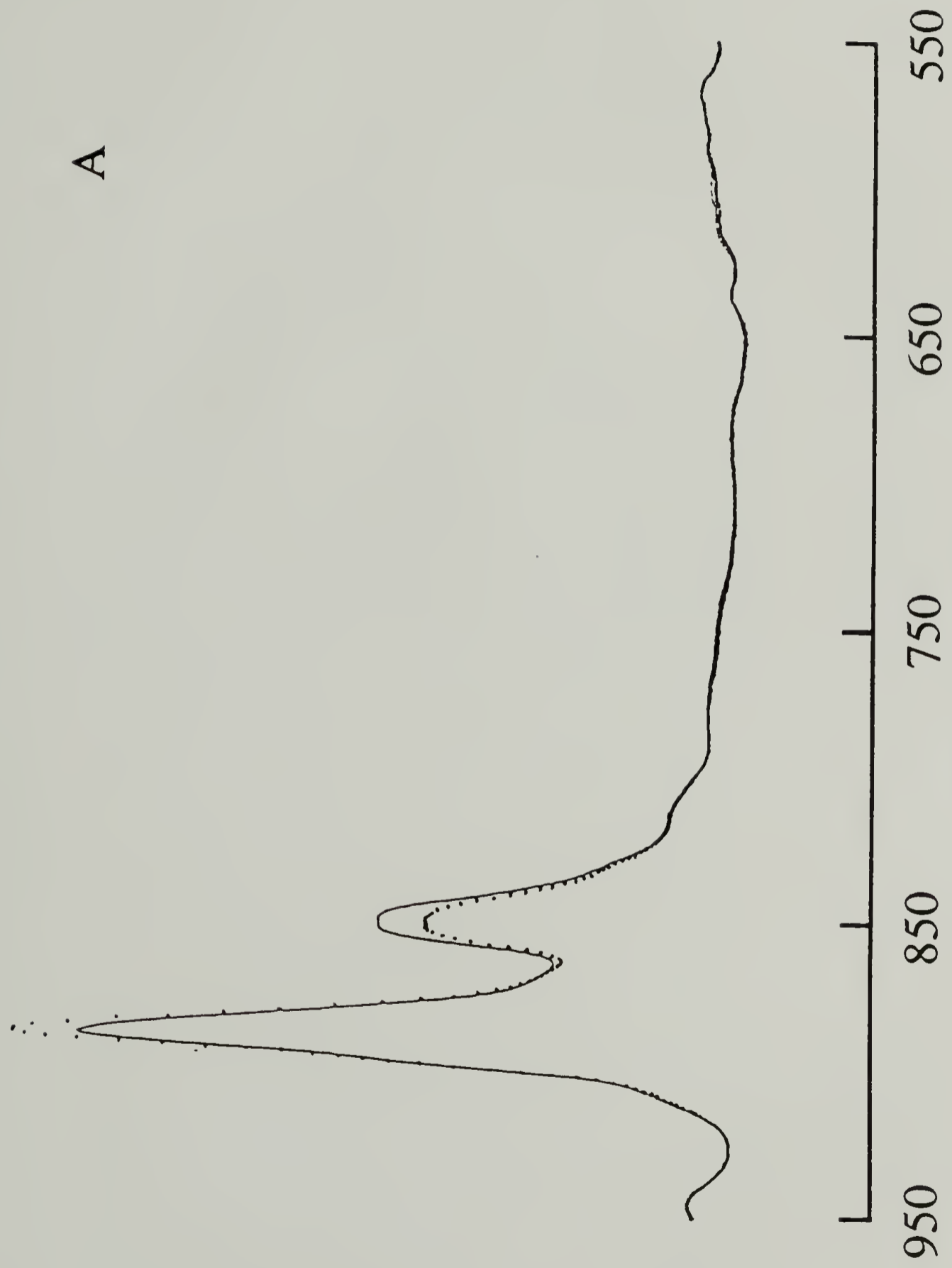
Spectra obtained before and during field application at 25°C and 125°C are shown in Figure 2.11. The larger degree of spectral change observed at high temperature is indicative of the increased mobility found above the Curie temperature. However above this temperature thermal energy removes most of the permanent structural change, so that the infrared intensity returns to near its initial value upon removal of the field, as shown in Figure 2.8. This is analogous to the loss of remnant polarization at the Curie temperature as measured by dielectric displacement hysteresis.³⁷⁻³⁹

A reduction in the coercive field is expected with increasing temperature due to greater chain mobility, and is observed in the D-E hysteresis of a 65/35 copolymer.³⁷ We observe a slight reduction of the coercive field from approximately 0.56 MV/cm at room temperature to 0.42 MV/cm at 94°C. These values are similar to those obtained from D-E hysteresis which measures a macroscopic polarization,^{37,38} while infrared spectroscopy is sensitive to localized dipole reorientation. Thus the agreement in values measured by these different techniques demonstrates the role of dipole orientation as the primary mechanism for polarization in these materials.

Irreversible Structural Change

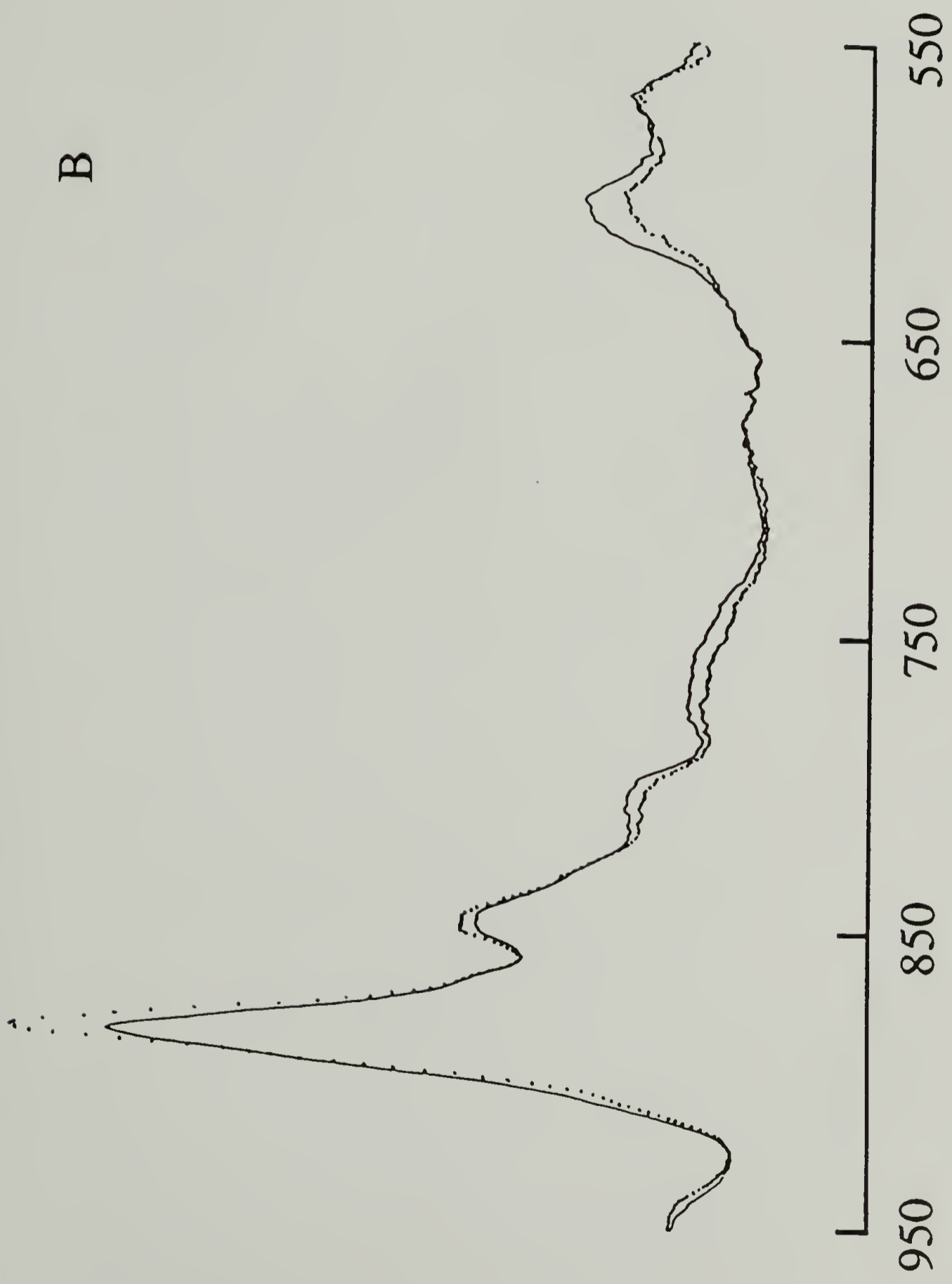
It is well established that piezoelectric activity can be enhanced significantly by the poling process.⁶ It has been shown previously that the structure of PVDF can be changed substantially by the application of an electric field at high temperatures.^{8,10} It is then interesting to compare the effects of an electric field on the chain conformation and packing of the PVDF-TrFE copolymer. Infrared spectra measured before poling and in the

FIGURE 2.11 Infrared spectra of 75/25 PVDF/TrFE obtained before and during the application of an electric field as a function of temperature; (950-550 cm^{-1}); (-) 0.0 MV/cm; (···) 1.0 MV/cm; (a) 20°C; (b) 125°C.



A

Wavenumbers



B

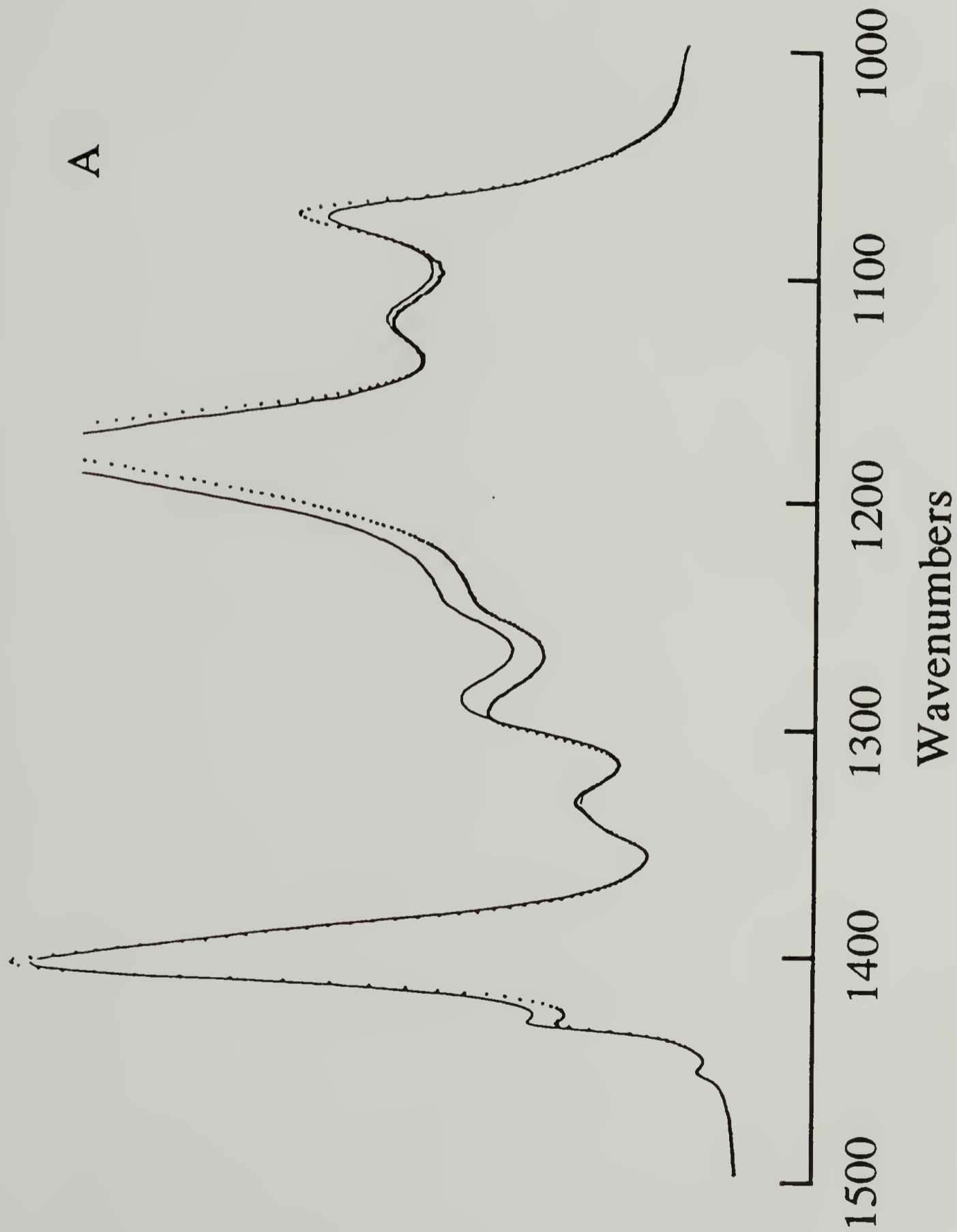
Wavenumbers

depolarized state are shown in Figure 2.12. When the residual polarization or chain orientation is removed by the application of the coercive field, it may be concluded that an irreversible structural change has taken place because the intensities of most of the bands differ in the depoled state as compared to the initial measurement.

As previously discussed, the 850 and 1290 cm^{-1} bands have been assigned to VDF sequences corresponding to sequences of trans isomers at least three or four units long. The intensity decrease for these bands would suggest that there is a reduction in the content of long trans sequences. However these bands along with the 883 cm^{-1} band are also highly sensitive to dipolar orientation. It is more probable that a residual dipole orientation remains even in the depolarized state. The removal of the overall macroscopic polarization does not necessarily imply that the original dipole orientation is regained. It is concluded that the dipolar orientation effect is the dominant factor controlling the field induced intensity change. This is shown from observation of poling uniaxially oriented samples.⁴²

Bands which exhibit polarization parallel to the chain axis such as the 1402 cm^{-1} CH_2 wagging, and 1076 cm^{-1} CC asymmetric stretching vibrations, are less sensitive to dipolar orientation, and are more reliable for determining the degree of conformation change. Spectra of a drawn film with incident polarization parallel to the draw direction before and after electric field application are shown in Figure 2.13. The 1076 cm^{-1} band is known to be related to the trans conformation as seen from annealing studies and results of factor analysis.⁴² This study has also shown the 1120 and 1243 cm^{-1} shoulder bands to be associated with the amorphous phase. The intensity increase after poling for the 1076 cm^{-1} band, as well as the decrease in the 1120 and 1243 cm^{-1} band intensities in Figures 2.11 and 2.12 demonstrate that the amount of trans sequences has increased. Previous x-ray diffraction studies have found no significant structural changes for a 75/25 copolymer upon poling. X-ray diffraction is sensitive to long range order, while infrared spectroscopy is sensitive only to very localized structural changes. Therefore the small increase in the trans isomer content may be too small to be observed by diffraction.

FIGURE 2.12 Infrared spectra of 75/25 PVDF/TrFE as a function of electric field. Spectra are obtained in the depolarized state; (-) 0.0 MV/cm; (....) 2.2 MV/cm; (a) 1500-1000 cm^{-1} ; (b) 1000-400 cm^{-1} .



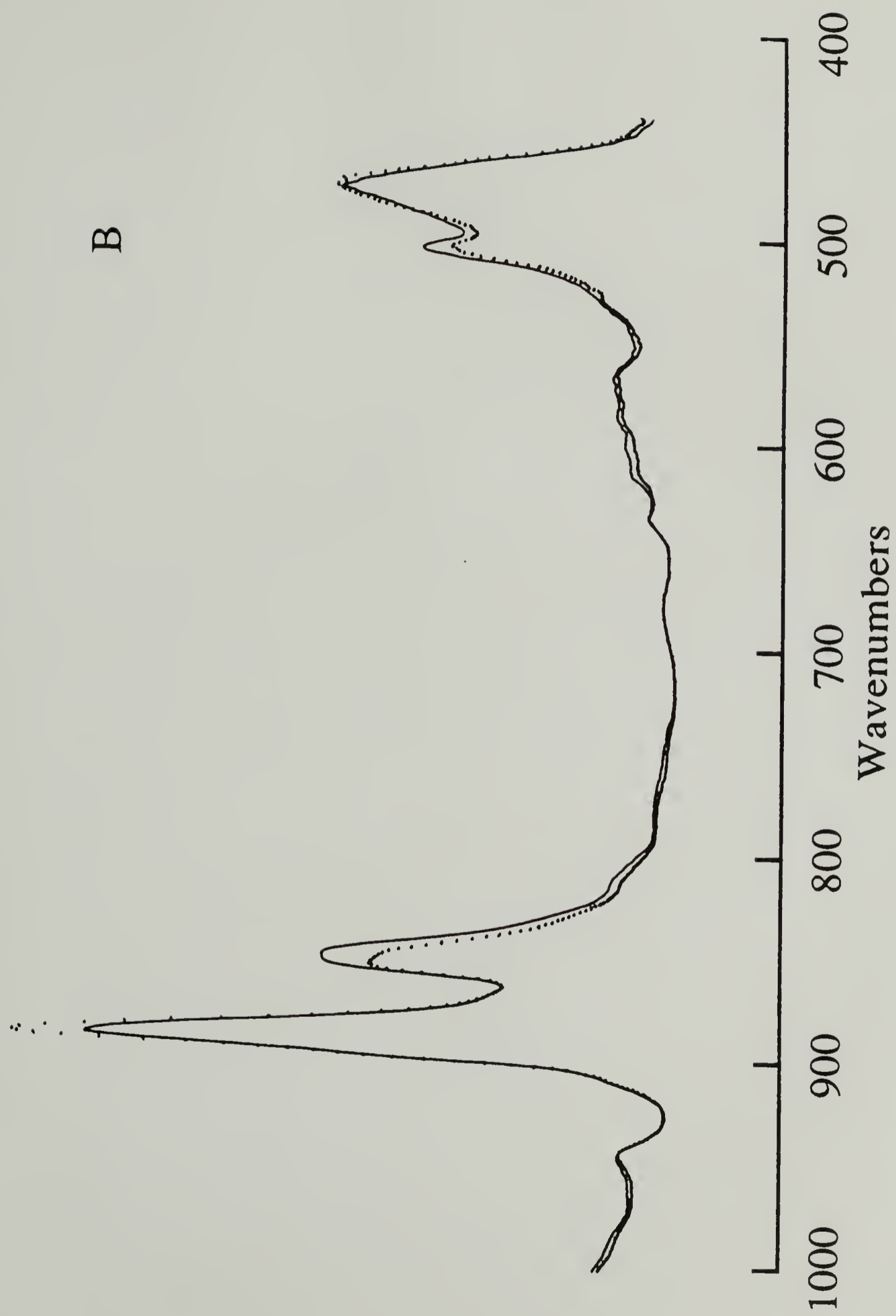
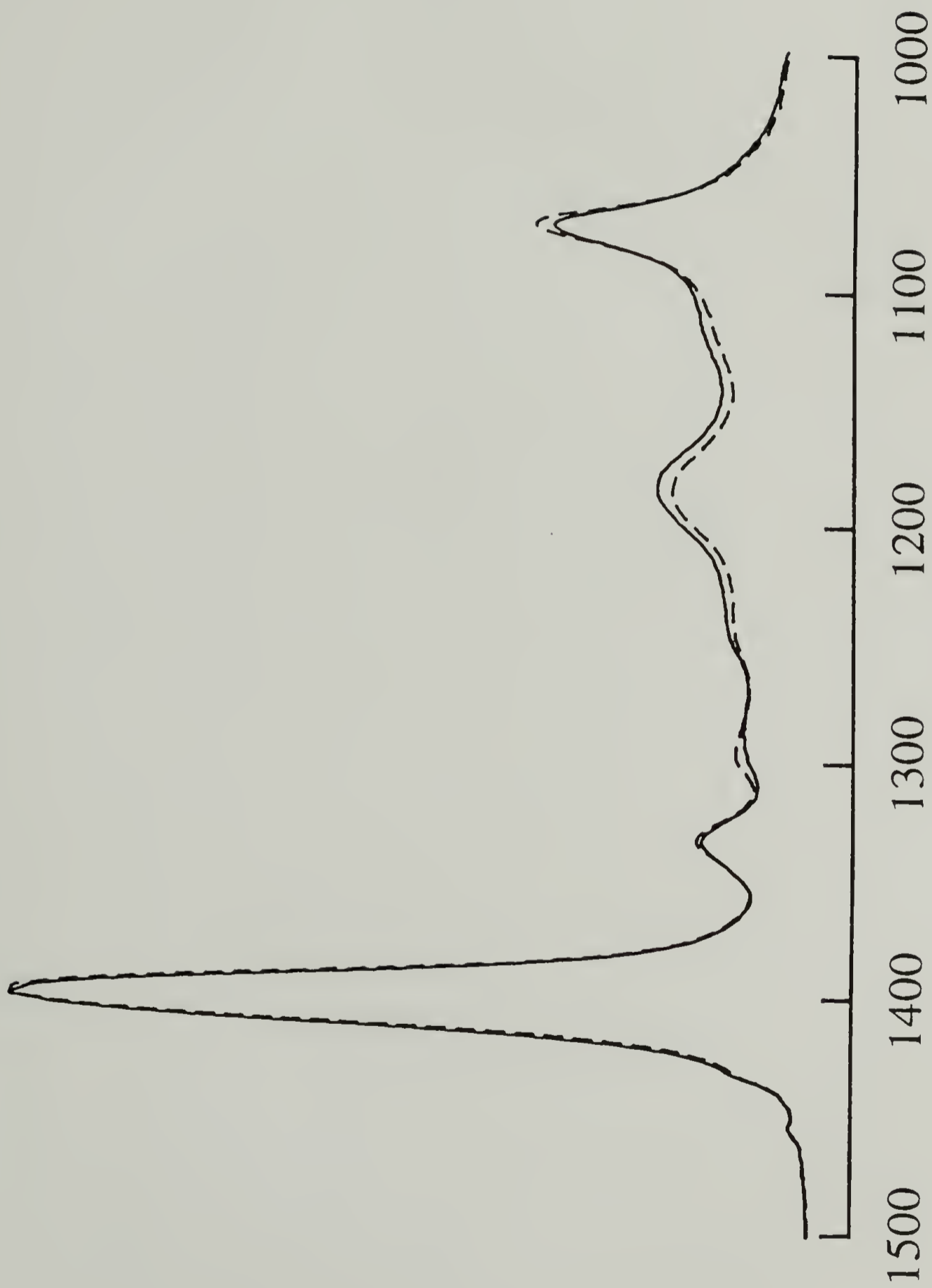


FIGURE 2.13 Parallel polarized infrared spectra of 75/25 VDF/TrFE copolymer film drawn to a draw ratio of 5, and annealed at 135°C; (—) before poling; (- - -) after depoling.



Wavenumbers

The relative contributions of dipolar orientation and conformation sensitivity to the infrared intensity of the 850 and 1290 cm^{-1} bands are observed to change at higher temperature. As seen in Figure 2.7, at 75°C the intensity change is slightly more reversible, and at 94°C the depoled intensity is greater than the initial intensity. Thus the intensity increase due to the increase in trans isomer content outweighs the decrease due to dipolar orientation. This is due to the greater conformation change possible at higher temperature in which the initial state contains greater conformational disorder than found at room temperature.

The increase in trans isomer content must be accompanied by a corresponding decrease in the gauche content. This indeed is confirmed by observing the vibrations sensitive to the gauche conformation found at 612 cm^{-1} and 802 cm^{-1} . The broad band near 612 cm^{-1} appears only weakly at room temperature. A previous study has shown from polarized spectra of drawn films a slight intensity decrease upon poling at room temperature for this weak parallel polarized band.⁴² As shown in Figure 2.11, at 94°C the 612 and 802 cm^{-1} bands show greater intensity due to an increase in gauche conformers. Under the electric field both bands demonstrate the decrease in gauche content. The 612 cm^{-1} band intensity hysteresis plot in Figure 2.10 shows the removal of the TG conformation at 94°C. At 125°C the same reversible behavior is seen as was displayed for the 1290, 883, and 850 cm^{-1} bands. This shows that the TG conformation reappears once the field is removed above the Curie temperature.

Effect of Copolymer Composition

The Curie transition temperature and the crystal structure of PVDF-TrFE copolymers are known to vary greatly with copolymer composition. For copolymers containing up to 65% VDF, three crystal phases have been observed.^{16,17,21} An all trans ferroelectric phase, similar to β phase PVDF, is termed the low temperature phase. Heating above the

Curie transition temperature transforms the low temperature phase to the high temperature paraelectric phase containing conformational disorder and loss of crystalline dipole moment. Cooling below the Curie transition temperature produces the "cooled" phase, which contains trans sequences connected by gauche linkages. Stretching or the application of a high strength electric field transforms the cooled phase to the low temperature phase.^{16,17,21}

Another goal of this study is to compare the effect of varying copolymer composition on the poling behavior. In this study we have examined copolymers containing 75% and 52% VDF. The 52% VDF-48% TrFE copolymer shows a higher degree of disorder due to the increased trifluoroethylene content. It exists at room temperature in the cooled phase, with trans sequences connected by gauche isomers. Being more disordered, it is expected to undergo a higher degree of structural change upon poling, compared to the 75/25 copolymer. This is in fact observed. The hysteresis in the 850 cm^{-1} trans isomer band intensity for both copolymers is shown in Figure 2.14. Upon reversal of the field, the intensity for the 52% VDF copolymer increases from that of the original state. This is due to a larger increase in the trans sequence content which outweighs the intensity decrease due to dipolar orientation. Thus the 52/48 copolymer, which exists in a more disordered state initially, undergoes a larger increase in trans sequence content for the same field strength.

The coercive field is also found to vary with composition. For a hysteresis cycle with a maximum field strength of 1.0 MV/cm , the coercive field was found to be 0.25 MV/cm during the first half poling cycle. This is compared to a value of 0.56 MV/cm for the 75/25 copolymer. This is due to the increased TrFE content, which increases the crystal lattice parameters, such that the steric hindrance for dipole rotation is less and reorientation occurs at a lower field strength. Both of these copolymers show lower coercive field values than those reported for PVDF samples of pure β , or δ phase, or a mixture of the two phases.³⁷ Again this is most likely related to the lattice expansion due to the TrFE units. Upon

FIGURE 2.14 Hysteresis in the 850 cm^{-1} band intensity for VDF-TrFE copolymers containing 75% and 52% VDF.

subsequent cycles it increases to 0.35 MV/cm. The coercive field represents the energy required to reverse the induced dipole orientation, and a higher value implies a more efficient crystalline packing or higher degree of structural order. For PVDF, higher coercive field values have been measured for the deuterated polymer, and this is thought to be related to the improved crystalline order due to a reduction in the amount of chain branching.⁴³ The increased coercive field measured for the 52% VDF copolymer after the first half poling cycle indicates such an increase in crystalline order with poling, and must be related to the increase in the trans isomer content.

Conclusions

The response of a 75 mole% VDF-25 mole% TrFE and a 52 mole% VDF-42 mole% TrFE copolymer to a high strength electric field has been studied by vibrational spectroscopy. Spectra obtained at different temperatures exhibit conformation sensitive bands which characterize the field induced microstructural change. For the 75% VDF copolymer, nearly all vibrational bands are sensitive to the applied field, suggesting that the trans β phase is the predominant structure. Vibrational assignments have been clarified by examining the effects of temperature, annealing, orientation, and electric field on the infrared spectrum. A band at 850 cm^{-1} is found to be sensitive to intermolecular interactions based on its two components which are more clearly resolved at low temperature and upon annealing. The polarization of these two components and their relative intensity changes seen upon poling suggest that the crystalline units are aligned in the draw direction and the chains within are rotated by the electric field. A cyclic electric field is applied in order to separate the orientation of dipoles from irreversible structural changes. This produces a hysteresis in the infrared intensity and the shape of the hysteresis changes significantly as a function of temperature. Values of the coercive field necessary to remove dipolar orientation are similar to those measured by dielectric displacement hysteresis, which measures a macroscopic polarization. Therefore dipolar orientation is the primary mechanism for polarization in these materials.

Bands assigned to both trans and gauche conformations are sensitive to the applied field, indicating that dipoles in both conformations couple to the field. Hysteresis curves show irreversible intensity changes when the field is applied below the Curie temperature, but nearly reversible behavior above this temperature. Here greater intensity changes are observed during poling and result from the increased dipole mobility found above the Curie temperature. The reversible intensity behavior above the Curie temperature when the field

is removed is analogous to the loss of remnant polarization measured at this temperature by dielectric displacement hysteresis.

The 1290 and 850 cm^{-1} bands, associated with trans sequences, show an intensity decrease after depolarization. However, these bands are highly sensitive to dipolar orientation as well as conformation. Residual dipolar orientation is present although the film is macroscopically depolarized, and therefore these intensity changes are not reliable indicators of irreversible structural change. Intensity increases in bands which are less sensitive to dipolar orientation show that room temperature poling produces a slight increase in long trans sequences. At higher temperatures intensity increases are related to a greater increase in long trans sequence content as the conformation change outweighs the effects of dipole orientation.

Poling behavior is observed as a function of copolymer composition. For the 52% VDF copolymer, bands associated with long trans sequences at 850 and 1290 cm^{-1} show intensity increases upon reversal of the electric field. This is because this material exists in a more disordered state initially with more gauche defects, so that the larger increase in trans content outweighs the effects of dipolar orientation. This material is observed to have a smaller coercive field value, as the larger crystal lattice reduces the degree of steric hindrance to dipole rotation under the field. The coercive field increases slightly after the first half poling cycle due to the increase in structural regularity and crystalline order which is induced upon poling.

References

1. Lovinger, A. J. *Science* **1983**, 220, 1116.
2. Date, M.; Takashita, S.; Fukada, E. *J. Polym. Sci., Part A-2* **1970**, 8, 61.
3. Miyata, S.; Yoshikawa, M.; Tasaka, S.; Ko, M. *Polymer J.* **1980**, 12, 857.
4. Maruyama, Y.; Sung, J. Y.; Inoue, Y.; Chujo, R.; Tasaka, S.; Miyata, S. *Polymer* **1987**, 28, 1087.
5. Litt, M. H.; Hsu, C.; Basu, P. *J. Appl. Phys.* **1977**, 48, 2208.
6. Lovinger, A. J.; *Developments in Crystalline Polymers*; Bassett, D.C., Ed.; Applied Science Publishers: Essex, UK, 1982; p 195.
7. Davis, G. T.; McKinney, J. E.; Broadhurst, M. G.; Roth, S. C. *J. Appl. Phys.* **1978**, 49, 4998.
8. Lu, F. J.; Waldman, D. A.; Hsu, S. L. *J. Polym. Sci., Polym. Phys. Ed.* **1984**, 22, 827.
9. Lu, F. J.; Hsu, S.L. *Polymer* **1984**, 25, 1247.
10. Hsu, S. L.; Lu, F. J.; Waldman, D. A.; Muthukumar, M. *Macromolecules* **1985**, 18, 2583.
11. Yagi, T.; Tatemoto, M.; Sako, J. *Polymer J.* **1980**, 12, 209.
12. Tashiro, K.; Takano, K.; Kobayashi, M.; Chatani, Y.; Tadokoro, H. *Polymer* **1981**, 22, 1312.
13. Lovinger, A. J.; Davis, G. T.; Broadhurst, M. G. *Macromolecules* **1982**, 15, 323.
14. Davis, G. T.; Furukawa, T.; Lovinger, A. J.; Broadhurst, M. G. *Macromolecules* **1982**, 15, 329.
15. Lovinger, A. J.; Furukawa, T.; Davis, G. T.; Broadhurst, M. G. *Polymer* **1983**, 24, 1233.
16. Tashiro, K.; Takano, K.; Kobayashi, M.; Chatani, Y.; Tadokoro, H. *Polymer* **1984**, 25, 195.
17. Tashiro, K.; Takano, K.; Kobayashi, M.; Chatani, Y.; Tadokoro, H.; *Ferroelectrics* **1984**, 57, 297.
18. Dvey-Aharon, H.; Sluckin, T. J.; Taylor, P. L.; Hopfinger, A. J. *Physical Review B* **1980**, 21, 3700.
19. Furukawa, T.; Date, M.; Ohuchi, M.; Chiba, A. *J. Appl. Phys.* **1984**, 56, 1481.
20. Reneker, D. H.; Mazur, J. *Polymer* **1985**, 26, 821.

21. Tashiro, K.; Kobayashi, M. *Polymer* **1986**, 27, 667.
22. Guy, I. L.; Unsworth J. *Appl. Phys. Lett.* **1988**, 52, 532.
23. Green, J. S.; Farmer, B. L.; Rabolt, J. F. *J. Appl. Phys.* **1986**, 60, 2690.
24. Stack, G. M.; Ting, R. Y. *J. Polym. Sci., Polym. Phys. Ed.* **1988**, 26, 55.
25. Green J. S.; Rabe, J. P.; Rabolt, J. F. *Macromolecules* **1986**, 19, 1725.
26. Tashiro, K; Kobayashi, M. *Polymer* **1988**, 29, 426.
27. Liang, C. Y.; Krimm, S. *J. Chem. Phys.* **1956**, 25, 563.
28. Moynihan, R. E. *J. Am. Chem. Soc.* **1959**, 81, 1045.
29. Brown, R. G. *J. Chem. Phys.* **1964**, 40, 2900.
30. Hannon, M. J.; Boerio, F. J.; Koenig, J. L. *J. Chem. Phys.* **1969**, 50, 2829.
31. Masetti, G.; Cabassi, F.; Morelli, G.; Zerbi, G. *Macromolecules* **1973**, 6, 700.
32. Boerio, F. J.; Koenig, J. L. *J. Polym. Sci., Part A-2* **1971**, 9, 1517.
33. Cessac, G. L.; Curro, J. G. *J. Polym. Sci., Polym. Phys. Ed.* **1974**, 12, 695.
34. Kobayashi, M.; Tashiro, K; Tadokoro, H. *Macromolecules* **1975**, 8, 158.
35. Tashiro, K.; Itoh, Y.; Kobayashi, M.; Tadokoro, H. *Macromolecules* **1985**, 18, 2600.
36. Lauchlan, L.; Rabolt, J. F. *Macromolecules* **1986**, 19, 1049.
37. Davis, G. T.; Broadhurst, M. G.; Lovinger, A. J.; Furukawa, T. *Ferroelectrics* **1984**, 57, 73.
38. Furukawa, T.; Date, M.; Fukada, E.; Tajitsu, Y.; Chiba, A. *Jpn. J. Appl. Phys.* **1980**, 19, L109.
39. Yamada, T.; Ueda, T.; Kitayama, T. *J. Appl. Phys.* **1981**, 52, 948.
40. Lines, M. E.; Glass, A. M.; *Principles and Applications of Ferroelectrics and Related Materials*; Clarendon Press: Oxford, 1977; p 103.
41. Guy, I. L.; Unsworth, J. *J. Appl. Phys.* **1987**, 61, 5374.
42. Kim, K. J.; Reynolds, N. M.; Hsu, S. L. submitted to *Macromolecules*.
43. Takase, Y.; Tanaka, H.; Wang, T. T.; Cais, R. E.; Kometani, J. M; *Macromolecules* **1987**, 20, 2318.

CHAPTER III

INFRARED STUDIES OF HIGHLY ORIENTED PVDF AND BLENDS WITH PMMA

Introduction

As stated in the last chapter, PVDF may crystallize into at least five different crystalline phases, with the most common one being the α phase crystallized at high degrees of supercooling.¹ The piezoelectric β phase usually can only be obtained at low degrees of supercooling, or upon deformation or application of an electric field.^{1,2} This chapter will deal with blends of PVDF with PMMA, in which the PMMA effects the phase contents and crystallization behavior of PVDF.

Blends of PVDF with poly(methyl methacrylate) (PMMA) are known to be miscible in the molten phase.³⁻¹² Crystallization of PVDF occurs for blends containing greater than approximately 30% PVDF. From melting point depression measurements, an interaction parameter of -0.3 at 160°C has been determined, indicating a strong enthalpic interaction between the components.⁴ It is known that the relative amounts of the α and β phases of PVDF, and the size and orientation of different crystallites all vary significantly with the blend composition and crystallization conditions.¹³⁻¹⁵ Pure β phase PVDF, however, is difficult to obtain unless the samples are crystallized under unusual conditions, such as under high pressure, on external substrates, or in the presence of a high external electrical field.^{2,16} In previous studies, it has been demonstrated that the β phase of PVDF can be successfully obtained when crystallized in a high longitudinal flow gradient.^{15,17-19} For blends of PVDF with PMMA, the β phase content is increased under these conditions.¹⁵ This is thought to occur due to the decrease in the crystallization temperature which occurs upon blending, such that the β phase can nucleate and grow more rapidly.¹⁴

When transition dipole moments of individual vibrations are well defined, infrared dichroism measurements provide a measure of the overall chain orientation. By comparing the dichroic behavior of bands assigned to each of the two polymers we can determine the orientation of both crystalline and amorphous components. The phase content, morphology, and chain orientation of PVDF are monitored with blend composition. The effects of annealing on these factors are also examined.

Experimental

PVDF samples were obtained from the Daikin Kogyo Corporation, Japan and the PMMA ($M_n = 60,000$; $M_w = 120,000$) was Plexiglas-Formmasse 8N supplied by Rohm GmbH, West Germany. Both components were dissolved in the appropriate weight fractions (100/0, 80/20, 60/40 and 50/50 PVDF/PMMA) in a common solvent (cyclohexanone). Extremely thin films approximately 100 nm thick were prepared according to the method of Petermann and Gohil, which provides a high extensional flow gradient during crystallization and large supercooling.²⁰ A schematic diagram illustrating this technique is shown in Figure 3.1. The melt draw temperatures for the various compositions were 150, 141, 131, and 125° C, respectively. Polarized infrared spectra were obtained with a Bruker IFS 113v FTIR. Samples ten layers thick were used for infrared and thermal analysis. These films were obtained by wrapping the film around the glass slide during drawing. Free standing films were obtained by floating the films onto water from the glass substrate. A wire-grid polarizer was used to obtain polarized radiation. For such thin films, generally 1000 scans at 2 cm⁻¹ resolution were collected in order to obtain high signal-to-noise ratio.

Samples were annealed under tension between 100 and 110°C for 10 minutes. This temperature range is below the onset of premelting, as determined by a differential scanning calorimeter operating at a heating rate of 10° C/min.

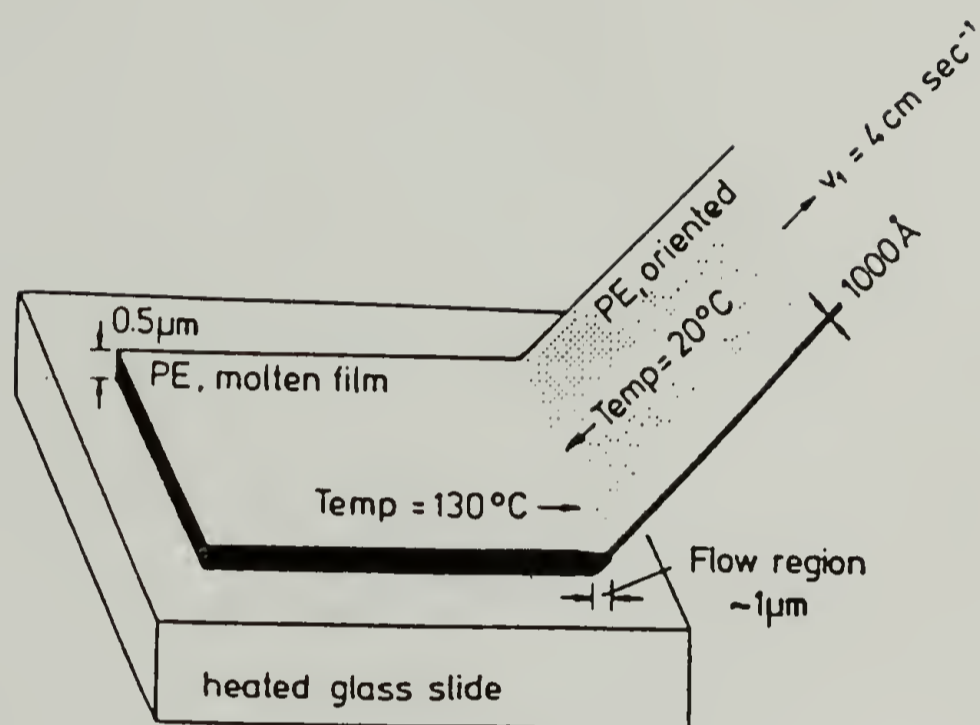


FIGURE 3.1 Schematic diagram illustrating the preparation of highly oriented melt drawn films. (from ref. 20)

Results and Discussion

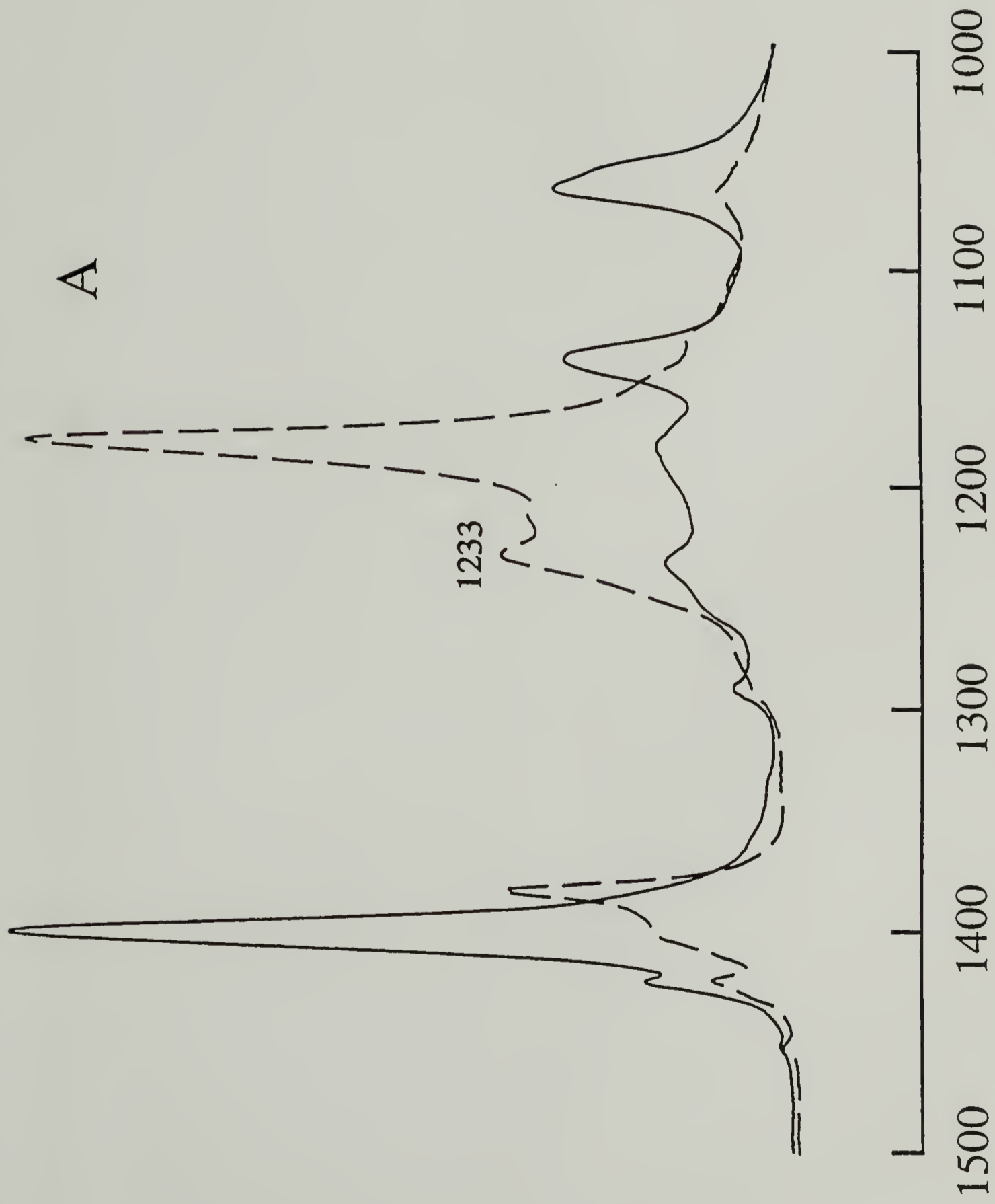
Electron microscopic and electron diffraction studies have shown a transformation from a lamellar morphology pure PVDF, to a mixed morphology containing lamellar and needle-like crystals in the 80% PVDF/ 20% PMMA blend, and then into a pure needle-like morphology in the 60% PVDF/ 40% PMMA blend.^{15,19} From these studies a qualitative picture of the molecular orientation associated with the PVDF crystals can be estimated from the angular misorientation of diffraction spots. For both compositions, the PVDF crystals have been found to be aligned nearly perfectly with their molecular axis parallel to the drawing direction. As we will demonstrate, infrared data will show PMMA and PVDF chains to be oriented.

Electron diffraction studies have shown that such highly drawn films of PVDF are predominantly α phase, with only very little β phase, and no γ phase present. It has been established by the electron diffraction and infrared results of Thomas and Yang that the β content in the sample increases with increasing PMMA content up to a concentration of 70% PVDF/ 30% PMMA.¹⁵

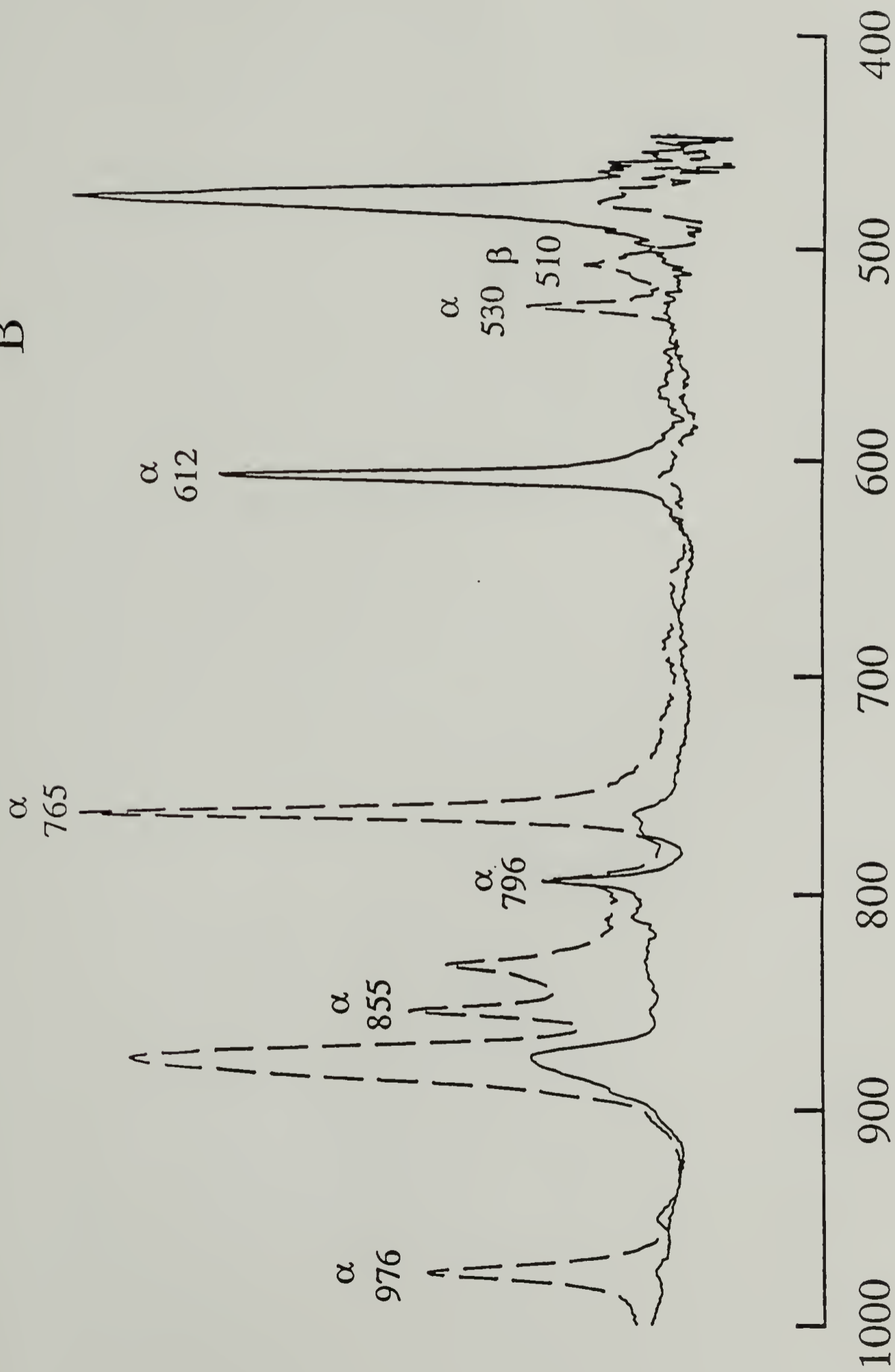
These qualitative results concerning overall molecular orientation and the phase contents can be considerably improved with quantitative infrared measurements, since additional information about local chain conformations, orientation of the amorphous PVDF and PMMA, and the relative amounts of the crystal phases can all be obtained. Preliminary infrared analysis has been performed on PVDF/PMMA blends to monitor the amount of β phase with blend composition and deformation.¹⁵ Polarized infrared spectra of the melt drawn PVDF and 80% PVDF/20% PMMA blend are shown in Figures 3.2a,b and 3.3a,b, respectively. In Figure 3.4a,b,c are shown polarized spectra for the 50/50 blend before and after annealing at 100° C.

From the spectra in Figure 3.2 it is clear that the PVDF film is very highly oriented. This is demonstrated by several bands such as the 976 cm^{-1} α phase band which appears

FIGURE 3.2 Polarized infrared spectra of drawn PVDF film; (a) 1500-1000 cm^{-1} region; (b) 1000-400 cm^{-1} region; (····) perpendicular polarization; (—) parallel polarization.



B



Wavenumbers

FIGURE 3.3 Polarized infrared spectra of 80% PVDF/ 20% PMMA blend; (a) 1800-1000 cm^{-1} region; (b) 1000-400 cm^{-1} region; (—) perpendicular polarization; (—) parallel polarization.

A



B

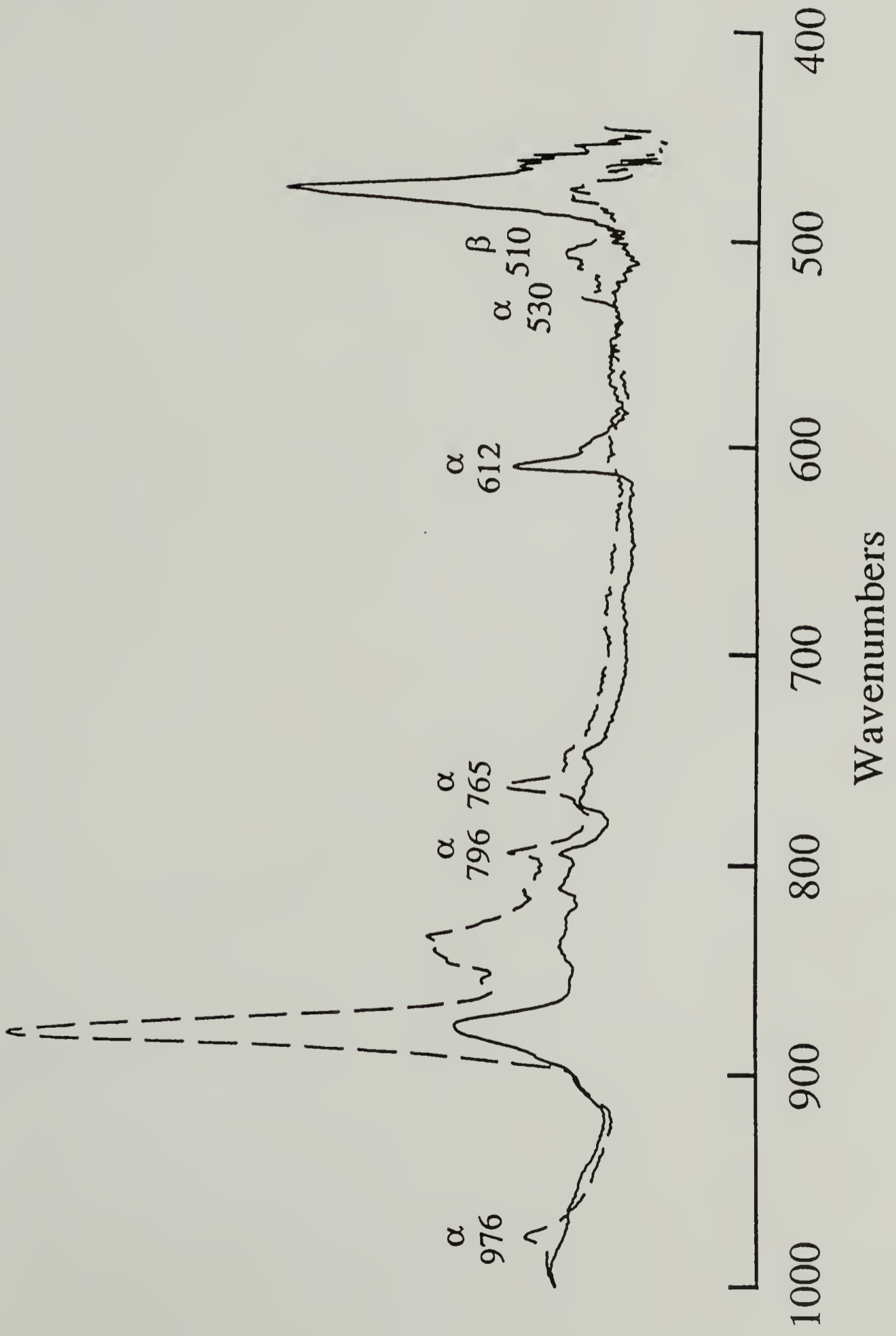
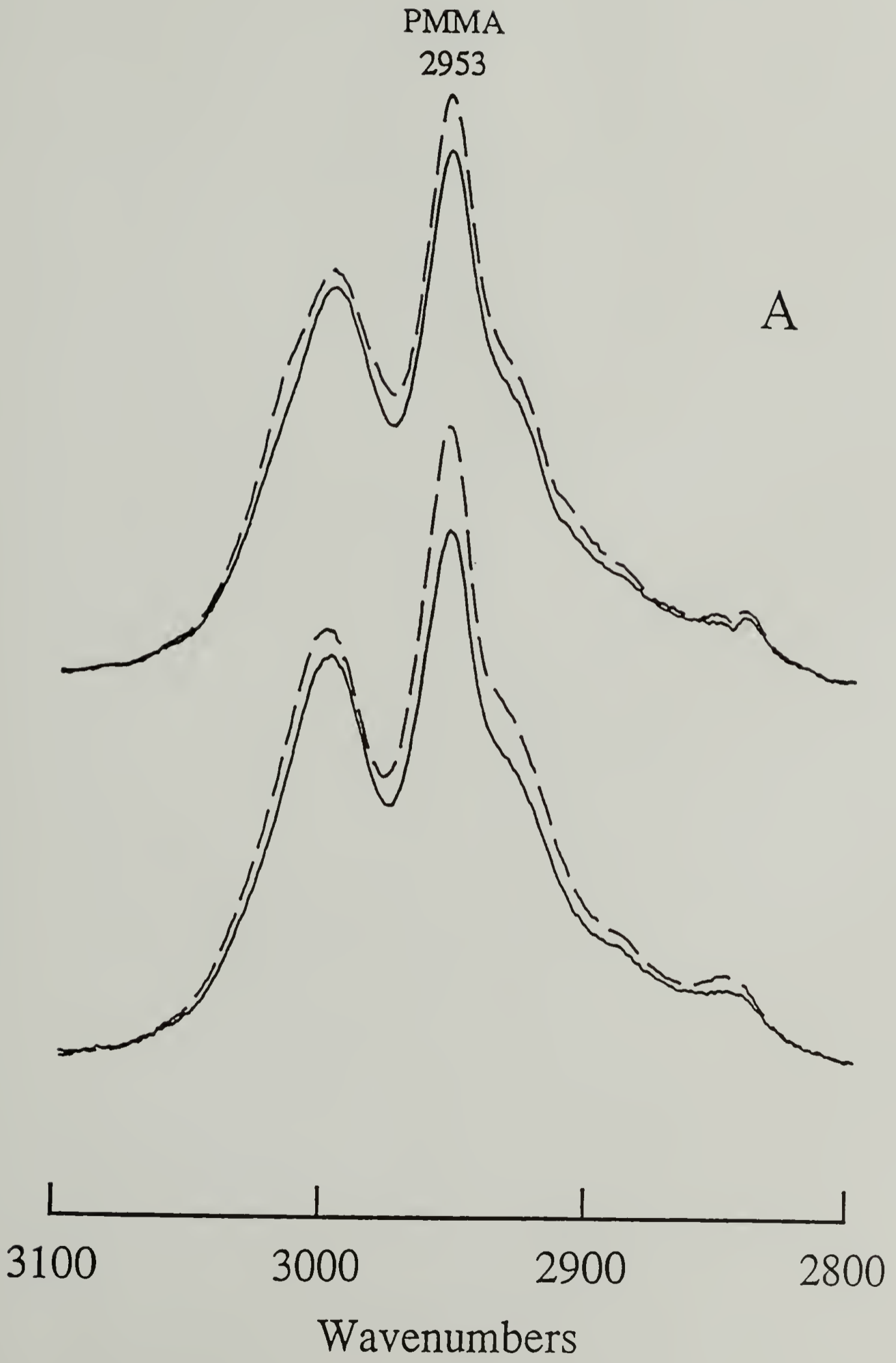


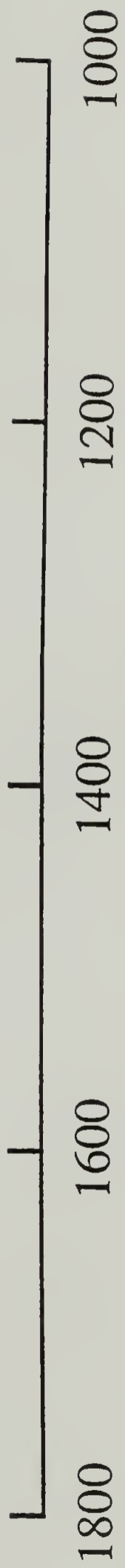
FIGURE 3.4 Polarized infrared spectra of 50% PVDF/50% PMMA blend; (a) 3100-2800 cm^{-1} region; (b) 1800-1000 cm^{-1} region; (c) 1000-400 cm^{-1} region; (....) perpendicular polarization; (—) parallel polarization; (bottom) as drawn; (top) after annealing at 100°C.



PMMA
1727

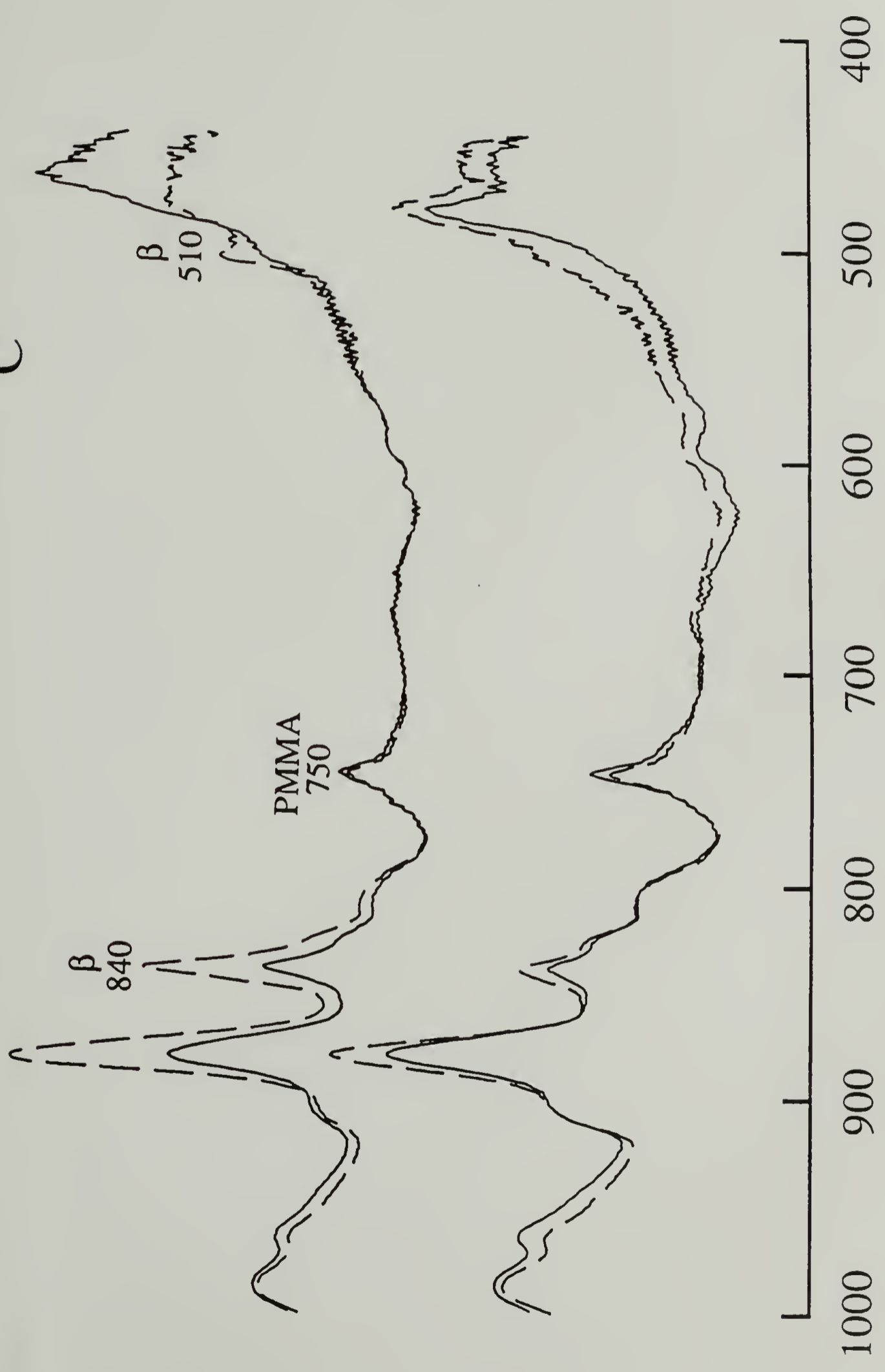
β
B 1177

1403



Wavenumbers

C



Wavenumbers

strongly with perpendicular polarization and is nearly extinct in the parallel polarized spectrum. This sample shows a remarkably high degree of orientation. The relative amounts of the α and β phases can be determined from the relative intensities of the 510 cm^{-1} (β or γ) and 530 cm^{-1} (α) bands, as has been performed in earlier studies.^{15,21} These bands have been assigned to the CF_2 bending mode for the two phases,²² and assuming that they have equivalent extinction coefficients, as done previously,²¹ allows us to calculate the α phase content to be 62%. A list of bands analyzed along with assignments, measured dichroic ratios, and calculated transition dipole moment angles for PVDF is given in Table 3.1.

Table 3.1 Calculated transition dipole moment directions for melt drawn PVDF.

	wavenumber ($A_{ }/A_{\perp}$)	dichroic ratio	transition moment angle		PED (ref.22)
			f=1	f=0.95	
α	976 \perp	0.044	82°	86°	CH_2 t (82%)
	855 \perp	0.140	75°	77°	CH_2 r (48%)
	796 $ $	0.988	55°	55°	CH_2 r (78%)
	765 \perp	0.096	78°	80°	$\text{CF}_2\delta$ (33%) $\text{CCC}\delta$ (21%)
	612 $ $	14.307	21°	18°	$\text{CF}_2\delta$ (24%) $\text{CCC}\delta$ (19%)
	530 \perp	0.0	90°	-	CF_2 δ (52%)
β	835 \perp	0.15	73°	75°	CF_2 r(60%) CF_2 v _a (31%)

Calculation of Transition Dipole Moments for PVDF

A perpendicular polarized band is observed at 1233 cm^{-1} and has been found by Kobayashi et al. to be associated with amorphous regions.²² The strong perpendicular polarization observed for this band therefore suggests that the amorphous regions of PVDF are also oriented in this material.

Due to the extremely high degree of orientation of the PVDF film as determined by electron diffraction and polarized infrared spectra, we can calculate the direction of transition dipole moments with respect to the chain axis with an initial assumption of perfect orientation. The second moment of the orientation function is described by the following relationship

$$f = (R_0 + 2) (R - 1) / (R_0 - 1) (R_0 + 2) \quad (3.1)$$

where R is the dichroic ratio $A_{\parallel} / A_{\perp}$, and R_0 is the dichroic ratio for a perfectly oriented sample calculated from

$$R_0 = 2 \cot^2 \alpha \quad (3.2)$$

where α is the angle between the transition dipole moment and the chain axis. For the 976 cm^{-1} band, a chain orientation function value of 0.936 is the lowest from which a positive R_0 value may be determined. This then gives us a lower limit for the degree of chain orientation. The effect of infrared beam divergence and the possibility of misalignment of the film layers are factors which would only reduce the observed dichroism. Therefore we conclude that within experimental error the second moment of the orientation function is greater than 0.94.

In Table 3.1 are given the experimentally measured transition dipole moment angles for several bands. Knowledge of these is useful as these may be compared to values determined from normal vibrational analysis and can be used to determine the validity of the force constant sets used in these calculations. It is also useful as infrared intensities have been used to measure the degree of dipolar orientation upon the application of an electric field for PVDF and copolymers of PVDF and TrFE.^{23,24} For such measurements, the transition moment angles of the selected bands must be well known. The bands in this frequency region are all coupled vibrations and so it is difficult to predict what the transition moment angles will be. For example the 612 cm^{-1} CF_2 bending and skeletal bending band shows extremely high parallel polarization. Therefore the transition moment for this mode is essentially parallel to the chain axis. The CF_2 bending and skeletal bending vibrations would be expected to possess transition moments in a direction closer to that perpendicular to the chain direction since the bisector of the CF_2 unit lies at 78° from the chain axis for the α phase. However the transition moment direction depends highly on the character of the vibrational mode and the degree of coupling between different vibrations. Thus it is very difficult to state whether the measured transition moment angle is consistent with the assignment given. The transition moment angles may be calculated from the Cartesian atomic displacements for each vibrational mode. These values have not been previously reported and such a calculation must be performed in order to assess whether or not the calculated transition moments of this study are in agreement with previous assignments.

Microstructure of PVDF/PMMA Blends

The infrared spectrum of an 80% PVDF/ 20% PMMA blend is shown in Figure 3.3. Again the very high orientation of the PVDF is clearly visible. From the very weak dichroism observed for the 1727 cm^{-1} carbonyl stretching band, we find that the PMMA shows relatively low degree of orientation as expected since these chains will relax at the

high drawing temperature employed. Similar to previous electron diffraction data, a lower α content is observed (42% α) as compared to pure PVDF. No definitive conclusions about the degree of orientation of the amorphous PVDF can be made for the blends, as PMMA exhibits absorptions which overlap the 1233 cm^{-1} amorphous PVDF band region.

The degree of morphological change with annealing is dependent upon blend composition. For the 80/20 blend, no changes in phase content are observed upon annealing at 100°C for 10 minutes. This is not true for samples having PMMA contents of 40% and more. Electron microscopic studies have shown that for a 60/40 blend, while the needle-like morphology is still maintained, the relative amount of the β phase increases after annealing.²⁵ In a highly drawn blend of 50% PVDF/ 50% PMMA the overall crystalline content of α and β phases in the sample is very small as estimated from diffraction data.²⁵ No ordered structure was observed at all. However upon annealing at 100°C for 10 minutes, a distinct lamellar morphology consisting primarily of β crystals was observed.²⁵

Infrared spectra of the 50% PVDF/ 50% PMMA blend are shown in Figure 3.4. The infrared bands of PVDF in this sample appear to be much less dichroic and thus the chains are less oriented than for pure PVDF or the 80/20 blend. There is no clear evidence for the presence of α phase in the as drawn 50/50 blend, since neither the 530 cm^{-1} nor the 612 cm^{-1} bands are present. A 510 cm^{-1} trans conformation band is only very weakly present. This is consistent with electron diffraction patterns which shows an unoriented amorphous structure.²⁵ Upon annealing, the 510 cm^{-1} β phase band appears. Therefore, in agreement with electron diffraction data, annealing the highly amorphous blend results in the direct formation of oriented β phase. Intensity increases in other β phase bands found at 1177 cm^{-1} (CF_2 asymmetric stretching and CF_2 and CH_2 rocking) and at 840 cm^{-1} (CF_2 symmetric stretching)¹¹ upon annealing provide further evidence for the formation of β phase.

Another interesting observation is the increase in the dichroism in the PVDF found upon annealing the 50/50 blend. This is clearly seen in all the PVDF bands, especially the 1403 cm^{-1} (CH_2 wagging and asymmetric skeletal stretching) and the 840 , and 510 cm^{-1} bands. After annealing we observe a slight decrease in the dichroism of the 750 cm^{-1} and 2953 cm^{-1} bands of PMMA. To evaluate the orientation of the amorphous PMMA, a transition moment angle of 90° is assumed for the 2953 cm^{-1} methyl asymmetric stretching band. The second moment of the orientation function has a value of 0.116 which decreases to 0.066 upon annealing as relaxation occurs.

The crystallization of β -PVDF from the weakly oriented amorphous blend of 50% PVDF and 50% PMMA (Figures 3.4a,b) is thought to occur due to the decrease in the crystallization temperature, at which the β phase may crystallize more readily.¹⁴ What is unusual is the great increase in PVDF chain orientation during its crystallization from this blend. It is likely that PVDF chains already in the trans conformation may be more able to diffuse to the growing crystals, resulting in a greater β phase content. The occurrence of diffusion controlled crystallization has been already suggested by Yang and Thomas,¹⁵ and the crystallization of β -PVDF from blends of 30-70% PMMA have also been reported by several authors,^{13,14} but few explanations have been offered for its occurrence as yet. The increase in segmental orientation during crystallization of the β -PVDF within this highly drawn blend can be understood from the formation of the β phase crystal nucleus oriented in the drawing direction and the decrease of gauche conformations by subsequent crystal growth.

Conclusions

In this study, the localized structures measurable by infrared spectroscopy differ significantly depending on blend composition or annealing conditions. Melt drawn PVDF films are very highly oriented with the second moment of the orientation function found to be greater than 0.94. The amorphous regions of this sample are also highly oriented. With samples of such high orientation, the transition moment angles of several infrared bands may be calculated. These may be useful for comparison with values obtained from normal coordinate calculations of PVDF. In agreement with previous reports, an increase in the β phase content is observed with the addition of PMMA (62% α in PVDF and 42% α in the 80/20 blend). The 50/50 blend shows a lesser oriented but amorphous structure. However annealing at 100°C for 10 minutes produces highly oriented β phase along with a reduction of the PMMA orientation. The orientation function value of PMMA decreases from 0.116 to 0.066 upon annealing as the amorphous chains relax. The increase in the PVDF orientation upon annealing is most likely due to the formation of highly oriented β phase nuclei. Chains in the trans conformation may more easily diffuse to the crystal surface, resulting in the formation of highly oriented β phase crystals.

References

1. Lovinger, A. J. *Science* **1983**, 220, 1116.
2. Lovinger, A. J. *Developments in Crystalline Polymers*; Bassett, D. C., Ed.; Applied Science Publishers: Essex, UK, 1982; p 195.
3. Noland, J. S.; Hsu, N. N. C.; Saxon, R.; Schmitt, J. M. *Adv. Chem. Ser.* **1971**, 99, 15.
4. Nishi, T.; Wang, T. T. *Macromolecules* **1975**, 8, 909.
5. Paul, D. R.; Altamirano, J. O. *Adv. Chem. Ser.* **1975**, 142, 371.
6. Coleman, M. M.; Zarian, J.; Varnell, D. F.; Painter, P. C. *J. Polym. Sci., Polym. Lett. Ed.* **1977**, 15, 745.
7. Hourston, D. J.; Hughes, J. D. *Polymer* **1977**, 18, 1175.
8. Paul, D. R. Barlow, J. W., Bernstein, R. E.; Wahrmund, D.R. *Polym. Eng. Sci.* **1978**, 18, 1225.
9. Roerdink, E.; Challa, G. *Polymer* **1978**, 19, 173.
10. Roerdink, E.; Challa, G. *Polymer* **1980**, 21, 509.
11. Wendorff, J. H. *J. Polym. Sci., Polym. Lett. Ed.* **1980**, 18, 439.
12. Morra, B. S.; Stein, R. S. *J. Polym. Sci., Polym. Phys. Ed.* **1982**, 20, 2243.
13. Morra, B. S.; Stein, R. S. *J. Polym. Sci., Polym. Phys. Ed.* **1982**, 20, 2261.
14. Leonard, C; Halary, J. L.; Monnerie, L.; Broussoux, D; Servet, B.; Micheron, F. *Polym. Comm.* **1983**, 24, 110.
15. Yang, D.; Thomas. E. L. *J. Mat. Sci. Lett.* **1987**, 6, 593.
16. Lu, F. J.; Hsu, S. L. *Macromolecules* **1986**, 19, 326.
17. Gohil, R. M.; Petermann, J. *Polymer* **1981**, 22, 1612.
18. Yang, D. C.; Thomas, E. L. *J. Mat. Sci.* **1984**, 3, 929.
19. Hausler, E.; Kaufmann, W.; Petermann, J.; Stein, L. *Ferroelectrics* **1984**, 60, 45.
20. Petermann, J.; Gohil, R. M. *J. Mat. Sci.* **1979**, 14, 2260.
21. Hsu, S. L.; Lu, F. J.; Waldman, D. A.; Muthukumar, M. *Macromolecules* **1985**, 18, 2583.
22. Kobayashi, M.; Tashiro, K; Tadokoro, H. *Macromolecules* **1975**, 8, 158.

23. Buchtemann, A.; Stark, W.; Geiss, D. *Acta Polymerica* **1988**, 39, 171.
24. Kim, K. J.; Reynolds, N. M.; Hsu, S. L. submitted to *Macromolecules*.
25. Kaufmann, W.; Petermann, J.; Reynolds, N.; Thomas, E. L.; Hsu, S. L. *Polymer* **1990**, 30, 2147.

CHAPTER IV

A SPECTROSCOPIC STUDY OF SYNDIOTACTIC POLYSTYRENE

Introduction

Fully syndiotactic polystyrene has been recently reported in the literature.¹⁻⁸ Only quite recently has the synthetic process been developed,^{1,2,7} however, only limited structural information is available. The attractive and interesting physical characteristics of this polymer can be summarized as follows: (1) a melting temperature of 270°C; (2) a fully trans planar zigzag backbone; and (3) the presence of a solid-solid phase transition.^{1,3-6} Because of its inherent backbone stiffness and strong intermolecular interactions, the macroscopic properties such as modulus and strength are expected to exceed those of most polymers, even those of some liquid crystalline polymers.

A variety of crystal forms have been suggested including a helical conformation upon crystallization from dilute solution, and an all trans conformation with annealing. The helical phase has been proposed to have a TTGG or T₃GT₃G' conformation.^{3,9} We are interested in the nature of these crystalline forms and the amorphous state, and the transition between them. Vibrational spectroscopy is our primary characterization technique. Its sensitivity to local conformation and chain packing changes allows us to observe microstructural changes with annealing, orientation or solvent treatments. In this report we examine structural differences between samples of different tacticities observed from their infrared spectra. Evidence will be presented for the presence of two different conformational forms, and the transition between them caused by thermal treatment or orientation.

Experimental

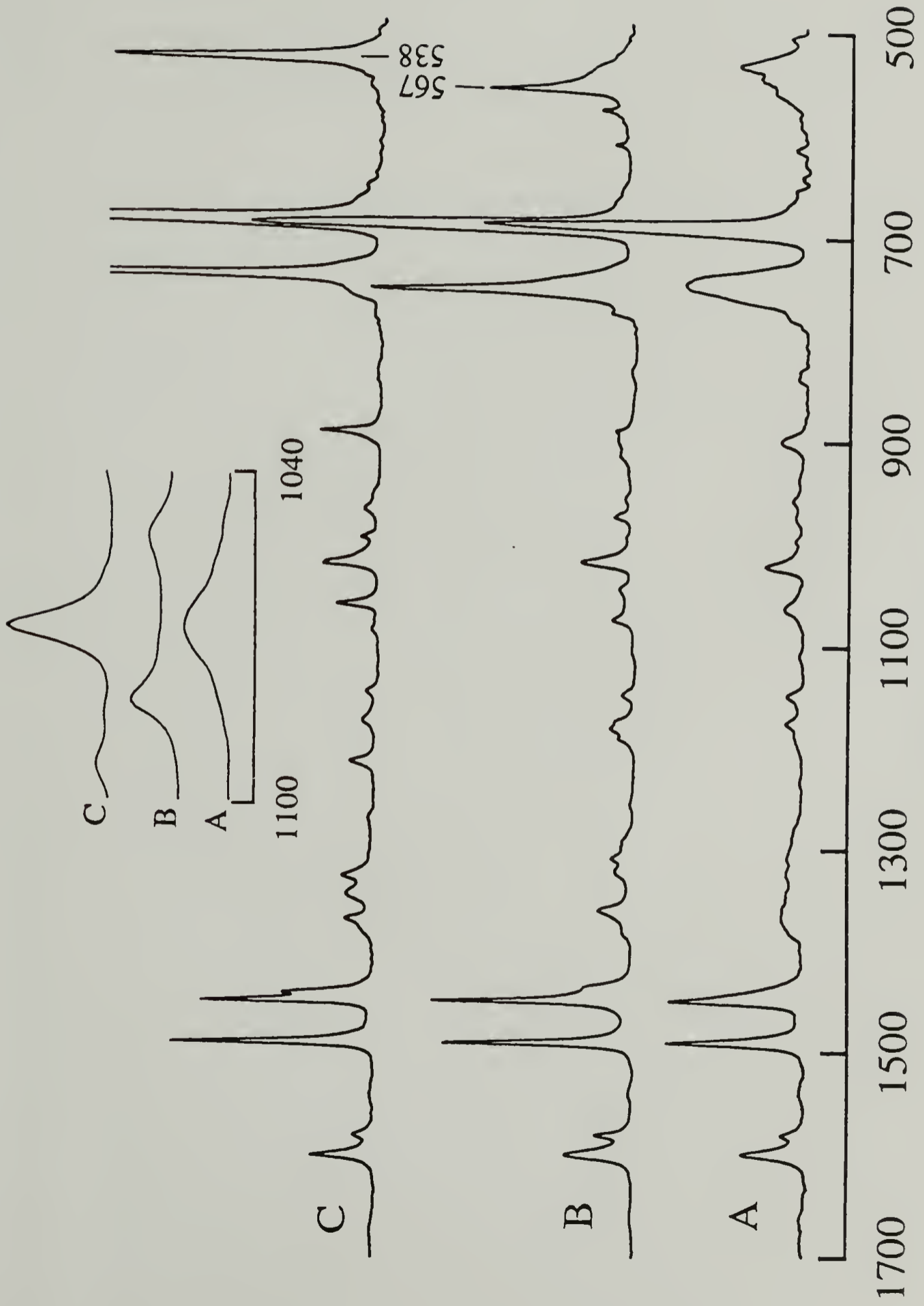
Polystyrene samples with syndiotacticity greater than 98% were obtained from Idemitsu Kosan Co. Ltd., Japan. Isotactic (90%) and atactic polystyrene samples were obtained from Scientific Polymer Products Inc., and Polysciences Inc., respectively. Thin films were obtained by casting from a 1 wt.% solution in chloroform and drying up to 14 days under vacuum at room temperature. Melt quenched films were prepared by heating the films cast on a AgCl window to 270°C under a nitrogen atmosphere in order to prevent oxidation, and then quenching into liquid nitrogen. Oriented samples were obtained by solid state coextrusion at 100°C in a polyethylene billet. Infrared spectra were obtained with a Bruker IFS 113v FTIR spectrometer. Generally 250 scans were collected at a resolution of 2 cm⁻¹. A gold wire grid polarizer was employed for obtaining polarized infrared spectra. For annealing experiments, samples were heated in a cell constructed in our laboratory. Low temperature spectra were obtained in a liquid nitrogen cooled cell.

Results and Discussion

The infrared spectra of atactic, isotactic, and syndiotactic polystyrene (sPS) are shown in Figure 4.1. Large differences in both the infrared and Raman data, related to the different chain conformations of these isomers, are observed, especially in the regions of 540, 750, 900, 1070, and 1200 - 1400 cm^{-1} . We have also found that the vibrational spectra can be perturbed significantly by thermal annealing. The spectra obtained for the sPS generally contain bands which are sharp (approximately 6 cm^{-1} in halfwidth) as compared to the relatively broad features observed for both isotactic or atactic isomers. From the intensity decrease in the helical bands and the corresponding sharpening of the spectroscopic features observed upon annealing, we intend to show that annealed sPS is of high crystallinity and has a planar zigzag backbone conformation. One of the primary objectives is to seek explicit evidence of vibrations which can be assigned to the all trans planar zigzag backbone.

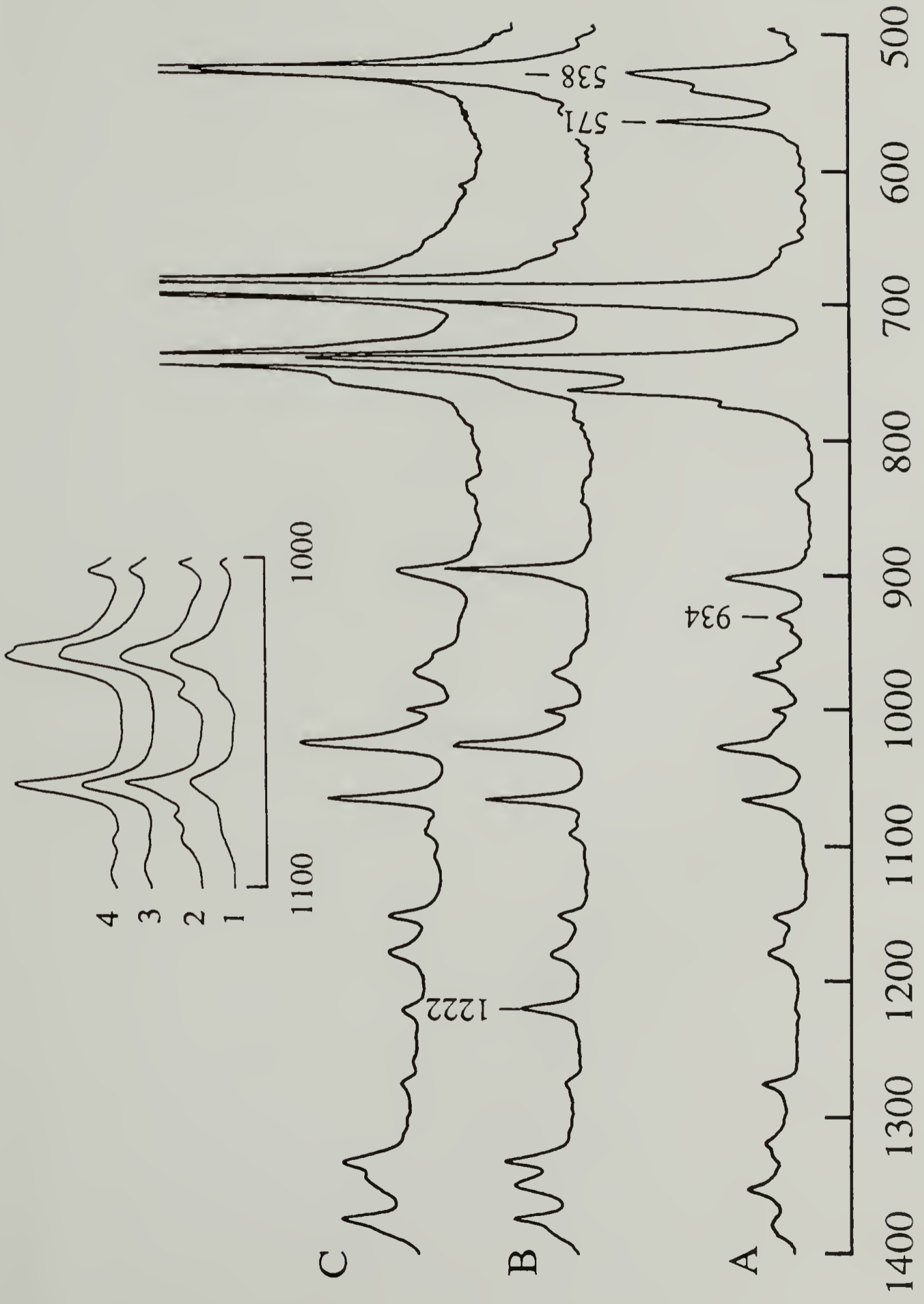
In Figure 4.2 are shown spectra of sPS as cast, upon annealing, and upon coextrusion. Spectra of a cast film at various temperatures are shown in Figure 4.3. In the 1100-1400 cm^{-1} region a number of conformation sensitive skeletal vibrations exist. It is also quite likely that these bands are sensitive to chain packing. The infrared spectrum of the cast film contains spectroscopic features which disappear when the sample temperature is raised. Some of the weak features, such as the 1079, 1086, and 1042 cm^{-1} bands which are hard to observe at room temperature are seen quite clearly at liquid nitrogen temperature, and this is shown in the inset region in Figure 4.2. The intensity and position of these weak features are especially sensitive to thermal annealing. One of the more interesting features observed for sPS is the 1030 cm^{-1} band. This band, assignable to the combination of CH in-plane-bending, CC ring stretching, and CCC ring bending vibrations,¹⁰ seems to be sensitive to chain packing, and appears splits into two components at 1030 and 1028 cm^{-1} at low temperature. However, these features are not

FIGURE 4.1 Infrared spectra of (a) atactic, (b) isotactic, and (c) syndiotactic polystyrene.



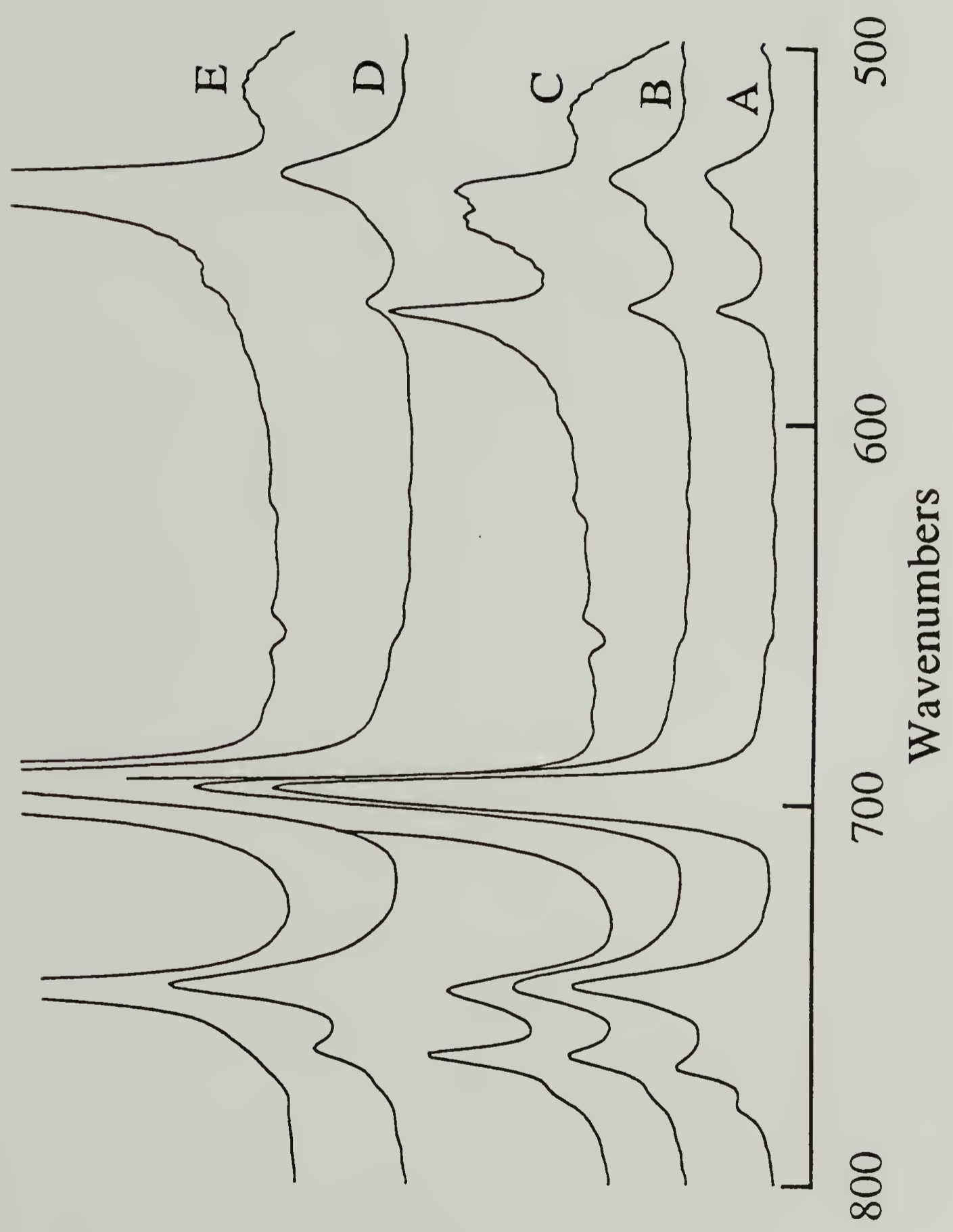
Wavenumbers

FIGURE 4.2 Infrared spectra of sPS (a) as cast, (b) after annealing at 295°C for 0.5 hour, and (c) coextruded at 100°C to a draw ratio of 4; inset region (1) as cast, (2) at liquid nitrogen temperature, (3) annealed at 200°C for 1 hour, and (4) annealed at 200°C and measured at liquid nitrogen temperature.



Wavenumbers

FIGURE 4.3 Infrared spectra of sPS at various temperatures; (a) 25°C, (b) 111°C, (c) 185°C, (d) 212°C, and (e) 238°C.



concluded to be due to crystal field splitting, and this will be explained further in the normal vibrational analysis which is presented in Chapter VI. A 1069 cm^{-1} band is present as a broad feature in the cast film. However, after annealing the band sharpens but remains as a singlet even at low temperature. Two bands of medium intensity have also been observed in this region for isotactic polystyrene (1052 and 1083 cm^{-1}). These bands seen in the inset region in Figure 4.1 have been assigned previously to ring-backbone and ring CC stretching, and to ring stretching and CH in plane bending, respectively. In that case, they are thought to be associated with the sequence length of preferred conformations in the amorphous phase.¹⁰ From our evidence we conclude that both of these medium intensity bands at 1030 and 1069 cm^{-1} in sPS are crystalline in nature. Atactic PS has been shown to possess a significant amount of syndiotactic trans isomers.¹¹ Therefore we expect the spectrum of sPS to be more similar than that of iPS to that of atactic polystyrene, and this is generally observed, although bandwidths for the syndiotactic isomer are much narrower.

As mentioned previously, a variety of crystal forms have been suggested for sPS including a helical structure upon crystallization from dilute solution.³ A TTGG conformation, which is also observed for syndiotactic propylene, has been proposed for these solution cast films.¹² Spectra of solution cast, annealed, and coextruded films are shown in Figure 4.2, while spectra of a cast film as a function of temperature are shown in Figure 4.3. A number of well defined bands are unique to sPS. Some appear in the solution cast film, but not in the annealed or drawn samples. One example is the doublet appearing at 943 and 934 cm^{-1} . The intensity of this pair changes even more dramatically than the bands in the 1000 cm^{-1} region, disappearing almost completely for annealed samples. We have assigned these two bands to the helical conformation found for the cast sample, which is removed by annealing. In the 500 cm^{-1} region, bands are observed at 571 , 548 , and 535 cm^{-1} . After annealing at 200°C , only a single band at 539 cm^{-1} remains. In iPS a single band at 567 cm^{-1} is observed and is assigned to the ν_{16b} skeletal out of plane mode of the aromatic ring.^{10,13} The sPS spectra in this region are consistent

with studies of polystyrene model compounds in which a 540 cm^{-1} band is observed when at least 4 backbone carbons atoms are in a trans conformation, whereas a band at 554 cm^{-1} is assigned to a second conformation containing gauche isomers.¹³ Thus the 539 cm^{-1} band of sPS is consistent with a syndiotactic all trans structure, while the cast film exhibits a 548 cm^{-1} band indicating the presence of gauche conformers. Atactic PS exhibits a broad band at 541 cm^{-1} suggesting a broad conformation distribution. As seen in Figure 4.2, extrusion of a cast film at 100°C produces spectral changes similar to those observed on annealing. It is expected that the drawing process would also transform the helical form present in the cast film to the more extended all planar zigzag form, and this is observed. Bandwidths are broader for this oriented sample than for the annealed film, indicating that thermal treatment produced greater structural regularity than extruding the sample to a draw ratio of four.

As seen in Figure 4.2, the 1222 cm^{-1} band is entirely absent in the cast film, but appears as a sharp band in the annealed sample spectrum. It is expected that for a solution cast film there must be a distribution of both trans and gauche conformations. The absence of the 1222 cm^{-1} band for the cast sample suggests that this band is associated with long trans sequences which are not present in large number in a solution cast film, but only in the annealed or drawn material. Upon annealing, all vibrational bands appear much sharper indicating an increase in structural regularity.

The transformation or the removal of structural defects is highly dependent on the temperature of annealing and this is observed in Figure 4.3. Only a small amount of structural transformation occurs below 200°C . Heating up to 185°C produces intensity increases of the 548 , 571 , and 769 cm^{-1} bands associated with the helical conformation. This is indicative of the increase in crystallinity of the helical phase upon annealing.

Heating to 212°C produces intensity decreases in the bands assignable to the helical conformation, and increases in the 1222 and 539 cm^{-1} bands assigned to the all trans conformation. The details of this structural transformation are unclear and will be

discussed in Chapter VI. Undoubtedly, the transition is a cooperative process and thus the rate and amount of transformation are strongly dependent on the specificity and magnitude of intermolecular interactions.

Conclusions

In conclusion, it is observed that infrared spectra of syndiotactic polystyrene obtained under different crystallization and thermal conditions are characteristic of the overall structural regularity and the specific chain conformations present. Spectra of samples cast from dilute solution from chloroform are consistent with previous studies suggesting a helical conformation. Annealing at temperatures up to 185°C causes an increase in the amount and perfection of the helical phase and further annealing near 200°C causes a transition to an all trans phase. Bands may be clearly identified which are indicative of each of these conformations. The transition to the trans state is also observed upon solid-state coextrusion at 100°C. Annealing near the melting point is seen to produce greater structural regularity, as determined by band widths, than extruding to a draw ratio of four.

References

1. Ishihara, N.; Seimiya, T.; Kuramoto, M.; Uoi, M. *Macromolecules* **1986**, *19*, 2464.
2. Zambelli, A.; Longo, P.; Pellecchia, C.; Grassi, A. *Macromolecules* **1987**, *20*, 2035.
3. Kobayashi, M.; Nakaoki, T.; Uoi, M. *Polym. Prep., Jpn.* **1988**, *37*, E432.
4. Greis, O.; Asano, T.; Xu, J.; Petermann, J. *Z. Kristallogr.* **1988**, *182*, 58.
5. Immirizi, A.; de Candia, F.; Iannelli, P.; Zambelli, A. *Makromol. Chem. Rapid Commun.* **1988**, *9*, 761.
6. Vittoria, V.; de Candia, F.; Iannelli, P.; Immirizi, A. *Makromol. Chem. Rapid Commun.* **1988**, *9*, 765.
7. Ishihara, N.; Kuramoto, M.; Uoi, M. *Macromolecules* **1988**, *21*, 3356.
8. Nyquist, R. A. *Appl. Spectrosc.* **1989**, *43*, 440.
9. Petermann, J. private communication.
10. Painter, P. C.; Koenig, J. L. *J. Polym. Sci., Polym. Phys. Ed.* **1977**, *15*, 1885.
11. Jasse, B.; Chao, R. S.; Koenig, J. L. *J. Raman Spectrosc.* **1979**, *8*, 244.
12. Kobayashi, M.; Nakaoki, T.; Ishihara, N. *Macromolecules* **1989**, *22*, 4377.
13. Jasse, B.; Monnerie, L. *J. Mol. Structure* **1977**, *39*, 165.

CHAPTER V

A NORMAL VIBRATIONAL ANALYSIS OF SYNDIOTACTIC POLYSTYRENE

Introduction

As explained in the previous chapter, syndiotactic polystyrene (sPS) is becoming a subject of great interest.¹⁻⁹ This material has several interesting physical characteristics: 1. A melting temperature of approximately 270°C, although with annealing at gradually higher temperatures we have observed a melting point as high as 285°C; 2. A variety of chain conformations including a fully trans planar zigzag backbone in addition to a helical conformation observed for solution cast films; and 3. The presence of a solid-solid phase transition at ~190°C involving changes in both chain conformation and packing.^{1,3-7}

Because of its inherent backbone stiffness and strong intermolecular , the macroscopic properties such as modulus and strength and their insensitivity to temperature are expected to exceed most polymers.

The structure of sPS is complex. Diffraction and spectroscopic studies have revealed that this polymer exists in a helical conformation upon casting from dilute solution and can easily transform to the all trans conformation upon annealing or drawing.^{3,5,6,10,11} The differences in the infrared and Raman spectra observed for different forms of sPS are striking. From the spectra obtained from samples of different tacticity, and from previous vibrational analyses of isotactic and atactic PS,¹²⁻¹⁴ preliminary analyses have been carried out for sPS.^{8,11} For example, infrared bands at 1222 cm⁻¹ or 538 cm⁻¹ were found to be associated with the trans conformation, while features at 571, 934, and 943 cm⁻¹ represent the helical structure.^{3,11,15} These preliminary assignments have been useful to clarify the microstructures and their changes. However the exact band assignments for sPS are still ill defined. Therefore a normal vibrational analysis of sPS is necessary for a thorough

analysis of the vibrational spectra in order to understand the microstructure and phase transition of this material.

A normal vibrational analysis for polystyrene is complicated because of the various cyclic and branching redundancies which exist and greatly increase the necessary number of internal coordinates needed for analysis. This overdefined set of coordinates is often used in order to take advantage of symmetry or to transfer force constants from one molecule to another. However the use of a larger than necessary number of coordinates increases the number of force constants so that the set is indeterminate, and thus the eigenvalue solution may not be unique. Therefore the force constants lose physical meaning and cannot be easily refined or adapted to polystyrene, and other polymers. It is also desirable to transfer well developed force field sets calculated for small ring molecules from first principles. In this study a set of force constants derived for a set of nonredundant symmetry coordinates is used for the phenyl ring, which were determined for benzene.¹⁶ These coordinates have been applied in the analysis of substituted benzenes and also for poly(p-phenylene terephthalamide).^{17,18} One goal of this study is to determine the degree of coupling of the ring vibrations to the backbone modes and to correlate these bands with those that are sensitive to the all trans conformation.

When the vibrational modes are well assigned it is possible to calculate the theoretical modulus from the slope of the dispersion curve for the longitudinal acoustic mode vibration at the zone center ($k=0$). Such a calculation is performed for sPS. Since this calculation involves the vibrations of a single infinite chain, the presence of intermolecular interactions and their effect on the mechanical properties are unaccounted for. Therefore the value calculated represents a lower limit of the theoretical modulus.

Experimental

Polystyrene samples which are greater than 99% syndiotactic ($M_n = 125,000$, $M_w = 660,000$) were obtained from Dow Chemical Co. Films were cast in aluminum pans from a 1% solution in chloroform and dried under vacuum. Oriented films with a draw ratio of 4 were obtained by solid state coextrusion at 100°C with the split billet technique.¹⁸ In this case the cast film was placed inside a high density polyethylene billet. Polarized infrared spectra were obtained with a Bruker IFS 113v FTIR spectrometer equipped with a gold wire grid polarizer. Generally 200 scans were collected at 2 cm^{-1} resolution. Low temperature infrared spectra were obtained in a liquid nitrogen cooled cell constructed in our laboratory. Polarized Raman measurements were made with a Jobin-Yvon U1000 spectrometer operating with a bandpass of 2 cm^{-1} . The highly polarized excitation radiation was the 5145 \AA line of a Spectra Physics 165-08 argon ion laser providing 100mW of power at the sample. A polarization scrambler, placed immediately following the analyzer, was used to remove intensity differences due to the anisotropic diffraction properties of the monochromator gratings. Two scattering geometries were employed for the polarized Raman measurements in order to correctly assign each vibration to a specific symmetry species. These are shown in Figure 5.1.

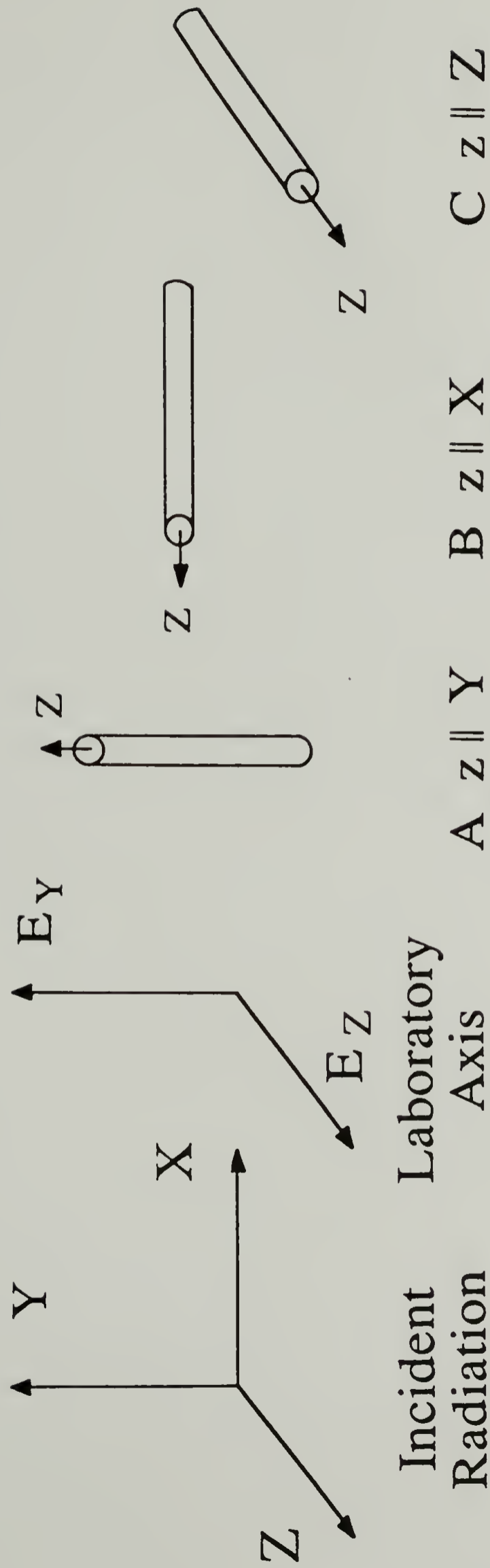


FIGURE 5.1 Schematic diagram of the sample orientation relative to the incident radiation for different scattering geometries.

Structure and Force Field

An all trans planar structure was used for our vibrational analysis. This is the accepted structure for annealed sPS determined from diffraction and spectroscopic studies and conformational analyses.^{1,3-11,20,21} As stated in Chapter V, the helical has been recently proposed to exist in a TTGG conformation.²² The all trans structure is a simpler structure and should possess higher mechanical properties. The factor group of the line group of the all trans conformation of sPS is isomorphous to the C_{2v} point group. Vibrational modes are distributed among the symmetry species as follows: 29 A_1 (\perp), 17 A_2 (IR inactive), 17 B_1 (\parallel), and 29 B_2 (\perp). The modes are calculated for two values of the phase angle between oscillators of adjacent chemical repeats. The A_1 and B_1 symmetry species are associated with a phase angle of 0° , while the A_2 and B_2 symmetry species are associated with a phase angle of 180° .

Many of the band assignments can be made from polarized Raman measurements with highly oriented samples, although these measurements are complicated by the lack of perfect orientation and by the presence of multiple scattering from small crystallites (these films are not completely transparent and exhibit a fibrous texture). The assignment of symmetry species to specific incident and scattered polarization directions has been performed for C_{2v} symmetry.^{23,24} With scattering geometry A the sample draw direction is positioned parallel to the Y axis in the laboratory frame as shown in Figure 5.1. Using this geometry, the X(YY)Z polarization, with parallel incident and scattered radiation, gives the totally symmetric A_1 symmetry species. The X(YX)Z or X(ZY)Z polarizations are associated with the A_2 and B_1 species, while the X(ZX)Z polarization gives the A_1 and B_2 symmetry species. With geometry B the draw direction is placed parallel to the X axis. Measurement with this geometry is needed to clearly distinguish between the A_1 and B_2 symmetry bands. As seen in Table 5.1, the X(YY)Z and X(ZY)Z polarizations give

Table 5.1 Raman scattering activities for C_{2v} symmetry

Scattering Geometry A				
Polarization	<u>Symmetry species</u>			
	A ₁	A ₂	B ₁	B ₂
X(YY)Z	α_{xx}	0	0	0
X(ZY)Z	0	α_{xy}	α_{xz}	0
X(YX)Z	0	α_{xy}	α_{xz}	0
X(ZX)Z	α_{yy}, α_{zz}	0	0	α_{yz}

Scattering Geometry B		
Polarization	<u>Symmetry species</u>	
	A ₁	B ₂
X(YY)Z	$1/32 (12\alpha_{yy}^2 + 8\alpha_{yy}\alpha_{zz} + 12\alpha_{zz}^2)$	$1/2 \alpha_{yz}^2$
X(ZY)Z	$1/32 (4\alpha_{yy}^2 - 8\alpha_{yy}\alpha_{zz} + 4\alpha_{zz}^2)$	$1/2 \alpha_{yz}^2$

identical scattering intensity for B₂ vibrations; however the totally symmetric A₁ vibrations will have greater intensity for the X(YY)Z polarization.

A schematic structure of sPS showing the internal coordinates is given in Figure 5.2. The indexing of the atoms for the internal coordinates is shown in Figure 5.3. The structural parameters and the internal coordinates are given in Tables 5.2 and 5.3, respectively. In this calculation a set of non-redundant symmetry coordinates is employed

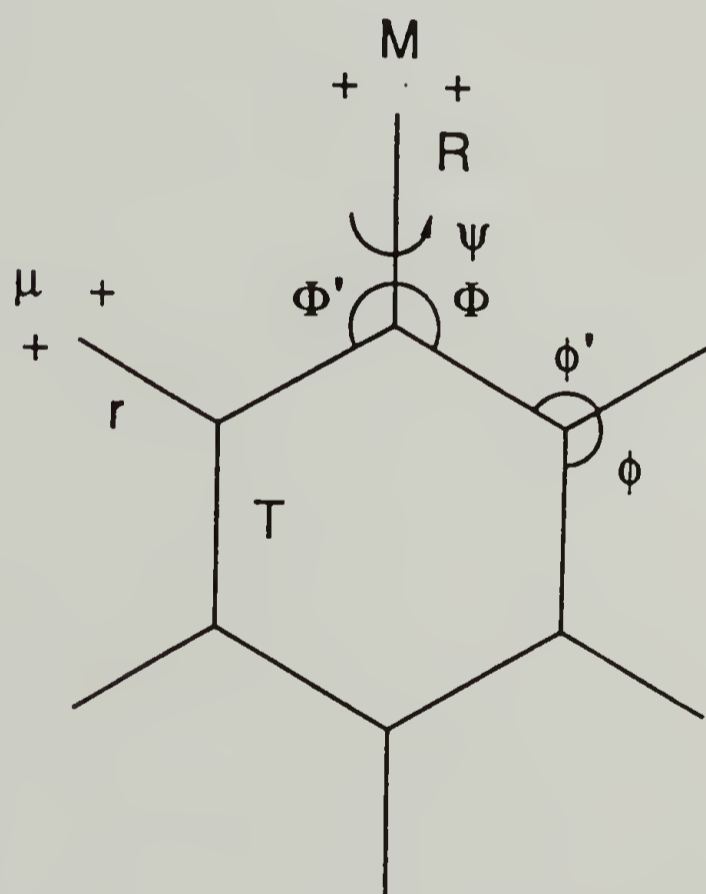
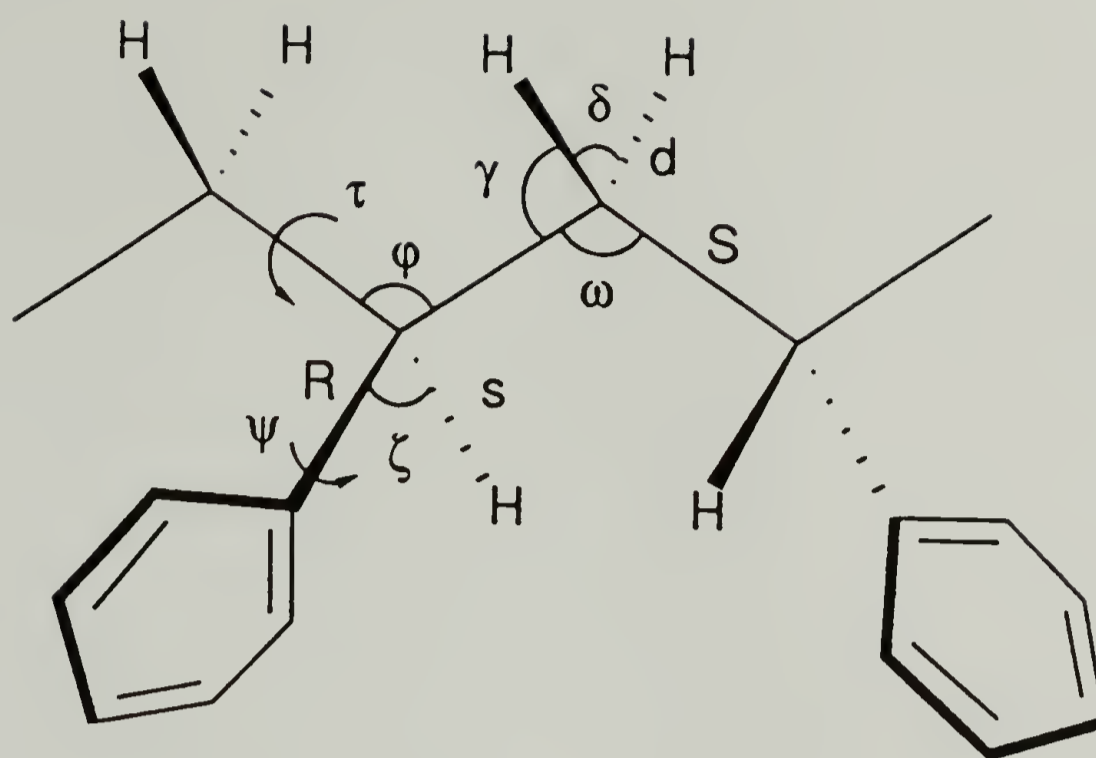


FIGURE 5.2 Schematic structure of sPS showing internal coordinates.

Table 5.2 Structural parameters for all trans syndiotactic polystyrene.

Length (Å)		Valence Angle (°)		Dihedral Angle (°)	
C-C	1.397	∠ (CCC)	120	τ(CCCC)	180
C-H	1.084	∠ (CCH)	120	τ(CCCH)	0
C-C'	1.51	∠ (CC'')	120	τ(CCC'')	0
C'-C'	1.54	∠ (C'C'C')	109.47	τ(HCCC')	180
C'-H	1.093	∠ (CC'H)	109.47	τ(C ₃ C'C'H ₁₆)	0
		∠ (C'C'H)	109.47	τ(C ₁ C'C'C ₁₈)	0
		∠ (HC'H)	109.47	τ(C ₁ C'C'H ₁₆)	120
		∠ (C'C'C')	109.47	τ(C ₁ C'C'H ₁₅)	240

C = ring carbon

C' = chain carbon

Table 5.3 Definition of internal coordinates for syndiotactic polystyrene

Stretching			
atoms		atoms	
$R_1 = r(\text{C}'\text{-C}')$	(2,17)	$R_{10} = r(\text{C-H})$	(4,9)
$R_2 = r(\text{C}'\text{-C})$	(2,3)	$R_{11} = r(\text{C-H})$	(5,10)
$R_3 = r(\text{C}'\text{-H})$	(2,14)	$R_{12} = r(\text{C-H})$	(6,11)
$R_4 = r(\text{C-C})$	(3,4)	$R_{13} = r(\text{C-H})$	(7,12)
$R_5 = r(\text{C-C})$	(4,5)	$R_{14} = r(\text{C-H})$	(8,13)
$R_6 = r(\text{C-C})$	(5,6)	$R_{15} = r(\text{C-H})$	(17,15)
$R_7 = r(\text{C-C}')$	(6,7)	$R_{16} = r(\text{C-H})$	(17,16)
$R_8 = r(\text{C-C})$	(7,8)	$R_{17} = r(\text{C-H})$	(17,17)
$R_9 = r(\text{C-C})$	(8,3)		
Angle Bending			
atoms		atoms	
$R_{18} = \angle (\text{C}'\text{C}'\text{H})$	(1,2,14)	$R_{24} = \angle (\text{C}'\text{C}\text{C})$	(2,3,4)
$R_{19} = \angle (\text{C}'\text{C}'\text{C})$	(1,2,3)	$R_{25} = \angle (\text{C}\text{C}\text{H})$	(3,4,9)
$R_{20} = \angle (\text{C}'\text{C}'\text{C}')$	(1,2,17)	$R_{26} = \angle (\text{H}\text{C}\text{C})$	(9,4,5)
$R_{21} = \angle (\text{H}'\text{C}'\text{C}')$	(14,2,17)	$R_{27} = \angle (\text{C}\text{C}\text{H})$	(4,5,10)
$R_{22} = \angle (\text{C}\text{C}'\text{H})$	(3,2,14)	$R_{28} = \angle (\text{H}\text{C}\text{C})$	(10,5,6)
$R_{23} = \angle (\text{C}\text{C}'\text{C}')$	(3,2,17)	$R_{29} = \angle (\text{C}\text{C}\text{H})$	(5,6,11)

Table 5.3 continued

Angle Bending			
	atoms		atoms
R ₃₀ = ∠ (HCC)	(11,6,7)	R ₃₉ = ∠ (CCC)	(6,7,8)
R ₃₁ = ∠ (CCH)	(6,7,12)	R ₄₀ = ∠ (CCC)	(7,8,3)
R ₃₂ = ∠ (HCC)	(12,7,8)	R ₄₁ = ∠ (CCC)	(8,3,4)
R ₃₃ = ∠ (CCH)	(7,8,13)	R ₄₂ = ∠ (C'C'C')	(2,17,18)
R ₃₄ = ∠ (HCC)	(13,8,3)	R ₄₃ = ∠ (C'C'H)	(2,17,15)
R ₃₅ = ∠ (CCC')	(8,3,2)	R ₄₄ = ∠ (C'C'H)	(2,17,16)
R ₃₆ = ∠ (CCC)	(3,4,5)	R ₄₅ = ∠ (HC'H)	(15,17,16)
R ₃₇ = ∠ (CCC)	(4,5,6)	R ₄₆ = ∠ (HC'C')	(15,17,18)
R ₃₈ = ∠ (CCC)	(5,6,7)	R ₄₇ = ∠ (HC'C')	(16,17,18)
Out-of-plane bending			
	atoms		atoms
R ₄₈ = CH opb	(4,9,5,3)	R ₅₁ = CH opb	(7,12,8,6)
R ₄₉ = CH opb	(5,10,6,4)	R ₅₂ = CH opb	(8,13,3,7)
R ₅₀ = CH opb	(6,11,7,5)	R ₅₃ = ring opb	(3,2,4,8)

Table 5.3 continued

Torsion			
	atoms		atoms
R ₅₄ = C'-C' tor	(2,17)	R ₅₉ = C-C tor	(5,6)
R ₅₅ = C'-C' tor	(17,18)	R ₆₀ = C-C tor	(6,7)
R ₅₆ = C-C' tor	(3,2)	R ₆₁ = C-C tor	(7,8)
R ₅₇ = C-C tor	(3,4)	R ₆₂ = C-C tor	(8,3)
R ₅₈ = C-C tor	(4,5)		

for the phenyl ring.¹⁶ A schematic diagram showing the atomic displacements for some of these coordinates is given in Figure 5.4. A list of the symmetry coordinates used in the calculation is given in Table 5.4. The force constants for the backbone chain were developed by Snyder and Schachtschneider for normal and branched alkanes and have been applied to many polymers such as polyethylene and polypropylene.²⁵ Force constants for the phenyl ring were obtained from *ab initio* quantum chemical calculations on benzene.¹⁶ Force constants describing the interaction of the ring with the backbone were taken from the work of La Lau and Snyder for substituted benzenes.²⁶ A complete list of the force constants used in this study is given in Table 5.5. The vibrational analysis was performed with Wilson's GF matrices with programs modified from Schachtschneider and Snyder's programs.²⁷ The calculated and observed frequencies along with the observed polarizations and calculated potential energy distribution are listed in Table 5.6.

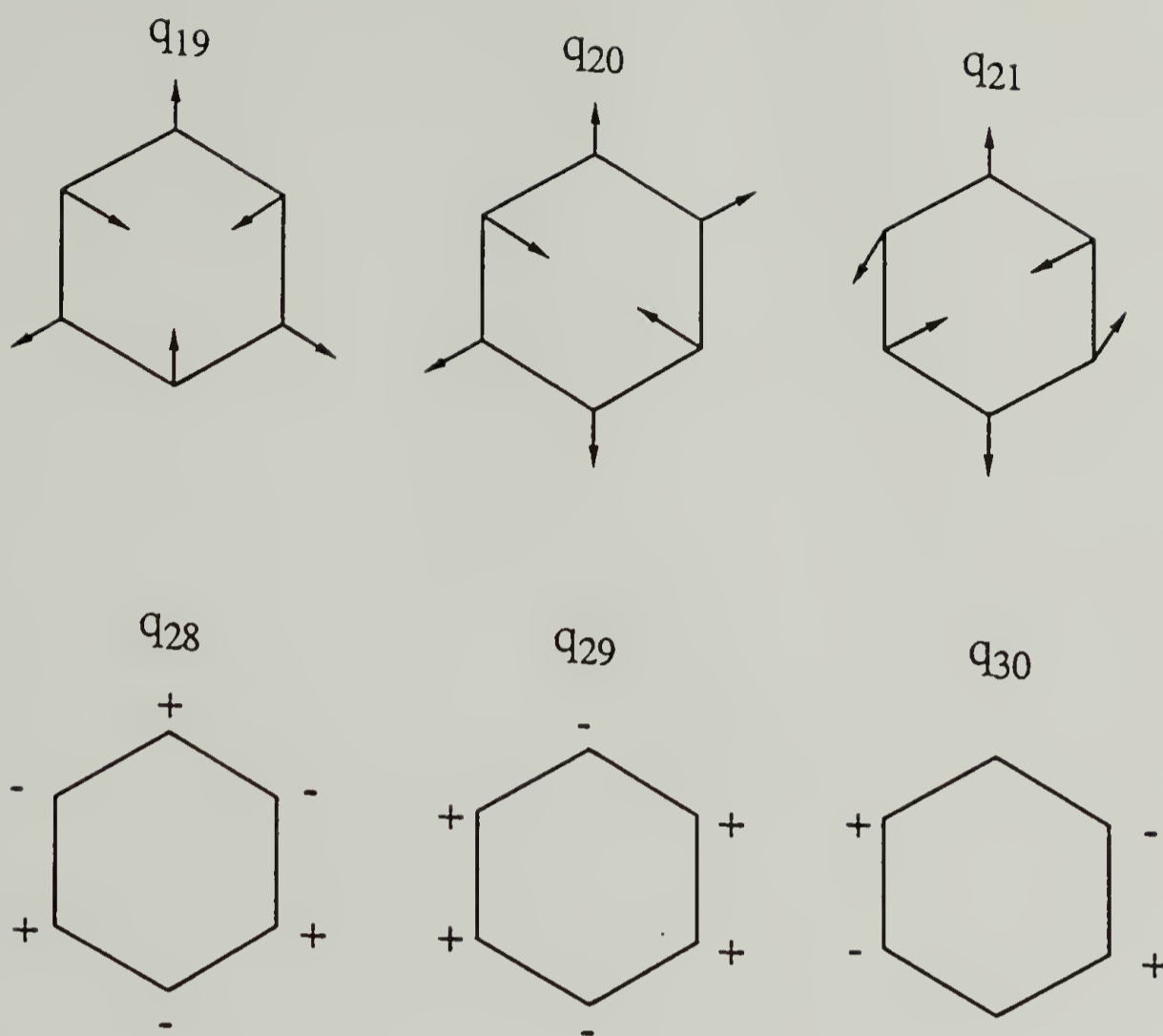


FIGURE 5.4 Definition of some of the nonredundant symmetry coordinates for the phenyl ring.

Table 5.4 Definition of symmetry coordinates for
syndiotactic polystyrene

Notation		
C'-C' str	S	$S_1 = R_1$
C'-C' str		$S_2 = R_{17}$
C'-C str	R	$S_3 = R_2$
C-C str	T	$S_4 = R_4$
C-C str		$S_5 = R_5$
C-C str		$S_6 = R_6$
C-C str		$S_7 = R_7$
C-C str		$S_8 = R_8$
C-C str		$S_9 = R_9$
C'-H' str	s	$S_{10} = R_3$
C'-H str	d	$S_{11} = R_{15}$
C'-H str		$S_{12} = R_{16}$
C-H str	r	$S_{13} = R_{10}$
C-H str		$S_{14} = R_{11}$
C-H str		$S_{15} = R_{12}$
C-H str		$S_{16} = R_{13}$
C-H str		$S_{17} = R_{14}$
C'C'H bend	ζ	$S_{18} = R_{18}$
HC'C' bend		$S_{19} = R_{21}$
CC'H bend		$S_{20} = R_{22}$

Continued next page

Table 5.4 continued

Notation		
C'C'C bend	φ	$S_{21} = R_{19}$
C'C'C' bend		$S_{22} = R_{20}$
CC'C' bend		$S_{23} = R_{23}$
C'C'C' bend	ω	$S_{24} = R_{42}$
C'C'H bend	γ	$S_{25} = R_{43}$
C'C'H bend		$S_{26} = R_{44}$
HC'C' bend		$S_{27} = R_{46}$
HC'C' bend		$S_{28} = R_{47}$
HC'H bend	δ	$S_{29} = R_{45}$
C'CC bend	Φ	$S_{30} = R_{24}$
CCC' bend	Φ'	$S_{31} = R_{35}$
CH9 ipb	β	$S_{32} = (R_{26}-R_{25})/2^{1/2}$
CH10 ipb		$S_{33} = (R_{28}-R_{27})/2^{1/2}$
CH11 ipb		$S_{34} = (R_{30}-R_{29})/2^{1/2}$
CH12 ipb		$S_{35} = (R_{32}-R_{31})/2^{1/2}$
CH13 ipb		$S_{36} = (R_{34}-R_{33})/2^{1/2}$
C'C ipb	β'	$S_{37} = (R_{24}-R_{35})/2^{1/2}$
trigonal def	q19	$S_{38} = (R_{41}-R_{36}+R_{37}-R_{38}+R_{39}-R_{40})/6^{1/2}$
asym def A	q20	$S_{39} = (2R_{41}-R_{36}-R_{37}+2R_{38}-R_{39}-R_{40})/12^{1/2}$
asym def B	q21	$S_{40} = (R_{36}-R_{37}+R_{39}-R_{40})/2$
CH9 opb	μ	$S_{41} = R_{48}$

Continued next page

Table 5.4 continued

Notation		
CH10 opb		$S_{42} = R_{49}$
CH11 opb		$S_{43} = R_{50}$
CH12 opb		$S_{44} = R_{51}$
CH13 opb		$S_{45} = R_{52}$
ring opb	M	$S_{46} = R_{53}$
puckering	q28	$S_{47} = (R_{57}-R_{58}+R_{59}-R_{60}+R_{61}-R_{62})/6^{1/2}$
asym tor A	q29	$S_{48} = (-R_{57}+R_{59}-R_{60}+R_{62})/2$
asym tor B	q30	$S_{49} = (-R_{57}+2R_{58}-R_{59}+R_{60}+2R_{61}-R_{62})/12^{1/2}$
C'C tor	ψ	$S_{50} = R_{56}$
C'C' tor	τ	$S_{51} = R_{54}$
C'C' tor		$S_{52} = R_{55}$

Table 5.5 Force constants for syndiotactic polystyrene

	<u>force constant</u>	<u>value</u>	<u>force constant</u>	<u>value</u>
(a) chain				
	K(d)	4.554	F(S ω)	0.417
	K(s)	4.588	F($\gamma\omega$)	-0.031
	K(R)	4.6813	F(R γ)	0.328
	K(S)	4.337	F(R γ')	0.079
	H(δ)	0.550	$f_{\gamma\zeta}^t$	0.127
	H(γ)	0.655	$f_{\gamma\zeta}^g$	-0.005
	H(ζ)	0.657	$f_{\omega\varphi}^t$	-0.011
	H(ω)	1.130	$f_{\omega\varphi}^g$	0.010
	H(φ)	1.084	$f_{\gamma\varphi}^t$	0.049
	H(ψ)	0.048	$f_{\gamma\varphi}^g$	-0.052
	H(τ)	0.072	$f_{\gamma\zeta}'^t$	0.002
	F(δ)	0.006	$f_{\gamma\zeta}'^g$	0.009
	F(SR)	0.101	$f_{\gamma\zeta}''^t$	-0.014
	F(γ)	-0.021	$f_{\gamma\zeta}''^g$	-0.025
	F(γ')	0.012	F(φ)	-0.041

Continued next page

Table 5.5 continued

(b) ring

<u>force constant</u>	<u>value</u>	<u>force constant</u>	<u>value</u>
K(r)	5.176	F(R ₁ β ₁)	0.167
K(R)	6.636	F(R ₁ β ₃)	-0.010
H(β)	0.512	F(R ₁ β ₄)	0.019
H(β')	0.7535	F(R ₁ β')	0.186
H(q ₁₉)	1.236	F(R ₁ q ₂₀)	0.134
H(q ₂₀)	1.236	F(R ₂ q ₂₀)	-0.268
H(q ₂₁)	1.236	F(R ₃ q ₂₀)	-0.067
H(γ)	0.5852	F(r ₂ q ₂₁)	-0.0857
H(γ')	0.6688	F(r ₃ q ₂₁)	0.0857
H(q ₂₈)	0.3763	F(R ₁ q ₂₁)	0.2321
H(q ₂₉)	0.3156	F(R ₃ q ₂₁)	-0.2321
H(q ₃₀)	0.3156	F(β) ^o	0.009
F(r) ^o	0.016	F(β) ^m	-0.010
F(r) ^m	0.005	F(β) ^p	-0.001
F(r) ^p	0.001	F(β ₂ q ₂₀)	-0.067
F(r ₁ R ₁)	0.079	F(β' ₂ q ₂₁)	0.07736
F(r ₁ R ₂)	-0.002	F(β ₂ q ₂₁)	-0.03863
F(r ₁ R ₃)	-0.022	F(γ) ^o	-0.092
F(r ₁ β ₂)	0.005	F(γ) ^m	-0.0004
F(r ₁ β ₃)	-0.007	F(γ) ^p	-0.0235

Continued next page

Table 5.5 continued

<u>force constant</u>	<u>value</u>	<u>force constant</u>	<u>value</u>
F(r ₁ q ₁₉)	0.105	F(γ ₁ q ₂₈)	-0.1681
F(r ₂ q ₁₉)	-0.105	F(γ ₂ q ₂₈)	0.1681
F(Rq ₁₉)	-0.105	F(γ ₁ q ₂₉)	-0.1700
F(r ₁ q ₂₀)	0.0495	F(γ ₂ q ₂₉)	0.085
F(Rq ₂₀)	-0.099	F(γ ₂ q ₃₀)	0.1472
F(R) ^o	0.633	F(γ ₃ q ₃₀)	-0.1472
F(R) ^m	-0.442	F(R ₁ R)	0.2506
F(R) ^p	0.440	F(Rβ')	0.5415

Table 5.6 Observed and calculated frequencies (in cm^{-1}) and potential energy distribution of sPS

IR	Polarization	Raman	Symmetry Species	Calculated	Potential Energy Distribution
3083	\perp			3092	r(99)
				3092	r(99)
				3081	r(100)
				3081	r(100)
				3071	r(100)
				3071	r(100)
3062	\perp	3062		3062	r(100)
				3062	r(101)
		3055		3054	r(100)
				3054	r(101)

Table 5.6 continued

IR	Polarization	Raman	Symmetry Species	Calculated	Potential Energy Distribution
2922	⊥			2929	d(95)
				2928	d(100)
		2906		2905	s(98)
				2903	s(95)
2846	⊥	2849		2856	d(100)
				2855	d(99)
				1647	T(74),β(17),q20(6),q21(5),R(5)
1601	⊥	1604	B ₂	1647	T(74),β(17),q20(6),q21(5),R(5)
				1566	T(86),β(21),q20(6),q21(5)
1583	⊥	1584	B ₂	1566	T(86),β(21),q20(6),q21(5)
1493	⊥			1505	β(52),T(38),R(9)

Continued next page

Table 5.6 continued

IR	Polarization	Raman	Symmetry Species	Calculated	Potential Energy Distribution
				1503	$\beta(55), T(38), R(8)$
				1459	$\delta(49), \beta(22), \gamma(15), T(12)$
1452	\perp	1454	B_2	1454	$\beta(56), T(34)$
				1453	$\delta(77), \gamma(21)$
				1450	$\beta(38), \delta(27), T(23), \gamma(7)$
1376	\perp	1375	A_1	1370	$\gamma(29), \beta(28), \zeta(22), R(15), T(8)$
				1358	$\beta(46), \zeta(30), T(13), R(12), S(6)$
1347	\parallel	1347	B_1	1357	$\zeta(42), \gamma(43), S(42)$
1334	\perp	1331	B_2	1330	$\zeta(64), \gamma(18), S(6)$
				1323	$\beta(74), T(13), \gamma(12)$
		1320	A_2	1323	$\gamma(58), \beta(25), T(8), S(8), \zeta(7)$
				1311	$T(76), \beta(36), \gamma(28)$

Continued next page

Table 5.6 continued

IR	Polarization	Raman	Symmetry Species	Calculated	Potential Energy Distribution
		1303	A ₁	1303	T(136), β (18), γ (9)
1279	\perp		B ₂	1279	T(69),R(19), β (18), γ (14), ϕ (5)
1253	\perp			1237	R(23), β (12), ζ (12),S(11),T(10), γ (9),q19(8), ω (5), ϕ (5)
1222		1222	B ₁	1235	γ (54), ζ (45),S(7)
		1205	A ₁	1210	ζ (34),R(14),T(14), β (12),q19(9), γ (8)
				1189	β (80),T(9)
1181	\perp	1182	B ₂	1189	β (78),T(10)
				1163	β (79),T(15)
				1163	β (80),T(17)
1155	\perp	1156	B ₂	1156	γ (73), ζ (19),S(14)

Continued next page

Table 5.6 continued

IR	Polarization	Raman	Symmetry Species	Calculated	Potential Energy Distribution
1092	⊥			1154	ζ(52), T(17), γ(25), β(8), S(8)
				1091	S(58), γ(23), φ(13)
				1084	T(28), β(26), S(17), γ(11)
				1080	S(32), ω(14), φ(13), q19(8), γ(6), β(6)
1069	⊥	1072		1065	T(50), β(32)
				1049	S(42), T(26), β(11), γ(9)
				1031	S(76), ζ(11), γ(8), φ(5)
				1024	T(52), β(20), q19(12)
1028	⊥	1031	A ₁	1021	T(49), q19(21), β(16)
				990	q19(47), T(46)
1004	⊥	1002	A ₁	990	q19(57), T(35)

Continued next page

Table 5.6 continued

IR	Polarization	Raman	Symmetry Species	Calculated	Potential Energy Distribution
				982	$\mu(136), q28(29)$
				982	$\mu(135), q28(28)$
				976	$\gamma(27), T(25), \zeta(16), S(14), q19(5)$
				964	$\mu(126), q30(12)$
				964	$\mu(126), q30(12)$
901			B ₁	911	$\mu(117), q28(14), q29(9), M(8)$
				909	$\mu(120), q28(13), q29(9), M(7)$
				854	$\gamma(64), \zeta(14), \phi(5), \mu(6)$
				839	$\mu(113)$
				839	$\mu(113)$
				776	$q28(83), \mu(43), M(31)$

Continued next page

Table 5.6 continued

IR	Polarization	Raman	Symmetry Species	Calculated	Potential Energy Distribution
		773	A ₁	760	R(26), T(23), q20(25), q19(11), ϕ (5)
750			B ₁	759	q28(86), μ (52), M(28), γ (11)
				751	q20(26), R(22), T(21), q19(9), γ (8), ϕ (5)
				697	μ (101), q28(49)
695			B ₁	696	μ (94), q28(61)
		622	B ₂	626	q21(80)
				622	q21(87)
				610	q28(44), ω (32), μ (18), ϕ (19), q29(8), ζ (7), S(6)
				556	q20(40), ϕ (29), R(11), Φ (9), T(6)
				548	ϕ (37), q20(33), q21(9), ζ (7), γ (6), Φ (6)
538			B ₁	536	q29(52), q28(30), M(28), μ (23), ϕ (20)

Continued next page

Table 5.6 continued

IR	Polarization	Raman	Symmetry Species	Calculated	Potential Energy Distribution
525		B ₂	508	$\varphi(26), \gamma(20), q20(19), \zeta(14), R(14), \Phi(12), \tau(7)$	
			465	$q29(86), M(37), \omega(26)$	
403		A ₁	402	$q30(159), \mu(28)$	
			402	$q30(159), \mu(28)$	
			396	$\Phi(27), q20(25), \varphi(15), T(7)$	
			327	$q29(78), \varphi(37), M(10), \mu(9), \tau(7)$	
232			257	$\varphi(53), q20(12), R(9), S(6)$	
			207	$q29(58), \varphi(16), \omega(16), \mu(14), M(5), q28(5)$	
			201	$\Phi(77), \varphi(15), \zeta(8), R(6)$	
177		A ₁	177	$\tau(36), M(27), q29(20), \mu(10)$	
			144	$\Phi(57), \varphi(19), R(14), \zeta(9), \tau(6)$	

Continued next page

Table 5.6 continued

IR	Polarization	Raman	Symmetry Species	Calculated	Potential Energy Distribution
				46	$\tau(38), M(24), Z(16), \phi(14)$
				40	$M(45), \phi(42), \omega(8)$
				36	$Z(93)$
				35	$Z(79), \tau(16)$
				20	$\tau(91)$

Results and Discussion

The goal of this analysis is to predict the frequencies and potential energy distribution of the infrared and Raman active bands and to correlate these with the observed spectra for use in structural analysis. We are particularly interested in the assignments of bands which are sensitive to the all trans chain conformation, which appears upon annealing at 200°C or upon drawing. Dramatic spectral changes are observed and are shown in Figure 5.5. Several localized modes assigned to ring vibrations are insensitive to the chain conformation. We are also interested in the degree of coupling of the ring to the backbone vibrations for the conformation sensitive bands in comparison to isotactic polystyrene.

Polarized infrared spectra of coextruded and annealed sPS are shown in Figures 5.6 through 5.8. Polarized Raman spectra obtained with scattering geometry A are shown in Figures 5.9 through 5.11. Raman spectra obtained with geometry B are shown in Figures 5.12 through 5.14. Several localized ring vibrations may be assigned upon comparison of frequencies calculated for sPS with those for toluene. Some of these calculated bands are found at 1647, 1566, 1505, 1323, 1303, 1189, and 1163 cm^{-1} . These modes all involve ring CC stretching and CH in-plane bending and many of these are also observed in atactic and isotactic polystyrene. The 1647 and 1566 cm^{-1} bands observed in the infrared at 1601 and 1584 cm^{-1} , respectively, have the same calculated frequencies in toluene. The agreement for these two bands is much less than satisfactory.²⁶ However this result is consistent with an earlier study where the nonredundant force constants were applied.¹⁸ These two bands show the worst agreement with the observed values aside from the CH stretching region which has never been successfully analyzed for aromatic materials. This region is shown in Figure 5.6, with all the CH stretching modes showing perpendicular polarization in the infrared.

The 1601 and 1584 cm^{-1} ring bands show high intensity for the ZX polarization for scattering geometry A and nearly identical intensity for the YY and ZY polarizations for

FIGURE 5.5 Infrared spectra of sPS (a) solution cast film, (b) after annealing at 295°C for 0.5 hours, and (c) coextruded at 100°C to a draw ratio of 4; inset region (1) cast film, (2) at liquid nitrogen temperature, (3) annealed at 200°C for 1 hour, and (4) annealed at 200°C and measured at liquid nitrogen temperature.

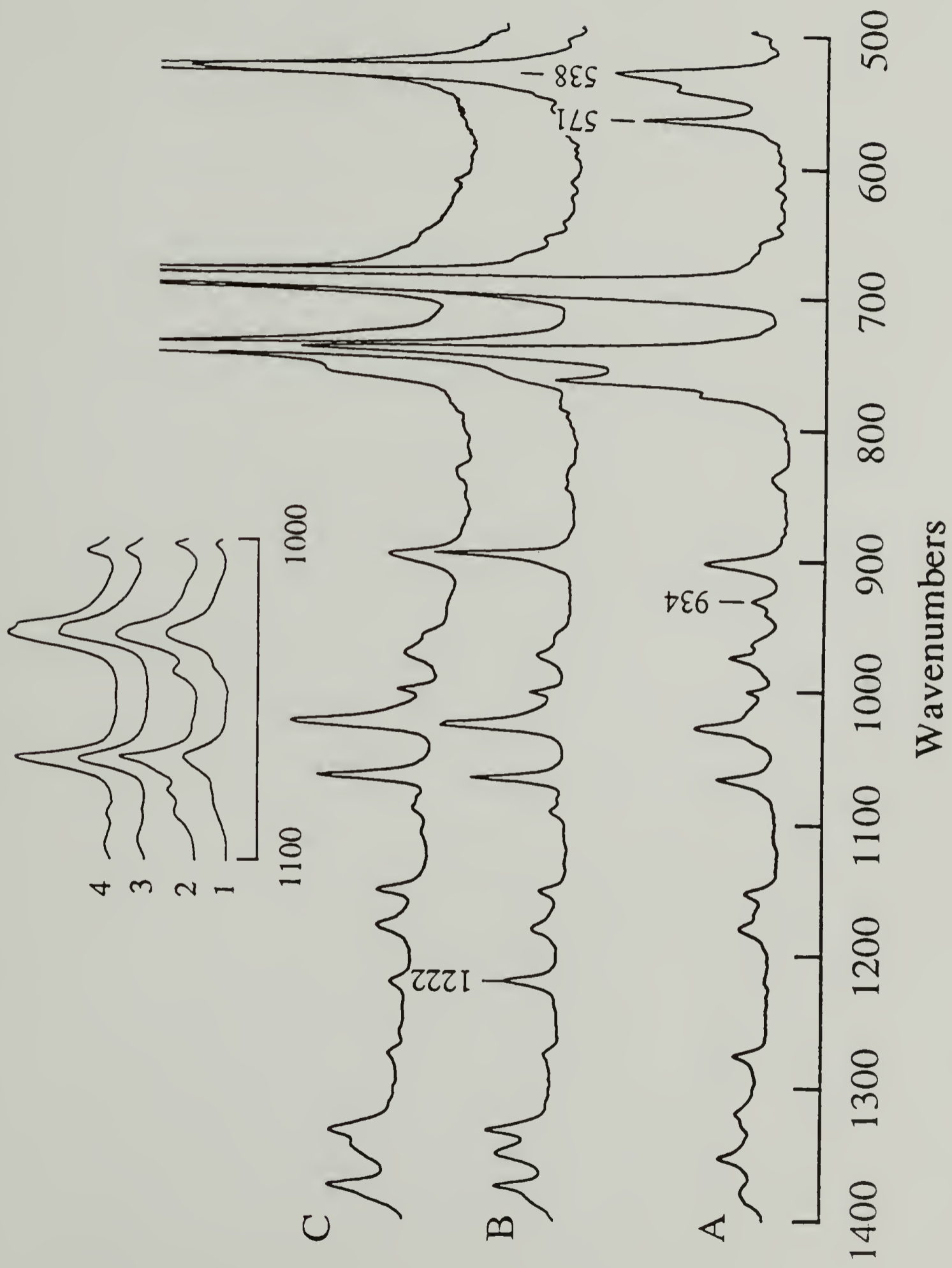


FIGURE 5.6 Polarized infrared spectra of coextruded sPS before and after annealing at 200°C. (3100 - 2800 cm^{-1}) Perpendicular polarization (—); parallel polarization (-----).

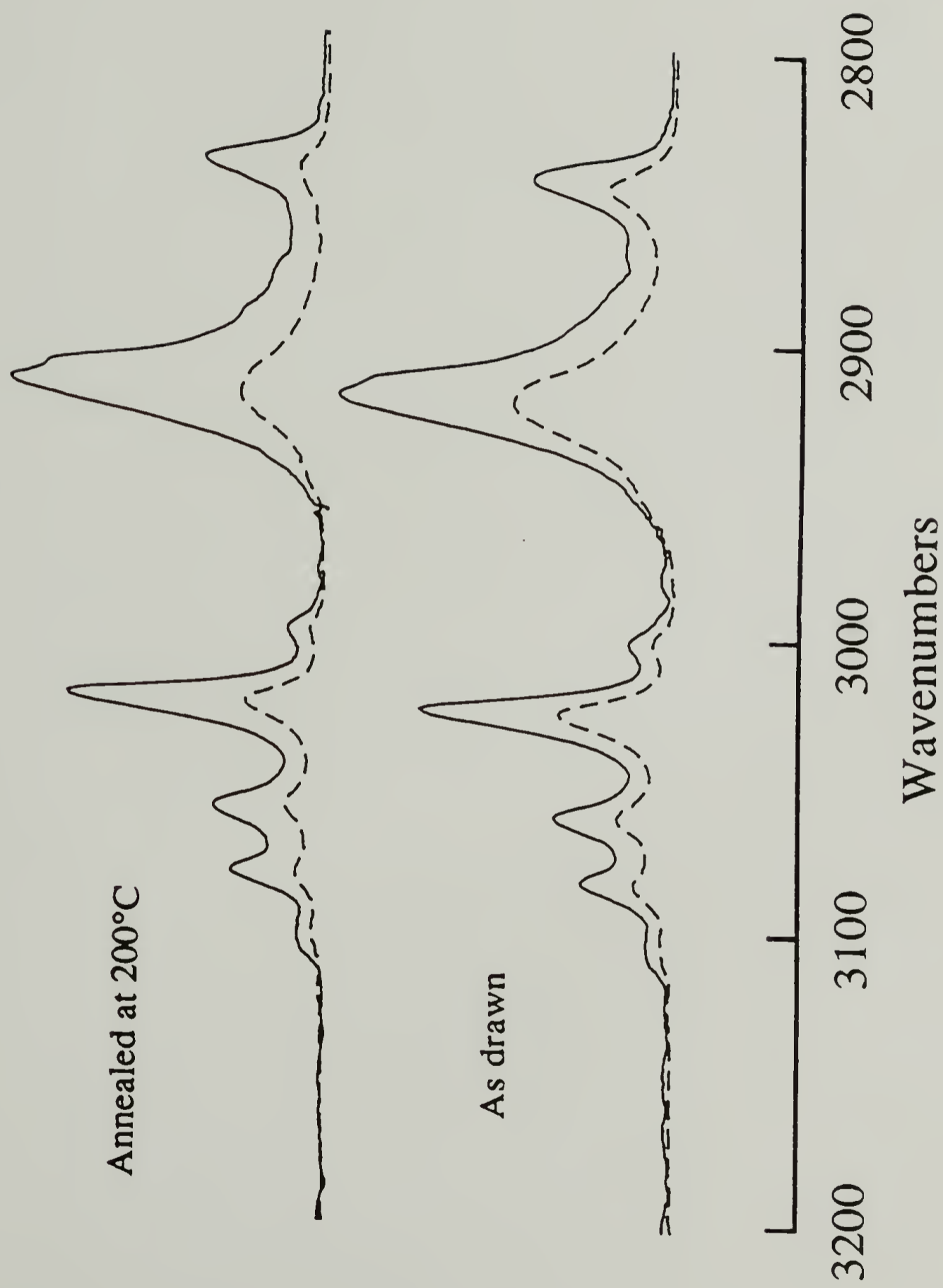


FIGURE 5.7 Polarized infrared spectra of coextruded sPS before and after annealing at 200°C. (1700 - 1000 cm^{-1}) Perpendicular polarization (——); parallel polarization (-----).

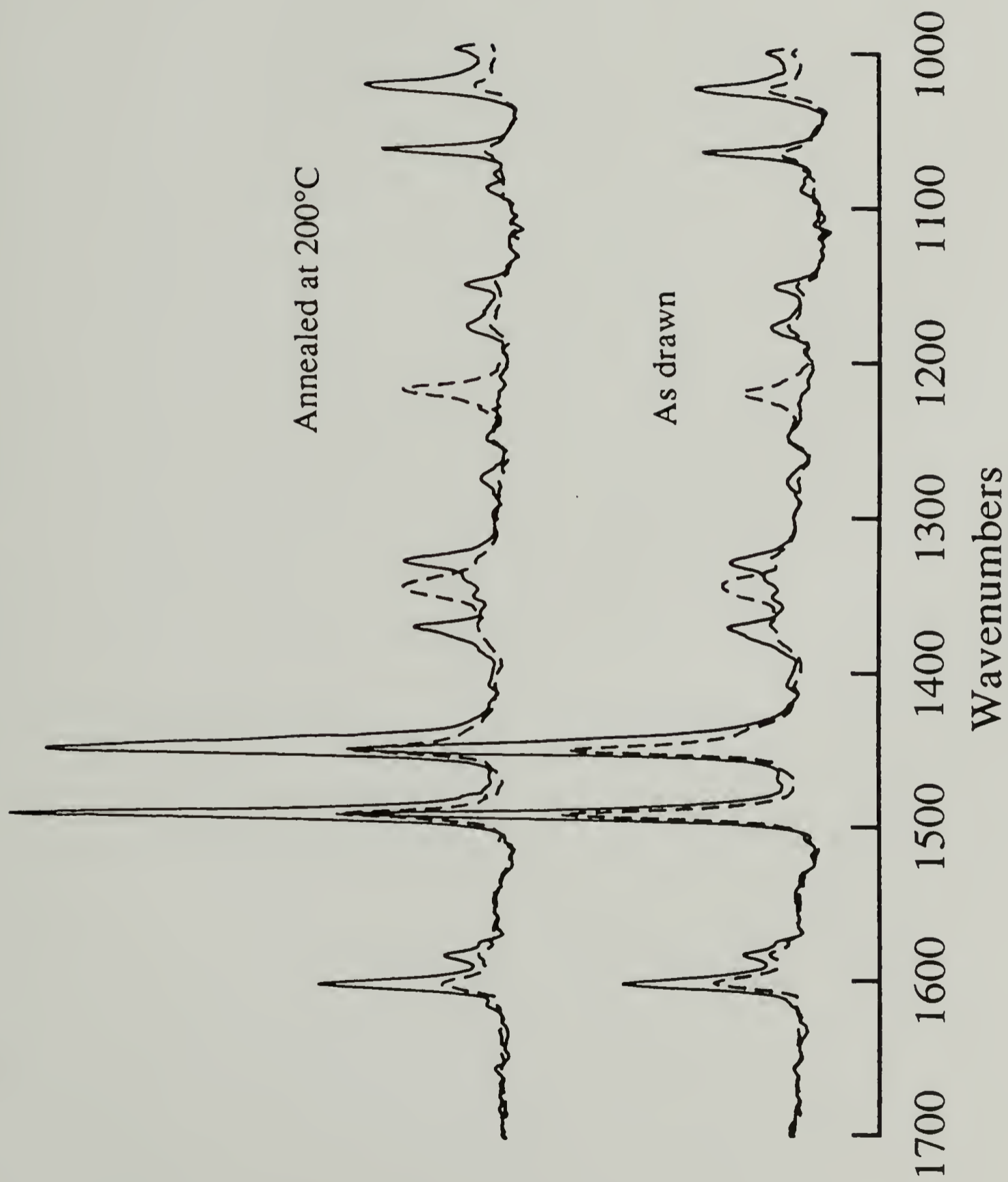


FIGURE 5.8 Polarized infrared spectra of coextruded sPS before and after annealing at 200°C. (1000 - 500 cm^{-1}) Perpendicular polarization (—); parallel polarization (-----).

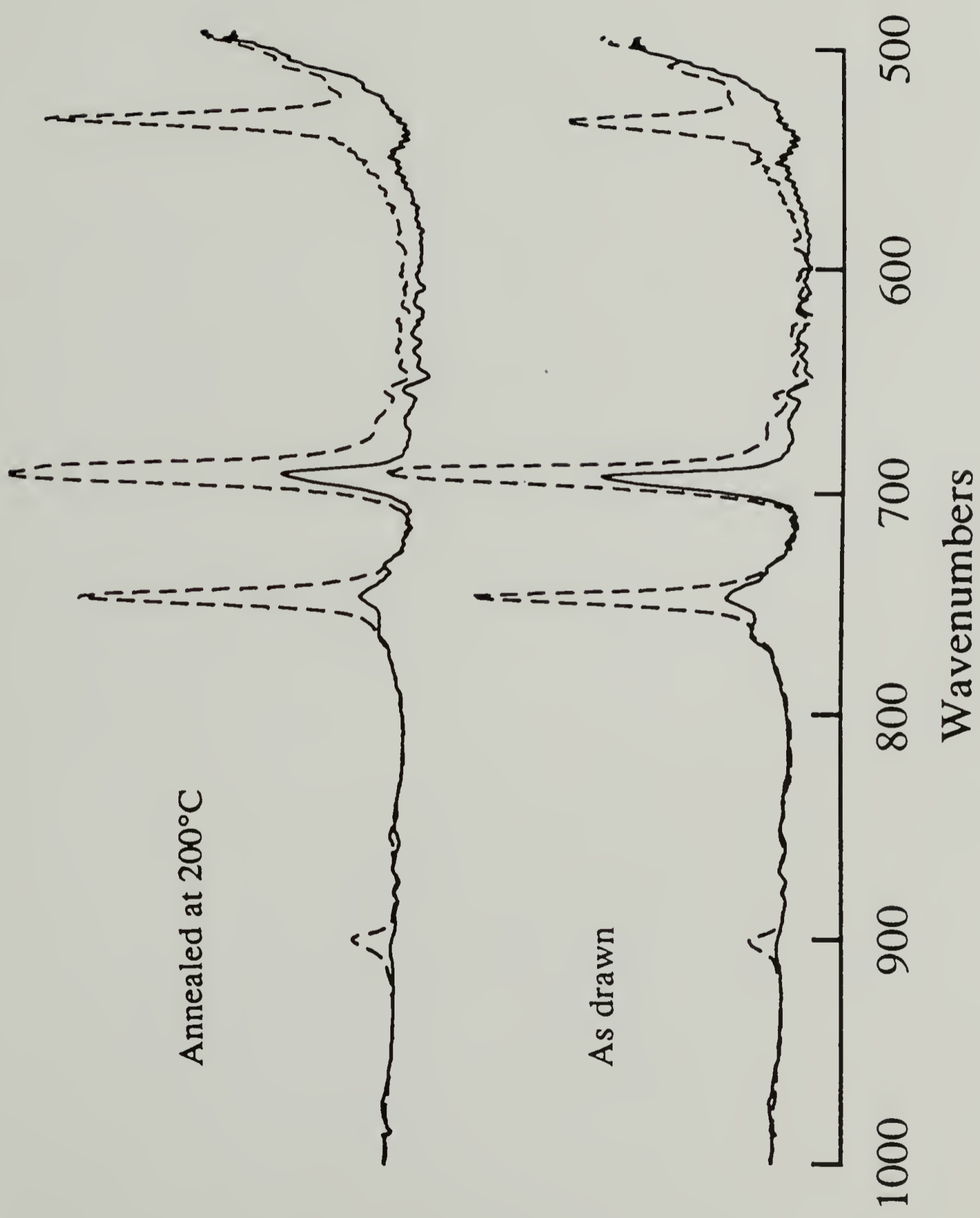


FIGURE 5.9 Polarized Raman spectra (scattering geometry A) of coextruded sPS after annealing at 210°C for 3 hours. (1700 - 1100 cm^{-1}).

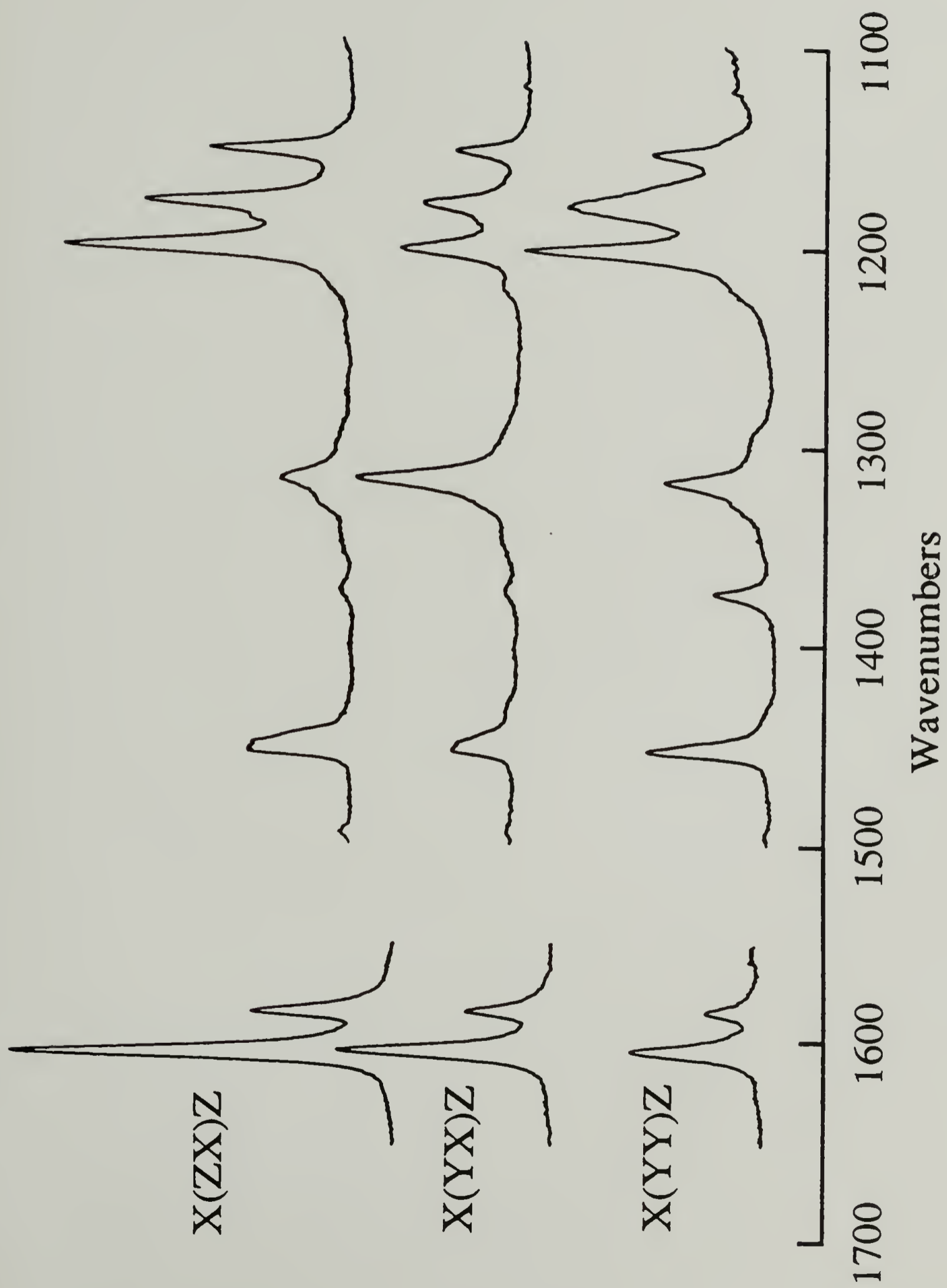


FIGURE 5.10 Polarized Raman spectra (scattering geometry A) of coextruded sPS after annealing at 210°C for 3 hours. (1100 - 900 cm^{-1}).

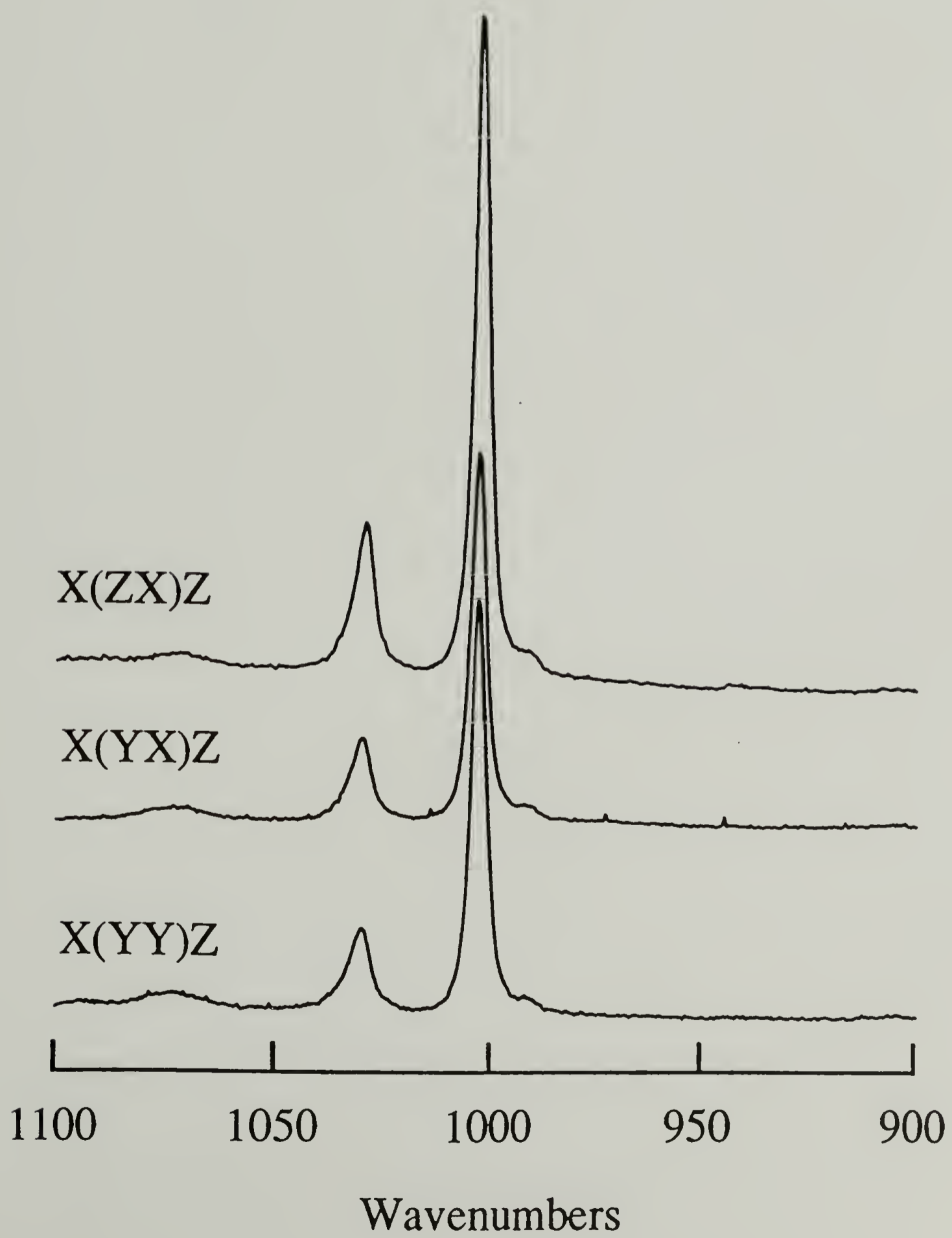


FIGURE 5.11 Polarized Raman spectra (scattering geometry A) of coextruded PS after annealing at 210°C for 3 hours. (900 - 100 cm^{-1}).

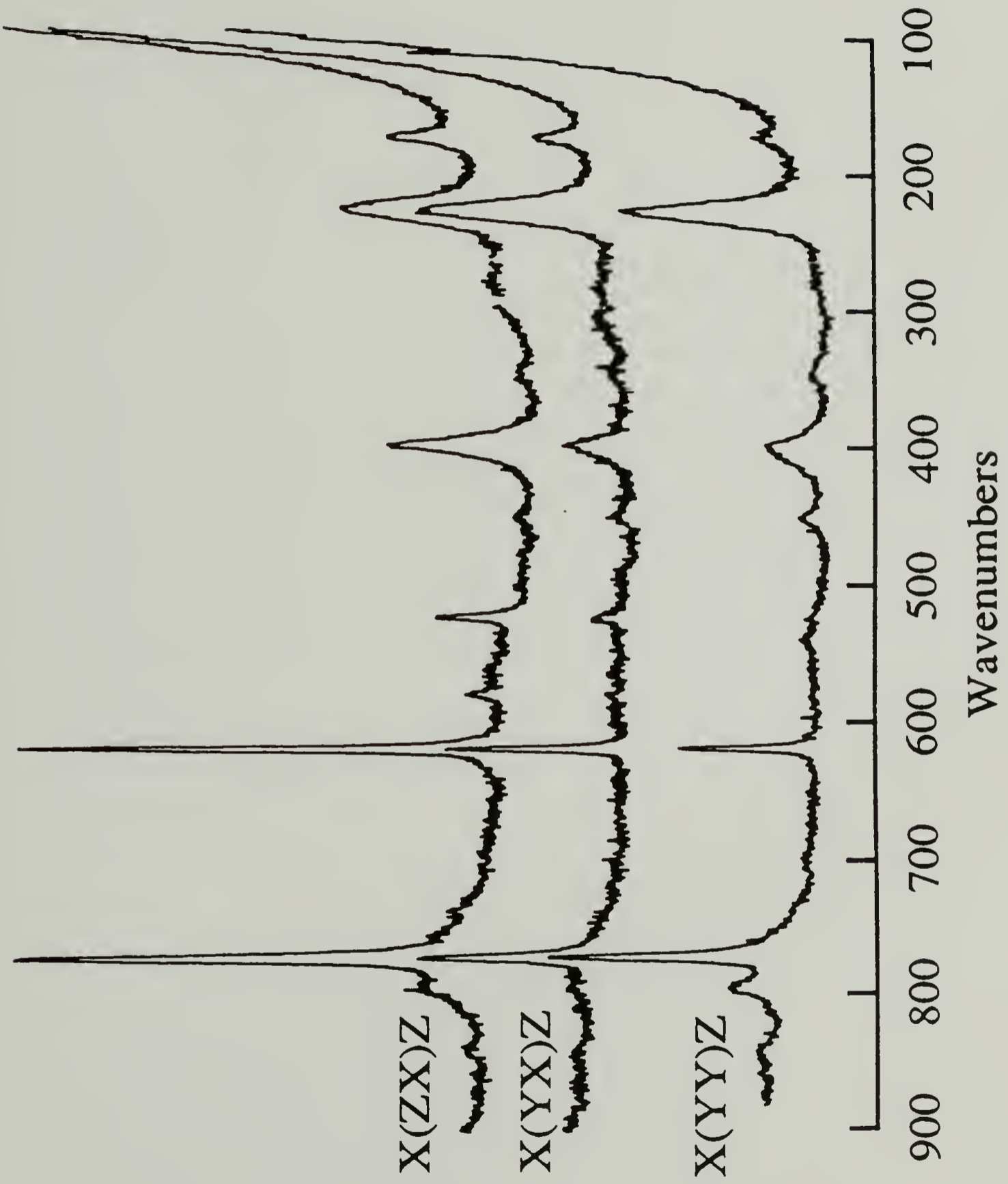


FIGURE 5.12 Polarized Raman spectra (scattering geometry B) of coextruded sPS after annealing at 210°C for 3 hours. (1700 - 1100 cm^{-1}).

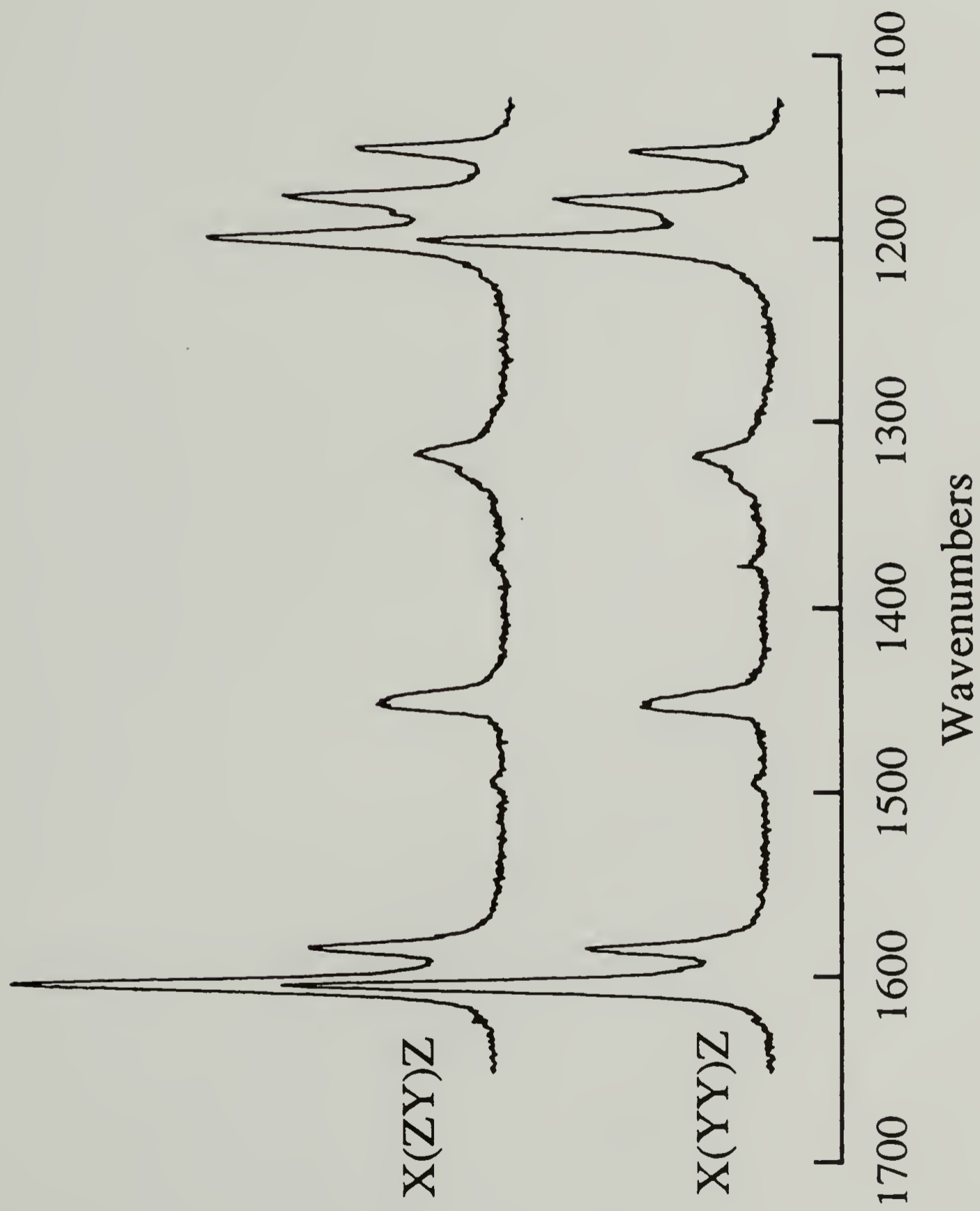


FIGURE 5.13 Polarized Raman spectra (scattering geometry B) of coextruded sPS after annealing at 210°C for 3 hours. (1100 - 900 cm^{-1}).

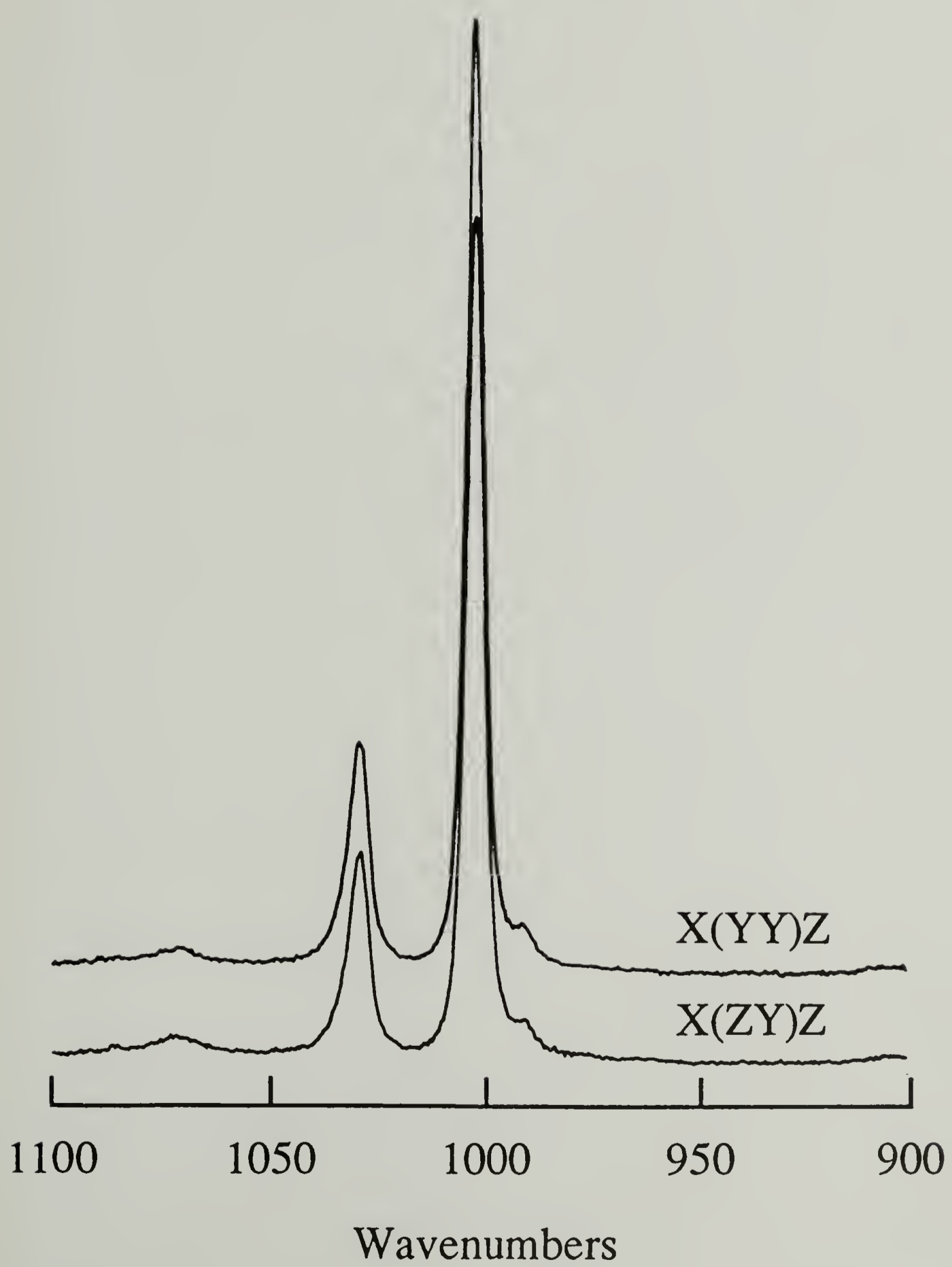
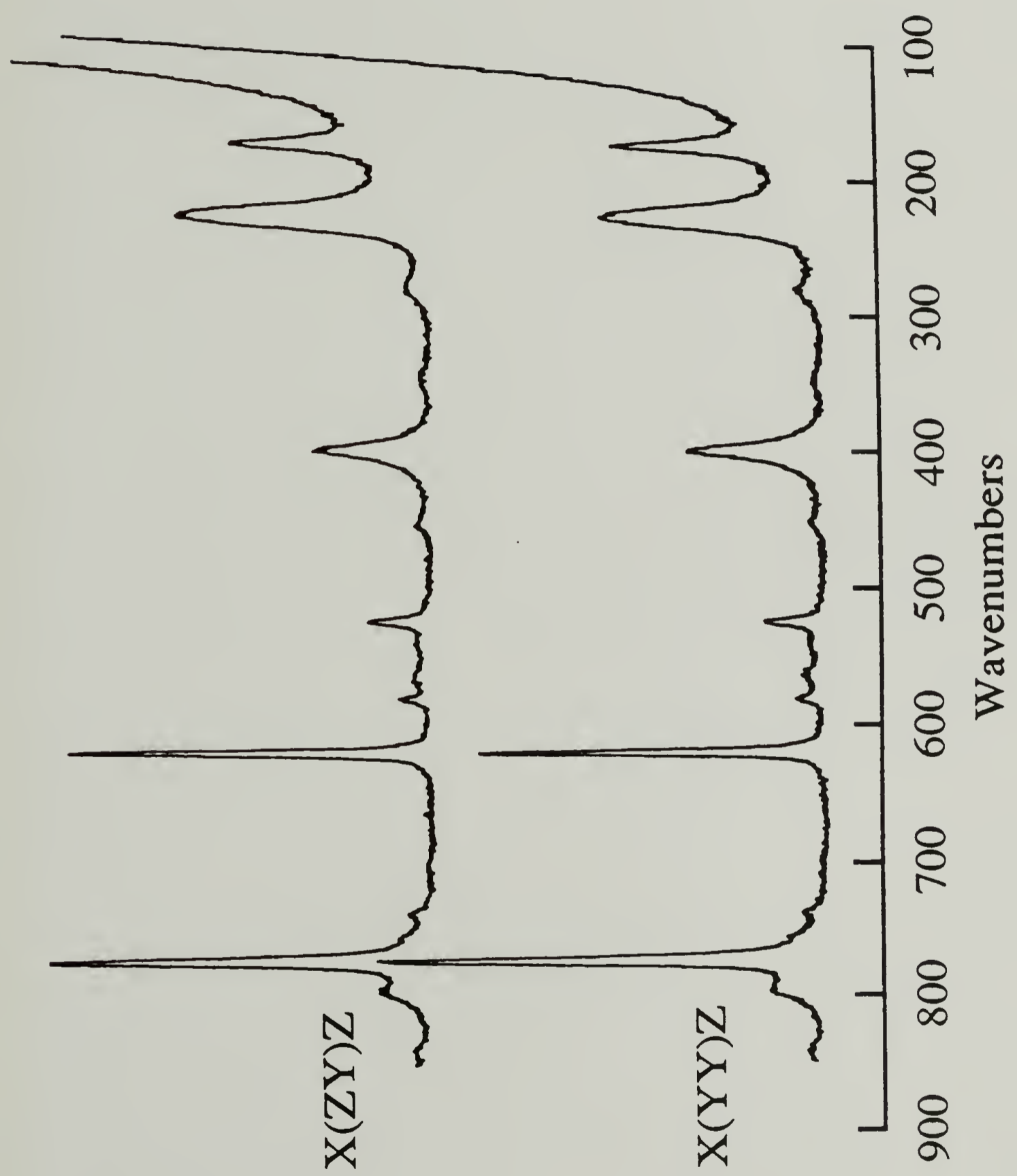


FIGURE 5.14 Polarized Raman spectra (scattering geometry B) of coextruded sPS after annealing at 210°C for 3 hours. (900 - 100 cm^{-1}).



geometry B, and therefore belong to the B_2 symmetry species. In a previous analysis of atactic polystyrene the 1601 and 1584 cm^{-1} bands were assigned to the B_1 and A_1 symmetry species. These assignments were made based on the symmetry analysis of monosubstituted benzenes in which the substituent, which represents the chain backbone, has no symmetry. A C_2 symmetry axis exists along the 1 and 4 carbons of the ring. However syndiotactic polystyrene has C_{2v} symmetry with the C_2 axis bisecting the CH_2 group. Because of the different position of the symmetry axis compared to monosubstituted benzenes, many of the symmetry species assignments are different.

Modes calculated at 1505 and 1323 cm^{-1} and assigned to CH in-plane bending and CC stretching are close in frequency to the corresponding toluene bands at 1495 and 1327 cm^{-1} , respectively. The latter appears in the Raman spectrum of sPS at 1320 cm^{-1} and shows higher intensity for the XY polarization with geometry A indicating it belongs to the B_1 or A_2 symmetry species. This band does not appear in the infrared and since the A_2 species is infrared inactive for C_{2v} symmetry, the 1320 cm^{-1} band may be tentatively assigned to the A_2 species.

Chain backbone vibrations are usually found in the 900 - 1200 cm^{-1} region and here substantial differences are seen in the spectra for different tacticities. One unique feature for sPS is the 1222 cm^{-1} band which shows strong parallel polarization. As mentioned in Chapter IV, it does not appear for the atactic and isotactic isomers. This band has a transition dipole moment parallel to the chain axis, as seen from the parallel polarization shown in Figure 5.7, and is present only upon annealing or drawing. Therefore it is due to a sequence of trans conformations. It is assigned to CCH bending of the CH_2 and CH groups parallel to the chain axis, and CC backbone stretching, and belongs to the B_1 symmetry species.

Several of the bands which are sensitive to chain conformation involve coupling of the ring vibrations to the backbone modes. The 1376 cm^{-1} band appears strongly in the Raman for the YY polarization for geometry A and belongs to the A_1 symmetry species. It

some of these bands may be assigned. Bands in this region, with the exception of the 403 cm^{-1} ring mode, all involve significant coupling of the chain to the backbone vibrations. This has also been observed for isotactic PS in which these vibrations are also highly conformation sensitive. A weak Raman band is observed at 527 cm^{-1} with ZX polarization (geometry A), and with equal intensity for YY and ZY polarization (geometry B) and is therefore assigned to the B_2 symmetry species. This band involves coupling of the ring to backbone and is predominantly backbone skeletal and CCH bending, and also ring asymmetric torsion.

A band observed at 403 cm^{-1} is assigned to ring asymmetric torsion and CH out-of-plane bending, and agrees well with the calculated frequency of 402 cm^{-1} . This band shows slightly greater intensity for the ZX polarization and is assigned to the B_2 symmetry species. This localized ring mode appears at 401 cm^{-1} in the toluene calculation and is also seen in atactic and isotactic PS. A broad intense Raman band observed at 232 cm^{-1} may correspond to the mode calculated at 257 cm^{-1} involving coupling of the backbone bending and asymmetric torsion, along with chain CC and CC' ring-chain stretching. It does not show significant polarization. Finally a band appears at 177 cm^{-1} , showing greater intensity for ZX polarization (geometry A) and for YY polarization (geometry B), thus belonging to the A_1 symmetry species. For isotactic polystyrene a band is observed at 225 cm^{-1} involving ring in-plane bending,¹³ which agrees with the present assignment for the 177 cm^{-1} band in sPS.

Conformation Sensitive Bands

As shown in Figure 5.5, significant changes in the infrared spectra occur upon annealing near 200°C or drawing a cast film indicating a change in the chain conformation and packing of the molecules. Several bands disappear such as the 943, 934, 769, 571, and 548 cm^{-1} bands in the infrared and the 800 cm^{-1} band in the Raman. Other features

appear such as the 1376, 1334, 1222 and 548 cm^{-1} bands. These frequency values are consistent with the calculated results. The 1376, 1334, 1222, and 548 cm^{-1} infrared bands which show increased intensity upon annealing or coextrusion can be correlated well with the calculated values. As previously stated, the 1376 and 548 cm^{-1} bands involve coupling of the ring to the backbone, while the 1334 and 1222 cm^{-1} bands are only associated with the chain backbone. Also appearing in the infrared with drawing or annealing is the weak 1092 cm^{-1} skeletal band. Some of the bands associated with the helical phase at 943, 934 (infrared), and 800 (Raman) cm^{-1} are not reproduced in the calculation. This supports the conclusion that these bands are not associated with the all trans conformation but with a structure containing gauche conformations.

The polarized infrared spectra in Figures 5.6 through 5.8 show a significant increase in dichroism upon annealing the free standing film at 200°C. Thus the overall segmental orientation increases even if the film is annealed without tension. This phenomena is very interesting since polyethylene shows a reduction in the overall orientation when annealed due to the relaxation of the amorphous regions.²⁸ Increases in orientation with annealing have also been observed for polypropylene²⁹ and for blends of polyvinylidene fluoride with poly(methyl methacrylate) as discussed in Chapter IV.³⁰ The increase in orientation for sPS is most likely also due to an increase in crystallinity upon annealing the drawn film. The crystalline orientation must be significantly higher than the amorphous orientation, and therefore an increase in crystallinity should increase the overall orientation. Oriented amorphous chains may be predominantly in an extended trans conformation. This conformation has been suggested to be the prevalent one for amorphous sPS.²² Therefore extended and oriented amorphous chains upon annealing should form oriented crystals. However it is not yet known how the amorphous orientation changes with annealing.

Calculation of Theoretical Modulus

Since the mechanical properties of sPS have yet to be reported, a determination of the theoretical modulus is desirable. Using the elastic rod model, the modulus E may be determined from the frequency of the longitudinal acoustic branch by the relationship

$$v = \frac{1}{2cL} \sqrt{\frac{E}{\rho}} \quad (5.1)$$

where L is the chain length, ρ is the density, and c is the speed of light. Strictly speaking, this calculation is only applicable to a chain of finite length L . However, we have calculated the acoustic branch by varying the phase angle of the equivalent vibration located at adjacent chemical repeats at approximately 0.5° increments from 0.5° to 4° . This phase angle is inversely proportional to the wavelength or the equivalent chain length, 875 - 112 Å respectively.³¹ In this fashion we can obtain the LAM frequency of various chain lengths, although the calculations are associated with an infinite chain. The density value of 1.00 g/cm^3 is determined from the crystal structure of Greis et al.⁴ A plot of the LAM dispersion curve is given in Figure 6.15. From the slope of this dispersion curve, a modulus value of 67 GPa is calculated. No theoretical or experimental modulus values have been reported as of yet. This value is based on the vibrational analysis of a single chain. Therefore the effects of intermolecular interactions, which would raise the modulus are not accounted for and this modulus value represents a lower limit. These interactions should be significant given the structure of Greis et al. consisting of a superstructure of clusters of three chains with overlapping of the phenyl rings. Such intermolecular interactions would produce a higher modulus value. However, the calculated value shown in this study, the lower limit, should provide a basis value for further investigations. This value is significantly lower than the value calculated for polyethylene of approximately 300

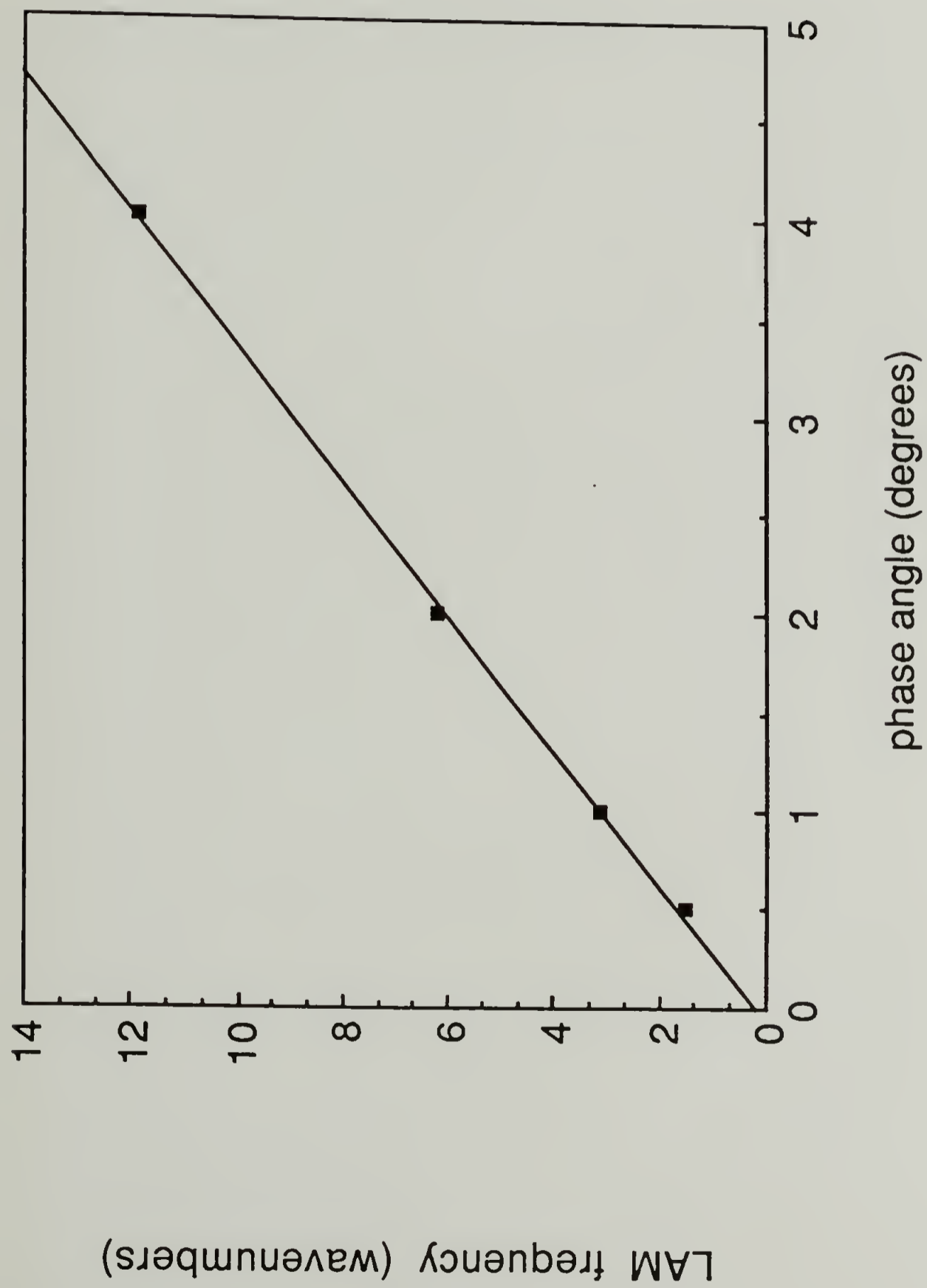


FIGURE 5.15 Dispersion curve of the longitudinal acoustic branch.

GPa. This is because the cross-sectional area of a polystyrene chain is significantly larger than that of a polyethylene chain due to the phenyl rings. Treloar's method has been employed in previous normal mode calculations without much success.¹⁸ When a reliable force field is available, normal vibrational analysis is the preferred method.

Conclusions

In this study a normal vibrational analysis has been performed for the trans planar form of syndiotactic polystyrene. A set of nonredundant symmetry coordinates was employed for the phenyl ring. No refinement has been made on the force constant set, yet the calculated frequencies agree well with the observed bands including polarization characteristics. Upon comparison with calculations on toluene, several localized conformation insensitive ring modes are identified. Comparison with the spectra of atactic and isotactic PS and previous normal coordinate analyses on isotactic PS shows features which are unique to the all trans structure of sPS. Bands such as the 1222 cm^{-1} band which only appear for the syndiotactic isomer in an annealed or drawn sample are identified in the calculation. Several bands involve significant coupling of the backbone and ring vibrations and some of these such as the 1374 and 538 cm^{-1} bands are sensitive to chain conformation.

Large intensity changes are observed upon annealing or drawing cast films, and several bands that are removed upon heating or drawing, such as the 943 and 934 cm^{-1} infrared bands and the 800 cm^{-1} Raman band are not reproduced by the calculation. This provides good evidence that these bands are representative of gauche conformations.

Solid-state coextrusion was found to be an effective method to produce highly oriented films for polarization studies. The high dichroism of the 1222 cm^{-1} skeletal band and the 538 cm^{-1} ring mode, both which are sensitive to trans conformations, suggests that the trans sequences have nearly perfect orientation. As the 538 cm^{-1} band is an out-of-plane ring mode the complete parallel polarization proves that the plane of the rings lies perpendicular to the chain axis, in agreement with previous studies. Annealing the freely standing drawn film results in a substantial increase in the segmental orientation. This orientation increase is thought to be due to the increase in crystallinity that occurs upon annealing.

The theoretical modulus has been calculated from the slope of the dispersion curve of the longitudinal acoustic branch near the Brillouin zone center at which the vibrations of adjacent repeat units are moving in phase. A value of 67 GPa was obtained. This value is based upon the vibrational modes of a single infinite chain, and does not include the effects of intermolecular interactions. However it should provide a basis value for further studies.

References

1. Ishihara, N.; Seimiya, T.; Kuramoto, M.; Uoi, M. *Macromolecules* **1986**, *19*, 2464.
2. Zambelli, A.; Longo, P.; Pellicchia, C.; Grassi, A. *Macromolecules* **1987**, *20*, 2035.
3. Kobayashi, M.; Nakaoki, T.; Uoi, M. *Polym. Prep., Jpn.* **1988**, *37*, E432.
4. Greis, O.; Xu, Y.; Asano, T.; Petermann, J. *Polymer* **1989**, *30*, 590.
5. Immirizi, A.; de Candia, F.; Iannelli, P.; Zambelli, A. *Makromol. Chem. Rapid Commun.* **1988**, *9*, 761.
6. Vittoria, V.; de Candia, F.; Iannelli, P.; Immirizi, A. *Makromol. Chem. Rapid Commun.* **1988**, *9*, 765.
7. Ishihara, N.; Kuramoto, M.; Uoi, M. *Macromolecules* **1988**, *21*, 3356.
8. Conti, G.; Santoro, E.; Resconi, L.; Zerbi, G. *Mikrochim. Acta* **1988**, *1*, 297.
9. Nyquist, R. A. *Appl. Spectrosc.* **1989**, *43*, 440.
10. Petermann, J. private communication.
11. Reynolds, N. M.; Savage, J. D.; Hsu, S. L. *Macromolecules* **1989**, *22*, 2867.
12. Painter, P. C.; Koenig, J. L. *J. Polym. Sci., Polym. Phys. Ed.* **1977**, *15*, 1885.
13. Snyder, R. W.; Painter, P. C. *Polymer* **1981**, *22*, 1633.
14. Liang, C. Y.; Krimm, S. *J. Polym. Sci.* **1958**, *27*, 241.
15. Jasse, B.; Monnerie, L. *J. Mol. Structure* **1977**, *39*, 165.
16. Pulay, P.; Fogarasi, G.; Boggs, J. E. *J. Chem. Phys.* **1981**, *74*, 3999.
17. Kim, P. K.; Hsu, S. L.; Ishida, H. *Macromolecules* **1985**, *18*, 1905.
18. Kim, P. K.; Chang, C.; Hsu, S. L. *Polymer* **1986**, *27*, 34.
19. Zachariades, A. E.; Mead, W. T.; Porter, R. S. *Chem. Rev.* **1980**, *80*, 351.
20. Yoon, D. Y.; Sundararajan, P. R.; Flory, P. J. *Macromolecules* **1975**, *8*, 776.
21. Doherty, D. C.; Hopfinger, A. J. *Macromolecules* **1989**, *22*, 2472.
22. Kobahaysi, M.; Nakaoki, T.; Ishihara, N. *Macromolecules* **1989**, *22*, 4377.

23. Wilson, E. B., Jr.; Decius, J. C.; Cross, P. G. *Molecular Vibrations The Theory of Infrared and Raman Vibrational Spectra*; Dover: New York, 1980; p.325.
24. Schlotter, N. E.; Rabolt, J. F. *Polymer* **1984**, 25, 165.
25. Snyder, R. G.; Schachtschneider, H. H. *Spectrochim. Acta* **1965**, 21, 169.
26. La Lau, C.; Snyder, R. G. *Spectrochim. Acta* **1971**, 27A, 2073.
27. Schachtschneider, H. H.; Snyder, R. G. *Spectrochim. Acta* **1963**, 19, 117.
28. Peterlin, A. *Colloid and Polymer Science* **1987**, 265, 357.
29. Samuels, R. J. *J. Polym. Sci., Polym. Phys. Ed.* **1979**, 17, 535.
30. Kaufmann, W.; Petermann, J.; Reynolds, N.; Thomas, E. L.; Hsu, S. L. *Polymer* **1989**, 30.
31. Snyder, R. G.; Schachtschneider, J. H. *Spectrochim. Acta* **1963**, 19, 85.

CHAPTER VI

A SPECTROSCOPIC STUDY OF PHASE TRANSITION KINETICS IN SYNDIOTACTIC POLYSTYRENE

Introduction

As described previously in Chapter IV, syndiotactic polystyrene (sPS) is an interesting material due to the presence of a solid-solid phase transition.¹⁻⁷ The transformation from the helical to the trans state is seen to occur upon heating to near 200°C or upon drawing.¹⁻⁷ It is irreversible except upon exposure to solvent vapors or immersion into solvents which will regenerate the helical structure.^{4,7-9} It has been observed that different solvents will give rise to unique helical crystal structures with differing chain packing arrangements. These studies also indicate the existence of at least two crystal packing orders for the all trans conformation as well.^{8,9} In this study, the transition will be shown to occur over a very narrow temperature range, which is unusual for high molecular weight polymers. An understanding of this phenomena is important as the trans phase is the most energetically favorable⁶ and should possess the highest mechanical properties. It is also a unique system in which to study a true crystal-crystal phase transition in polymers.

The energy barrier in transforming the helical TTGG conformation to the extended trans state has been calculated to be 2-3 kcal/mole from conformational analysis and molecular dynamics simulations.⁶ It is desirable to measure the transition kinetics upon heating and to discover what factors control the rate in order to gain insight into its mechanism. In this study the rate of structural transformation from the helical to the trans phase is determined by monitoring the infrared intensity of bands associated with each phase as a function of time and temperature. Infrared spectroscopy is a valuable technique for this investigation, since spectra may be obtained in less than one minute in order to

follow the rapid structural transformation. The evolution of the trans phase will be measured for samples as a function of annealing temperature in order to determine the dependence of the transition rate on the thermal history. A nucleation and growth model will be applied to describe the formation of the trans structure. This process involves the transition of helical crystal phase to the trans phase as well as crystallization of amorphous material.

Experimental

Polystyrene samples which are greater than 98% syndiotactic ($M_n = 125,000$, $M_w = 660,000$) were obtained from Dow Chemical Co. Films were cast in aluminum pans from a 1% solution in toluene and dried under vacuum. Samples were annealed under vacuum at 120°, 150°, and 170°C. The absence of solvent in these films was confirmed by infrared spectra. Melt quenched samples were obtained by heating films to 290°C under nitrogen atmosphere and quenching into a bath of cyclohexane and liquid nitrogen. The amorphous structure of these samples was confirmed by WAXS scans collected with a Siemens D500 diffractometer operating at a 2θ range from 3° to 40°. These X-ray scans appeared identical to those of atactic polystyrene. Infrared spectra were obtained with a Bruker IFS 113v FTIR spectrometer. Samples were heated in a heating cell constructed in our laboratory, and controlled by an Omega 6000 temperature controller. In order to obtain spectra rapidly during kinetics measurements, 20 to 50 scans were collected at 2 cm^{-1} resolution. DSC measurements were made with a Perkin-Elmer DSC-7 calorimeter operating at a scan rate of 20°C/min.

Results and Discussion

A schematic structure of the two known conformations of sPS are given in Figure 6.1. In this study the transition from the helical to the trans conformation is monitored by the intensity of bands at 1222 cm^{-1} for the all trans state, and at 943 and 934 cm^{-1} for the helical conformation. Integrated intensity values were measured and were normalized for variations in sample thickness with the integrated intensity of the 1601 and 1585 cm^{-1} bands. These bands are due to CC stretching in the phenyl ring and are insensitive to thermal treatment or tacticity. All of the bands described were shown previously in Figure 5.5. Infrared bands are frequently associated with specific conformational sequences. However, the fact that these particular bands are completely absent in quenched amorphous samples, which must contain a large distribution of conformations, indicates that these features are sensitive to long conformational sequences found in the trans and helical crystal phases.

The variation of intensity of the 1222 cm^{-1} trans isomer band at different temperatures is shown in Figure 6.2 for samples annealed at 150°C for 1 hour. A substantial intensity increase is observed to occur during the first few minutes of heating, followed by a very gradual increase at longer times. The initial rapid increase occurs within the first two minutes. The equilibrium intensity of this band measured at long times at each temperature is shown in Figure 6.3. This intensity increase occurs simultaneously with the intensity reduction of features due to the helical conformation, such as the 934 , 943 , and 869 cm^{-1} bands. These intensity changes can be seen in Figure 6.4.

From Figure 6.3, it is apparent that the trans content is observed to increase significantly at 192°C . This transition is extremely sharp, which is unusual as polymers generally exhibit diffuse phase transitions in the solid state such as the ferroelectric to paraelectric crystal transition discussed previously in Chapter II for the PVDF-TrFE

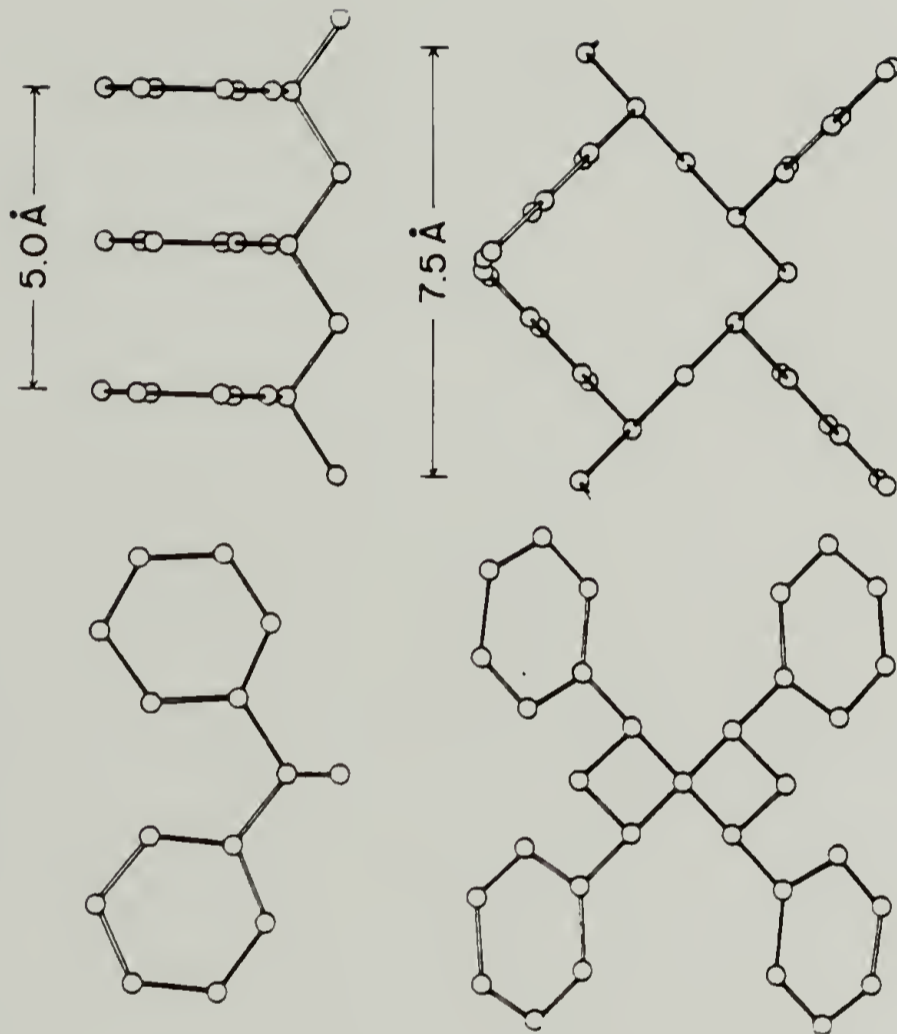


FIGURE 6.1 Schematic diagram of different conformations of syndiotactic polystyrene. (from ref. 7)

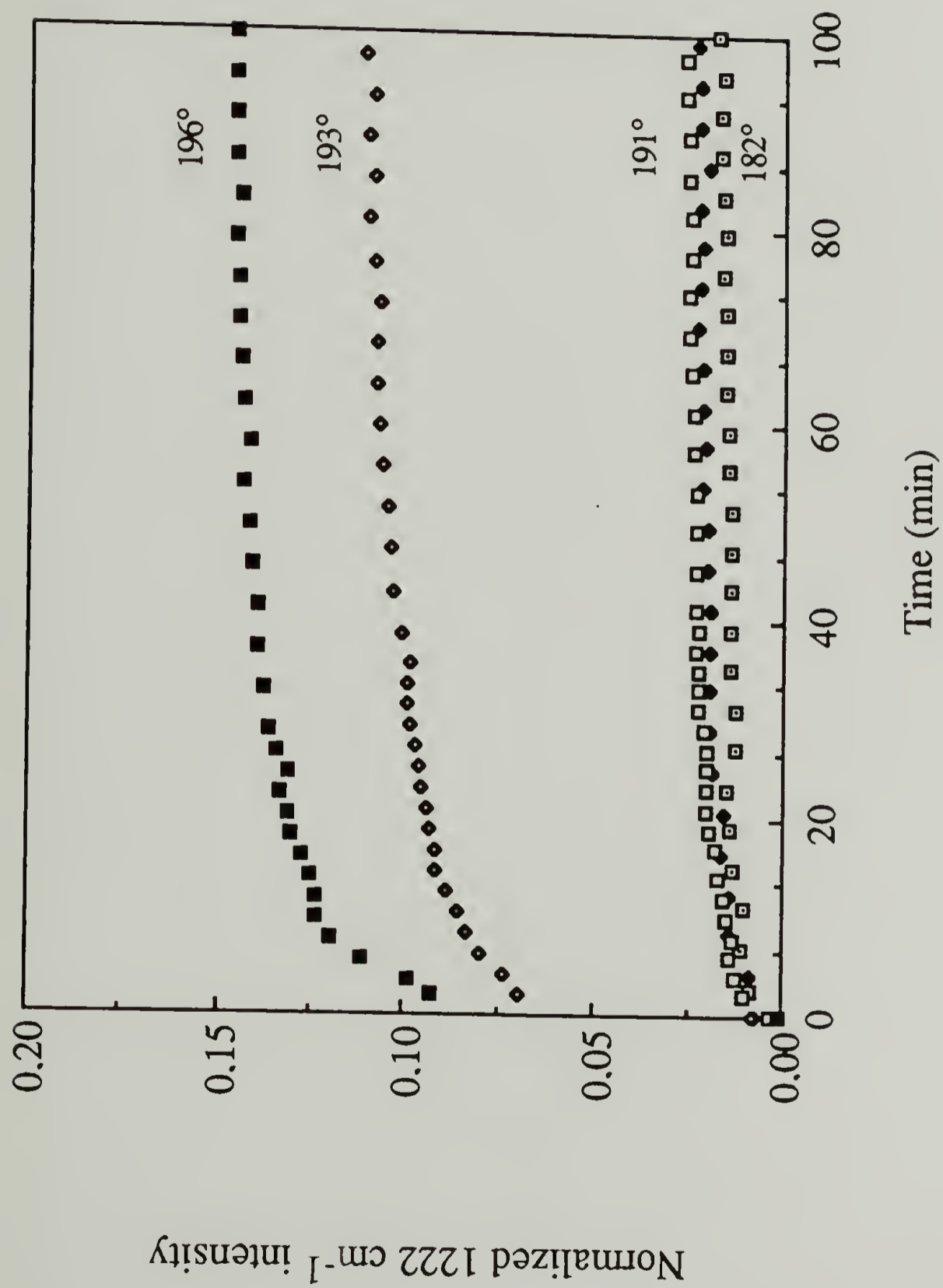


FIGURE 6.2 Integrated intensity of the 1222 cm^{-1} trans band with time at temperatures for a sample annealed at 150°C .

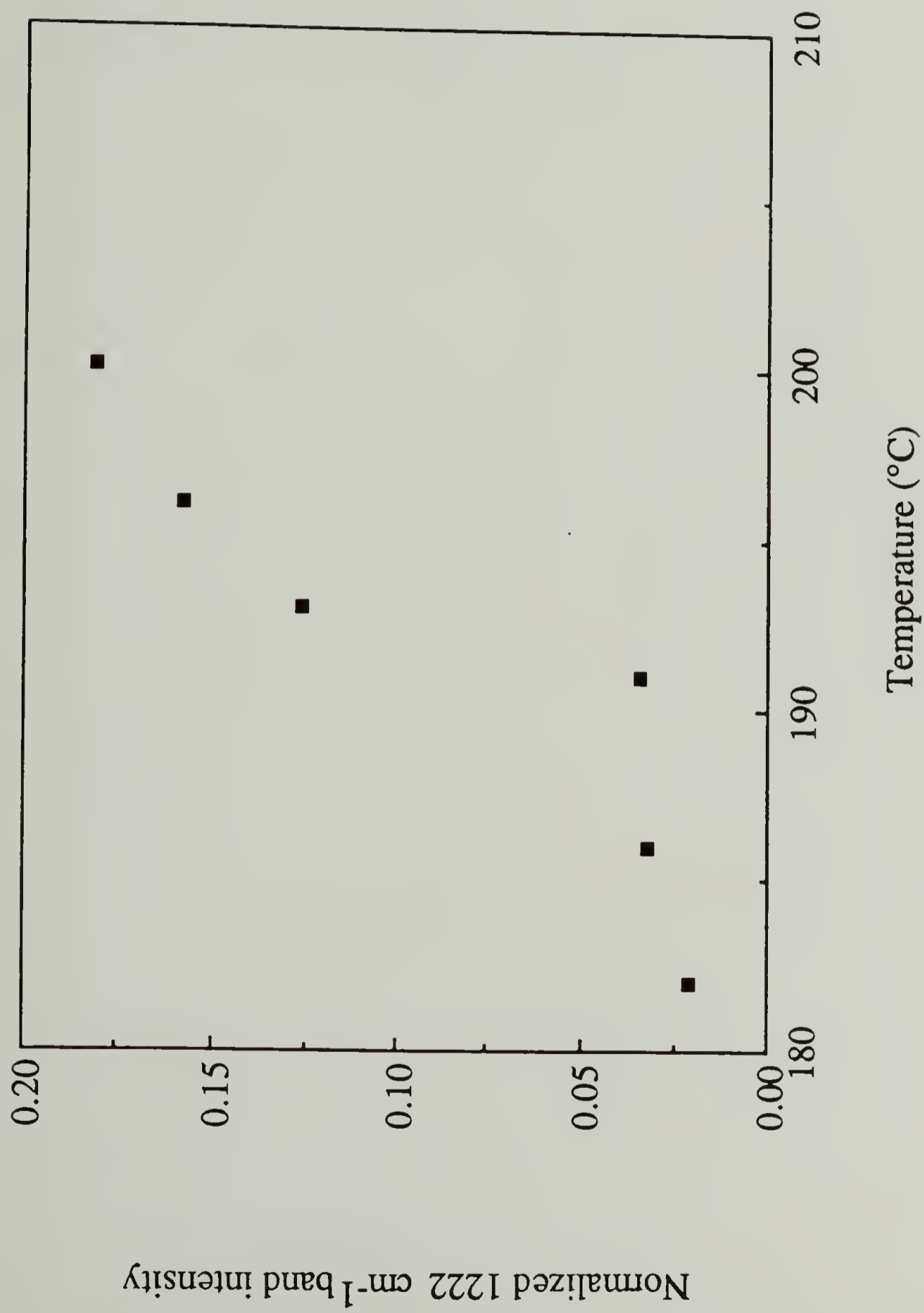


FIGURE 6.3 Integrated intensity of the 1222 cm⁻¹ band measured at equilibrium at various temperatures for a sample annealed at 150°C.

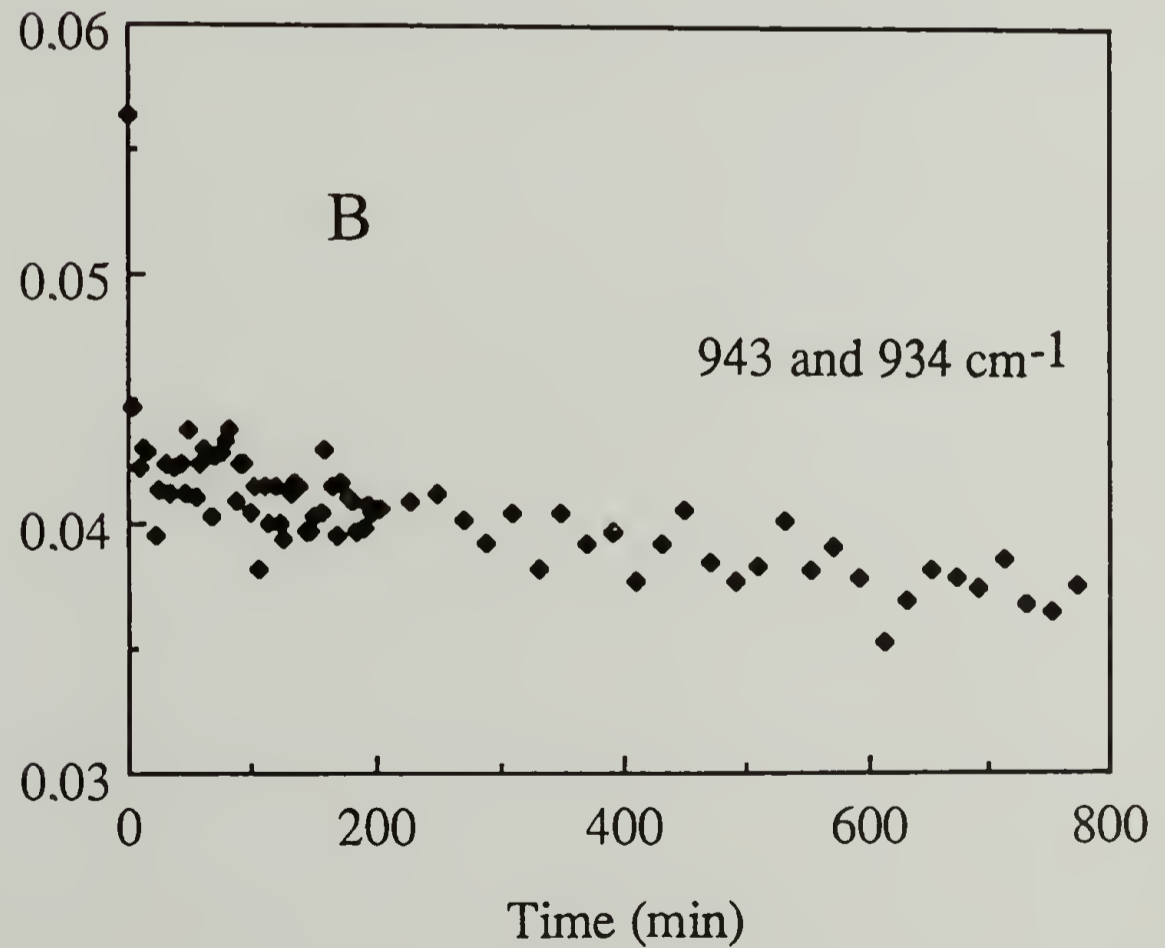
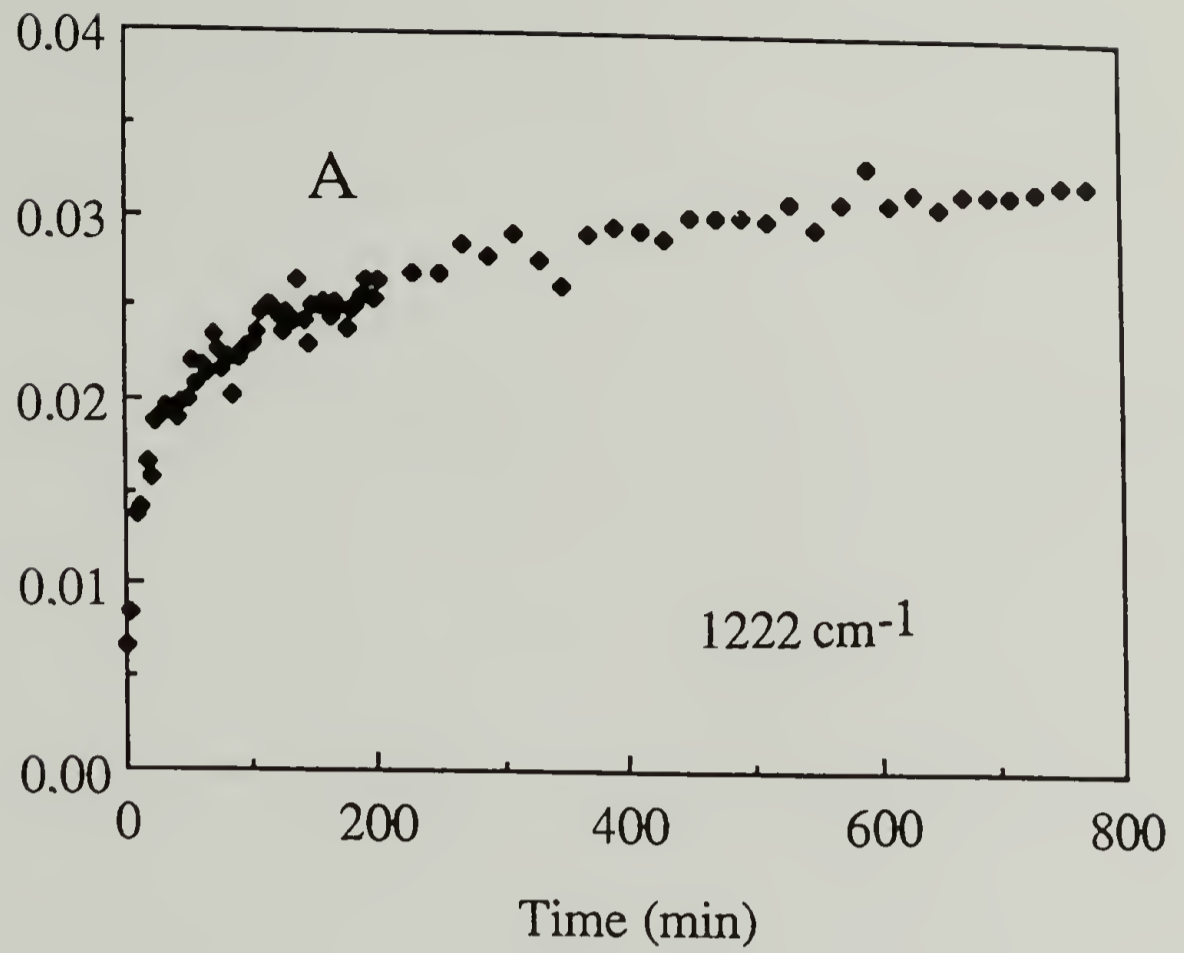


FIGURE 6.4 Integrated intensities at 191°C as a function of time for a sample annealed at 170°C ; (a) 1222 cm^{-1} ; (b) $943\text{ and }934\text{ cm}^{-1}$.

copolymers. The sharpness of the transition implies that this process involves a high degree of cooperativity of molecular motion.

The degree and rate of transition is also highly dependent upon the annealing history. The formation of the trans phase at 191°C for samples annealed at 120, 150, and 170°C is shown in Figure 6.5. Here the transition is observed to occur more rapidly for samples annealed at lower temperatures. Lower annealing temperatures result in a lower degree of crystallinity and smaller more imperfect crystals. Such a structure contains a high degree of disorder and therefore requires less energy for phase transformation than samples annealed at 170°C. At that temperature, as shown previously in Figure 4.3, an increase in the amount and perfection of helical crystal phase occurs. The critical temperature at which substantial phase transition occurs then must be lower for samples of lower crystallinity.

The trans crystal phase content may be determined by the band intensity for a sample of known crystallinity. Values for the degree of crystallinity may be determined by measuring the change in heat capacity at the glass transition. The ratio of this quantity to that of an entirely amorphous sample provides a measure of the amorphous content. This method has been applied to many semi-crystalline polymers.¹⁰ A sample was heated up to the melt and allowed to slow cool to room temperature, and therefore contained only trans crystal phase and amorphous material. No helical structure was observed. Such samples exhibited a ΔC_p value at T_g of 0.16 J/g°C. A melt quenched amorphous sample showed a value of 0.61 J/g°C, giving an amorphous content of 26%. This indicates a degree of crystallinity of 74%, which is very consistent with values measured by vapor sorption in samples slow cooled from the melt.¹⁰ The measured degree of crystallinity may now be used to normalize the band intensity in order to determine the amount of trans phase. This was performed for the equilibrium intensity data measured as a function of temperature and is shown in Figure 6.6.

The phase transition may also be observed by calorimetry.^{7,8} DSC scans from 150 to 250°C for samples annealed at 150 and 170°C are shown in Figure 6.7. For the sample

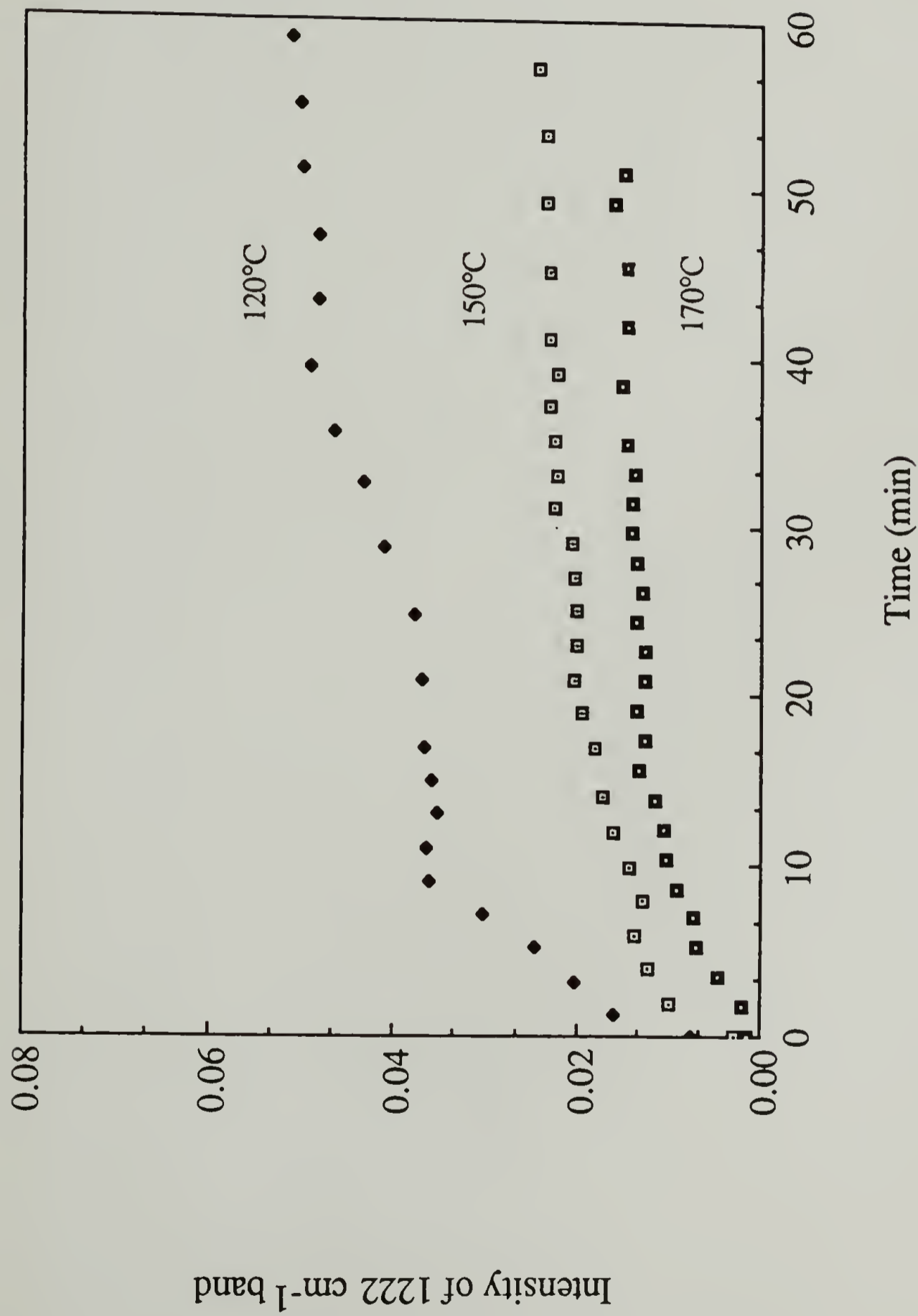


FIGURE 6.5 Integrated intensity of the 1222 cm^{-1} band with time at 191°C for samples annealed at 120°C, 150°C, and 170°C.

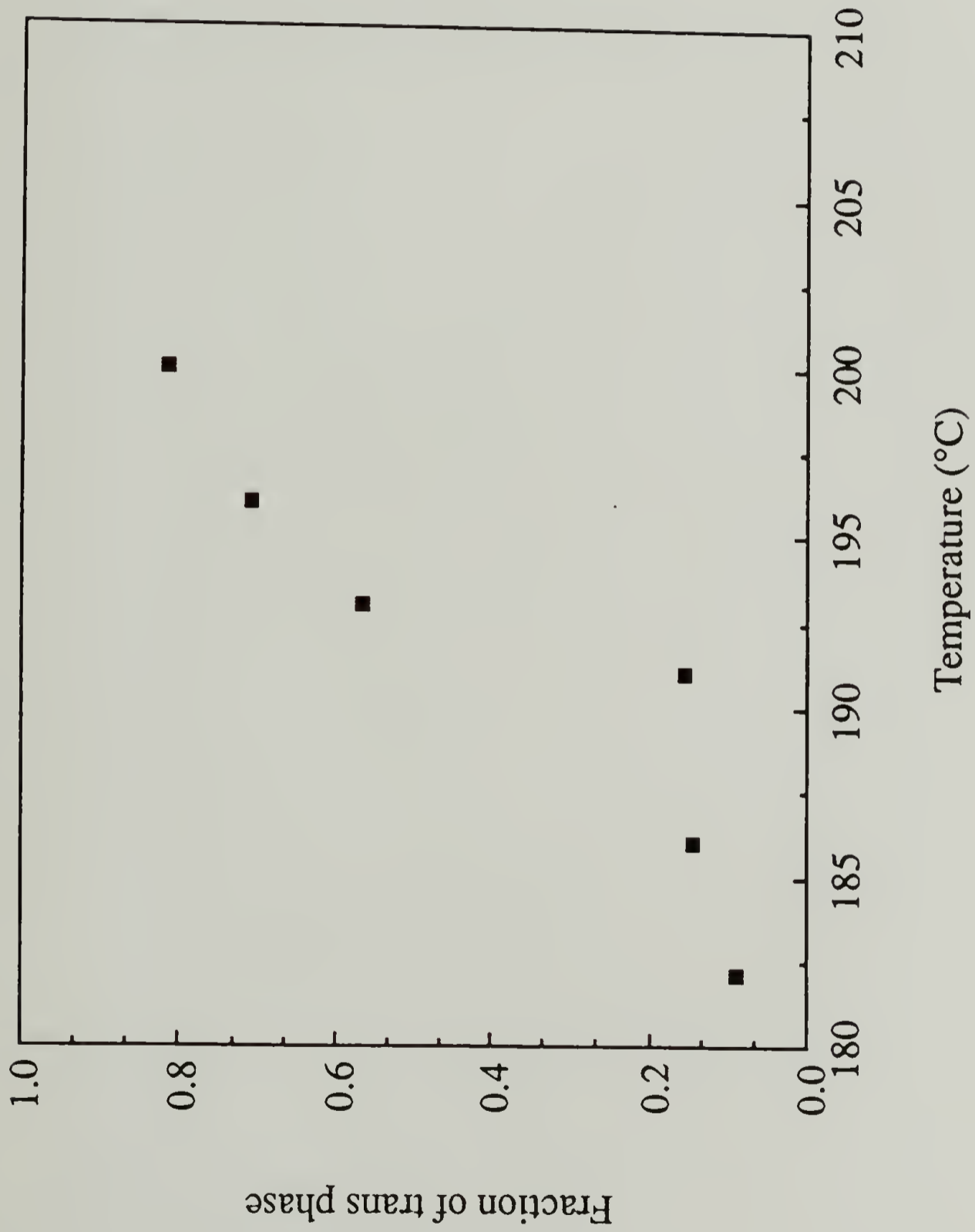


FIGURE 6.6 Trans crystal phase content measured at equilibrium as a function of temperature for samples annealed at 150°C.

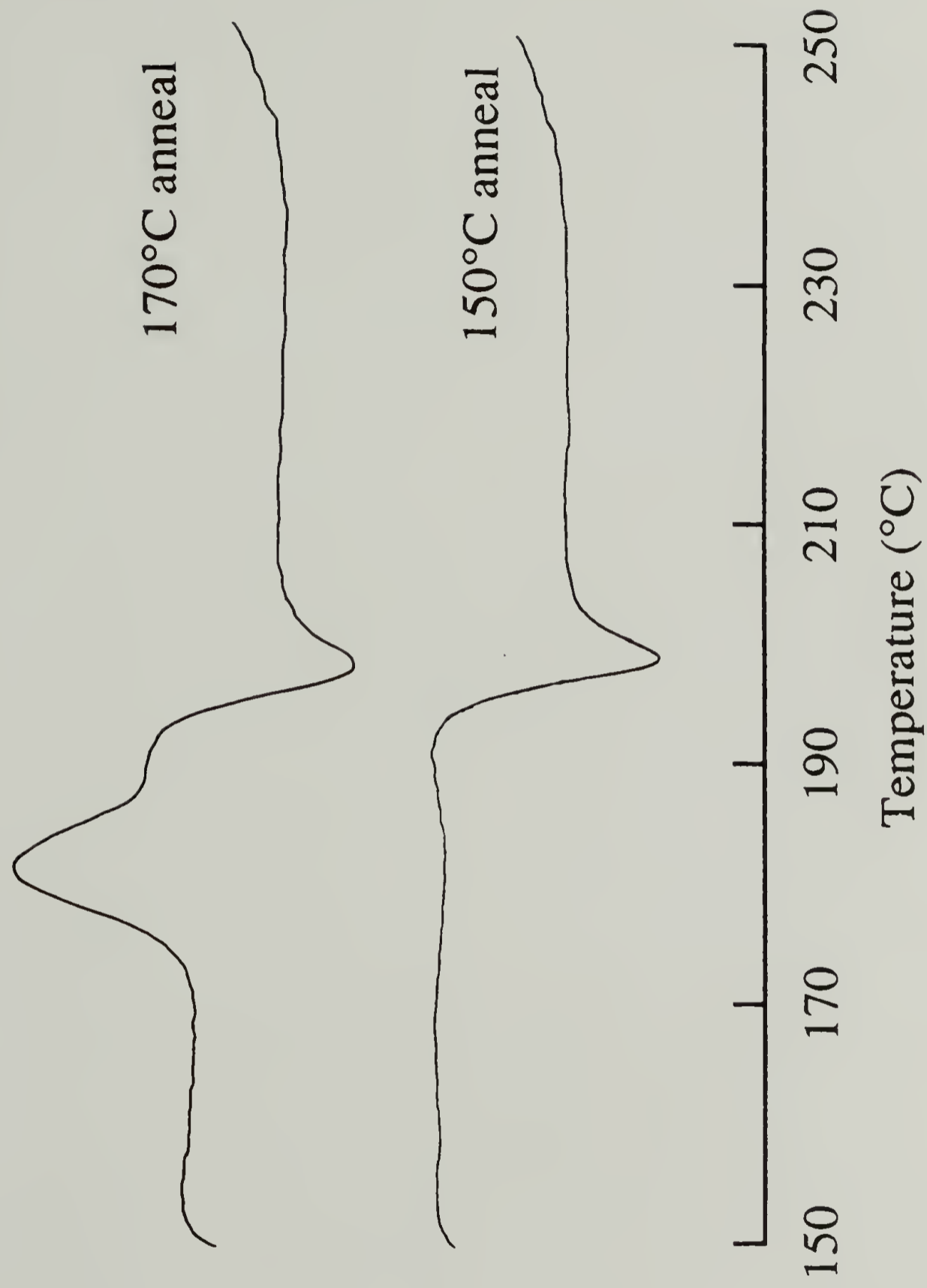


FIGURE 6.7 DSC scans of samples annealed at 150°C and 170°C.

annealed at 170°C, an endotherm is observed at approximately 182°C, which is due to the helical to trans crystal phase transition. At 197°C an exotherm appears which is associated with crystallization of amorphous material into the trans crystal phase. The sample annealed at 150°C does not show the lower temperature endotherm as it contains a lower amount of helical crystal phase. For samples annealed at 180°C, the endotherm is more intense and appears at higher temperature so that it overlaps the crystallization exotherm. The endotherm observed for the 170°C is quite small, only 4.1 J/g. Thus the two processes which produce the increase in all trans phase may be separated by thermal treatment.

Due to the extremely sharp increase in the trans crystal phase content with temperature, it was the original intent of this study to apply a cooperative phase transition model in order to interpret the transition behavior. Such a model has been applied to the helix-random coil transition in polypeptide chains in which dramatic conformation changes are observed from small variations in temperature or solvent quality.¹¹⁻¹³ This model employs two statistical parameters which are equilibrium constants, the first of which describes the energy difference between the two states, while the second parameter is related to the energy barrier which must be overcome for transition to occur. It is this second parameter which is a measure of the degree of cooperativity of the process. With this model, the transition enthalpy can be used to calculate the first parameter. However this model is only strictly applicable to reversible phase transitions. The crystal phase transition in sPS is nonreversible and therefore involves an overall increase in entropy. This entropic contribution precludes the calculation of the statistical parameters based upon the transition enthalpy.

An alternative is to model the phase transition behavior as one of nucleation and growth, an approach which has been widely applied to the crystallization kinetics of polymers.¹⁴⁻¹⁷ In this case nucleation may involve the formation a trans segment in the helical crystal from thermal fluctuations and which propagates through the crystal through

cooperative motion, causing rapid transformation. Using this type of model, the trans phase content at time t , $M(t)$, can be expressed by the Avrami equation as

$$M(t) / M(0) = 1 - \exp (-Kt^n) \quad (6.1)$$

where $M(0)$ is the initial content of trans crystal phase. The infrared intensity of the 1222 cm^{-1} band is proportional to the trans phase content and its variation with time can be described by

$$\frac{M(t) - M(\infty)}{M(0) - M(\infty)} = \frac{I(t) - I(\infty)}{I(0) - I(\infty)} = \exp (-Kt^n) \quad (6.2)$$

where $I(t)$, $I(0)$, and $I(\infty)$ are the band intensities at time t , at the initial measurement time, and at equilibrium, respectively. This equation may be rearranged into its more usual form as

$$\ln \left(-\ln \left(\frac{I(t) - I(\infty)}{I(0) - I(\infty)} \right) \right) = \ln K + n \ln t \quad (6.3)$$

An Avrami plot of the intensity increase with time at 191°C for a sample annealed at 170°C is given in Figure 6.8.

With the nucleation and growth model, the exponent of time, n , is frequently used to determine the dimensionality of crystal growth. The Avrami plot given in Figure 6.8 shows linear behavior with a slope of 1.1 and a correlation coefficient of 0.94. Such a value implies a linear growth mechanism. However, without some knowledge of the overall morphology and crystallization behavior, it is difficult to assign a growth mechanism to this process although the same value has been measured for the crystal phase transition in polybutene-1.¹⁸ In this case a tetragonal crystal modification transforms into a hexagonal crystal phase with time at room temperature, while stretching the sample accelerates the process. For sPS virtually nothing has been reported about the morphology

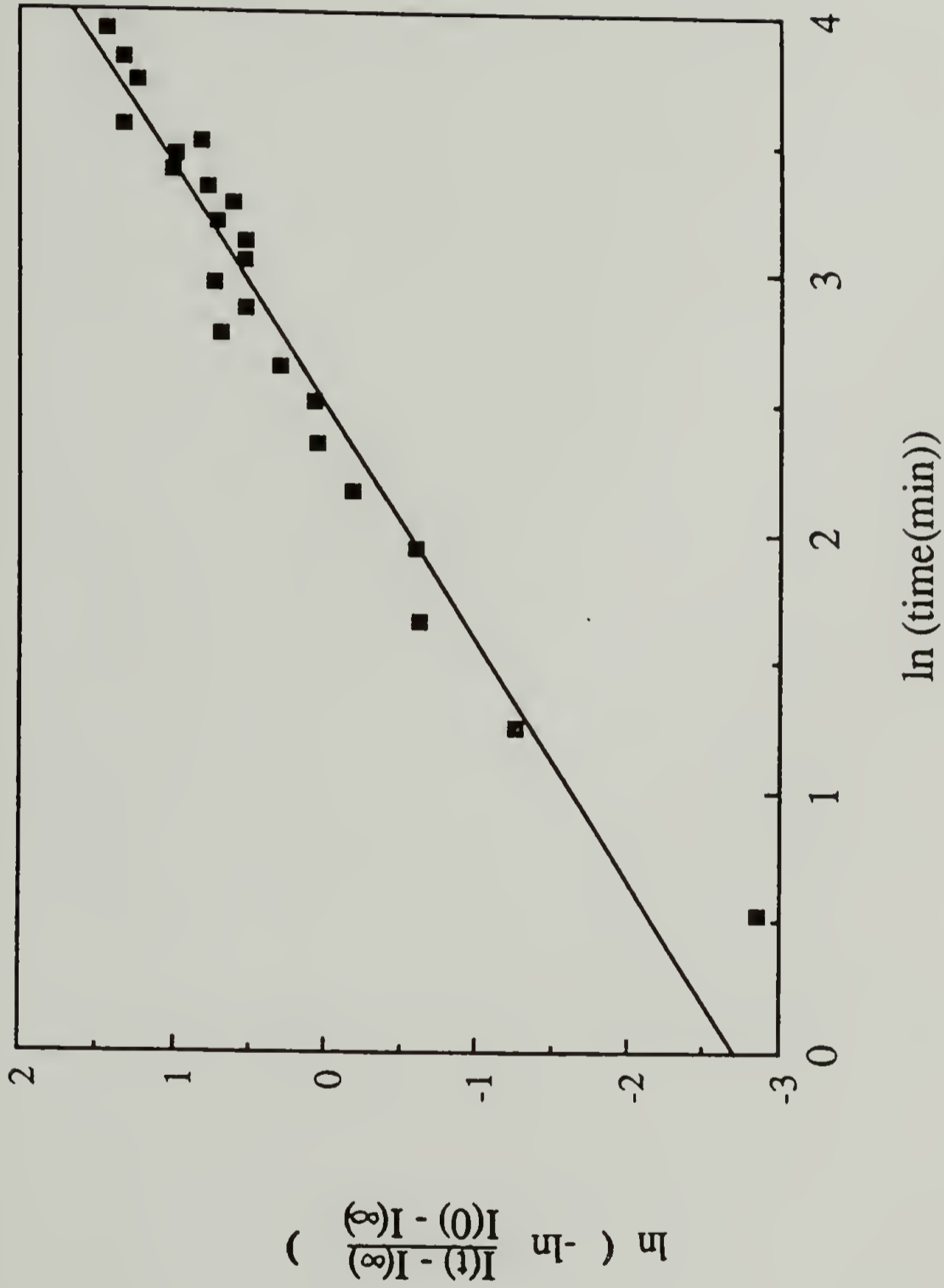


FIGURE 6.8 Avrami plot of the 1222 cm^{-1} band intensity as a function of time for a sample annealed at 170°C.

and crystallization kinetics, or the ultimate degree of crystallinity obtained. Such information is essential for a complete understanding of the phase transition behavior. Crystalline phase transitions often involve substantial strains in the crystal as the new phase forms, and these strains can rupture crystals. It is not yet known if such high strains are present in this case. Undoubtedly the phase transition mechanism is complicated by the presence of the various polymorphs. However, a nucleation and growth mechanism does appear to be consistent with the observed data of this highly cooperative irreversible phase transition.

It is also interesting that crystallization of the amorphous material occurs just above the phase transition temperature. Previous studies have shown crystallization in completely amorphous sPS samples to occur at 140°C. It is probable that in a highly crystalline material the amorphous portion is constrained between crystals, with many tie chains between the crystallites possessing less mobility than that of a totally amorphous sample. At the phase transition the helical TTGG conformation having a 7.5 Å repeat distance transforms to a TTTT conformation which has a length of 10 Å. Therefore at the transition, crystalline lamellae should lengthen approximately 33%. This extension of crystalline chains could allow greater conformational freedom for constrained amorphous chains, allowing them sufficient mobility to crystallize and producing the observed crystallization exotherm just above the phase transition endotherm.

Conclusions

In this study, the solid-solid phase transition in syndiotactic polystyrene has been measured by spectroscopic analysis. Bands sensitive to specific conformations have been monitored in order to observe the kinetics of the transition from the helical crystal phase to the all trans phase at various temperatures and annealing histories. The transition is observed to occur very rapidly and for samples annealed at 150°C, a substantial amount of transition occurs above a critical temperature of 192°C. Here approximately 60% of the transformation occurs within two minutes. At 200°C, the sample contains nearly 80% trans crystal phase. The rate of structural transformation is highly dependent on the annealing temperature. Samples annealed at lower temperatures show more rapid transition, as a more disordered and less stable structure requires less energy for phase change.

By measuring the change in heat capacity at the glass transition temperature and comparing it to that of a totally amorphous sample, a degree of crystallinity of approximately 74% was determined for a sample slow cooled from the melt. This value is consistent with values determined by previous vapor sorption experiments for a similarly prepared sample. By measuring the intensity of such a sample of known crystallinity, band intensity data at equilibrium conditions for different temperatures may be converted to trans crystal phase content.

The phase transition has also been observed by DSC. Annealing at 170°C prior to DSC scans allows the observation of a weak endotherm of 4.1 J/g associated with the helical to trans crystal phase transition. Just above this temperature an exotherm is seen indicative of crystallization of amorphous material. Thus the amorphous material experiences an increase in mobility just above the phase transition temperature. The transition process has been modeled as a nucleation and growth process with nucleation occurring within the helical crystal. An Avrami analysis has been applied, and a linear plot is generated with a slope of 1.1. This value suggests a linear growth mechanism for this

transformation. Further studies of the morphology of sPS will be helpful in interpreting the transition behavior.

References

1. Ishihara, N.; Seimiya, T.; Kuramoto, M.; Uoi, M. *Macromolecules* **1986**, *19*, 2464.
2. Kobayashi, M.; Nakaoki, T.; Uoi, M. *Polym. Prep., Jpn.* **1988**, *37*, E432.
3. Immirizi, A.; de Candia, F.; Iannelli, P.; Zambelli, A. *Makromol. Chem. Rapid Commun.* **1988**, *9*, 761.
4. Vittoria, V.; de Candia, F.; Iannelli, P.; Immirizi, A. *Makromol. Chem. Rapid Commun.* **1988**, *9*, 765.
5. Petermann, J. private communication.
6. Doherty, D. C.; Hopfinger, A. J. *Macromolecules* **1989**, *22*, 2472.
7. Kobahaysi, M.; Nakaoki, T.; Ishihara, N. *Macromolecules* **1989**, *22*, 4377.
8. Guerra, G.; Vitagliano, V. M.; De Rosa, C.; Petraccone, V.; Corradini, P. *Macromolecules* **1990**, *23*, 1539.
9. Vittoria, V.; Russo, R.; De Candia, F. *J. Macromol. Sci.-Phys.* **1989**, *B28*, 419.
10. Menczel, J.; Wunderlich, B. *J. Polym. Sci. Polym. Lett. Ed.* **1981**, *19*, 261.
11. Zimm, B. H.; Bragg, J. K. *J. Chem. Phys.* **1958**, *28*, 1246.
12. Zimm, B. H.; Bragg, J. K. *J. Chem. Phys.* **1959**, *31*, 526.
13. Poland, D.; Scheraga, H. A. *Theory of Helix-Coil Transitions in Biopolymers*; Academic Press: New York, 1970.
14. Avrami, *J. Chem. Phys.* **1939**, *7*, 1103.
15. Avrami, *J. Chem. Phys.* **1940**, *8*, 212.
16. Avrami, *J. Chem. Phys.* **1941**, *9*, 177.
17. Wunderlich, B. *Macromolecular Physics Vol. 2*; Academic Press: New York, 1976.
18. Asada, T.; Onogi, S.; *Structure and Properties of Polymer Films*; Lenz, R. W.; Stein, R. S., Ed.; Plenum Press: New York, 1973, p. 235.

CHAPTER VII

RECOMMENDATIONS FOR FUTURE WORK

Results and Recommendations

In this study the phase transition behavior in three semi-crystalline polymer systems has been studied with vibrational spectroscopy. This technique has proved to be very useful in understanding the conformational distribution, as well as the segmental and dipolar orientation in polymers. Study of the changes in these properties during phase transitions provides information about the mechanism of structural transformation. In this chapter, the main achievements of this work will be summarized and recommendations for future work will be presented in three sections.

Copolymers of PVDF and TrFE

In Chapter II, the effects of a high strength electric field on the microstructure of piezoelectric copolymers of vinylidene fluoride and trifluoroethylene was studied. Their structure was found to be highly dependent upon the annealing history, orientation, and the application of an electric field. The application of an electric field up to 2.2 MV/cm was found to produce changes in dipolar orientation and also changes in chain conformation, with the content of long sequences of trans isomers seen to increase upon poling. This effect is greater just under the Curie transition temperature. Application of the field above the Curie temperature gave reversible behavior as the field was reduced to zero. This is analogous to the loss of remnant polarization found as the Curie transition is reached.

In comparison with PVDF, smaller spectral changes were observed for a 75/25 copolymer, however nearly all bands in the spectra exhibited some intensity change, while

PVDF demonstrated more significant intensity changes and frequency shifts for selected bands. This is because the copolymer is already predominantly in the extended trans state, allowing it couple to the field more readily than PVDF, which must undergo greater conformational rearrangements to reach the polar β or γ phases. Poling above 60°C was necessary for significant α to β phase change in PVDF, while both copolymers exhibited an increase in the all trans conformation upon room temperature poling to 1.0 MV/cm.

The coercive field necessary to reverse the dipolar orientation for the 75/25 copolymer was found to decrease with temperature as dipolar mobility increased. Poling above the Curie temperature and cooling under the field was found to increase the coercive field, and this is associated with an increase in structural regularity. Values of this coercive field were found to agree well with those obtained from dielectric displacement hysteresis which measures a macroscopic polarization. This demonstrates that dipolar orientation is the primary mechanism for polarization in these materials.

Electrical poling behavior was examined for two copolymer compositions which show substantial differences in structure and Curie temperature. The copolymer with higher trifluoroethylene content showed a greater increase of long sequences of trans isomers, as it contained more disorder initially. It also exhibited a smaller coercive field value, indicative of the greater mobility of dipoles in the larger crystal lattice resulting from higher TrFE content.

The ferroelectric to paraelectric phase transition in PVDF-TrFE copolymers has been modeled as a cooperative first order phase transition.¹ In future studies various models could be applied to interpret the structural changes and disordering which occur at this transition. By quenching from the high temperature paraelectric phase to low temperature and monitoring the formation of the ferroelectric phase isothermally, a nucleation and growth model could be applied to describe the transition.

The molecular mechanism of polarization for ferroelectric polymers is probably the most desirable information of interest. Molecular modeling studies would provide a means

to determine the mechanism by which chain dipoles couple to the field and induce conformation change. In the crystalline lattice, the motion must be cooperative among neighboring chains, and various models have been proposed to explain the field induced structural change.¹⁻⁶ One of these involves the nucleation and subsequent growth of domains with dipole moments parallel to the field direction,² while another model involves a soliton type motion propagating down the chain.³ Molecular dynamics simulations may elucidate which model is most feasible.

Another area of interest is determination of the distribution of polarization in piezoelectric materials. Nonuniform polarization can result from a nonuniform poling field due to space charges or conductivity. These effects are especially important at high temperatures. It may also result from a nonuniform coercive field due to material inhomogeneities.⁷ Thermal pulse experiments on biaxially oriented PVDF films poled at room temperature have shown that films pole more easily in the middle region, which implies a higher coercive field for polarization reversal near the film surfaces.⁷ Other workers have observed that films poled at high temperature and cooled under the applied field exhibit maximum polarization near the poling anode.⁸ Similar studies have shown that when poling in a temperature gradient, the strongest polarization occurs on the cooler side of the film.⁹ It is interesting to know if the polarization distribution in these materials can be correlated with the amount of the polar and nonpolar phases. In PVDF, there are infrared bands associated with the α and β phases. By poling layers of films and measuring spectra before and after poling and depolarizing, the distribution of these crystal phases could be determined and compared with previous polarization distribution results.

Copolymers of PVDF and TrFE are known to crystallize predominantly in the all trans phase. It is of interest to determine how the presence of the copolymer may alter the crystallization behavior of the PVDF homopolymer. It has been shown by WAXS and DSC that PVDF-TrFE copolymers of similar composition may cocrystallize and thus change their Curie transition behavior.¹⁰ It is possible that the presence of a high VDF

content copolymer could alter the crystallization of PVDF, changing the relative amounts of the α , β , and γ phases. This may not be the result of cocrystallization, but merely a change in the nucleation and growth processes, as with blends of PVDF with PMMA. Studies of the electric field induced structural changes of such blends are also of interest. Such experiments would determine if the presence of the copolymer, which is in the trans phase and couples easily to the electric field, allows the PVDF to couple to the field more readily and undergo greater phase change from the α phase to the polar β or γ phases. These studies are relevant as they may lead to a better understanding of the molecular interactions in these materials, as well the development of materials of high piezoelectric activity.

Blends of PVDF and PMMA

The orientation and microstructure of highly oriented blends of PVDF and PMMA has been studied. Melt drawn films of PVDF show a value of the second moment of the orientation function of nearly unity. Infrared spectroscopy has been employed to determine the content of α and β phase of PVDF for two highly drawn blends and for the homopolymer. A significantly higher β phase content was observed for a 70/30 blend compared to pure PVDF. The effects of annealing on the phase content and segmental orientation have been measured. A weakly oriented 50/50 blend showed no evidence for α or β phase in agreement with electron diffraction studies. Upon annealing at 100°C, crystallization of highly oriented β phase occurred, along with relaxation of PMMA. The formation of highly oriented β phase crystals from the oriented amorphous state is concluded to occur by the formation of highly oriented nuclei. Polarized data obtained from PVDF films with nearly perfect segmental orientation have been used for determination of the transition dipole moment directions of selected bands.

The measurement of transition dipole moment directions is very useful because it provides information which will complement vibrational assignments from normal

coordinate analysis. Many of the low frequency bands such as the 510 cm^{-1} CF_2 bending vibration are associated with the β or γ phases and also sensitive to dipolar orientation.^{11,12} In order to determine the angular orientation of dipoles from the sample film plane by infrared band intensity, the transition moment directions must be clearly defined. From a normal coordinate analysis, the Cartesian displacements can be determined and the transition moment angles may be calculated. It would be useful to calculate these values and compare to the experimental values from this study in order to assess the validity of the force constants used in previous normal coordinate calculations.¹²

Microstructure of Syndiotactic Polystyrene

The microstructure of various phases of syndiotactic polystyrene has also been studied. The presence of a helical structure in a solution cast film, and an all trans conformation upon annealing or drawing was shown. An irreversible transition to the all trans phase was observed to occur very rapidly near 200°C . Spectral features which are sensitive to specific conformations and packing order were identified. Upon annealing or extrusion, bands appear which are associated with long trans sequences.

A normal coordinate analysis has been performed using nonredundant coordinates and force constants for the phenyl ring. Force constants for the chain are obtained from studies of paraffins. The use of nonredundant coordinates for the ring removes errors which can result from overdefined internal coordinate sets which can give a nonunique solution to the eigenvalue equation. Assignment of the infrared and Raman bands and their polarization characteristics has been made upon comparison of the calculated results with the observed spectra. No refinement of the force constants was made. Bands which involve coupling between the ring and backbone vibrations were found to correlate well with the observed bands which are associated with the trans conformation.

Solid-state coextrusion was found to be successful in producing highly oriented trans phase. The extremely high dichroism of a ring mode sensitive to the all trans conformation shows that these trans sequences possess nearly perfect orientation and that the rings are aligned with the ring planes normal to the chain axis. The theoretical modulus of a single chain has been calculated from the dispersion curve of the longitudinal acoustic branch near the Brillouin zone center, and a value of 69 GPa was obtained. This value, which is based on the vibrational modes of a single chain, provides a lower limit of the theoretical modulus as intermolecular interactions have been neglected.

The kinetics of the irreversible phase transition in syndiotactic polystyrene has been measured as a function of temperature and annealing history, in order to determine the effect of thermal history on the transition behavior. The transition occurs over a very narrow temperature range of approximately 2°C, implying a high degree of cooperativity is involved. Samples annealed at lower temperatures undergo transformation more rapidly, as the more disordered structure requires less energy for phase transformation. The enthalpy of the transition was measured and the crystallinity of a sample slow cooled from the melt was determined to be approximately 74%. For samples annealed at temperatures just below the phase transition, the enthalpy due to the crystal phase transition can be separated from the higher temperature exotherm due to crystallization of amorphous material. The rapid formation of the all trans phase was modelled as a nucleation and growth process with nucleation occurring within the helical phase crystals. Avrami analysis shows a linear plot with a slope of 1.1 which suggests a linear growth process.

Only very little structural information is available about this material. The complete crystal structure for the various polymorphs are not yet known. Wide angle X-ray and electron diffraction will be useful techniques in determining the structure of each crystal phase. Knowledge of the crystal structures will be very important in understanding the mechanism of phase transition. The effect of crystallite size may also play an important role in the transition behavior. Small angle x-ray scattering would be a valuable technique

for the measurement of crystallite size and its change due to the effects of annealing and heating through the phase transition. Certainly the overall morphology is an important factor in understanding structural transformations and in applying any model or fully interpreting the value of the Avrami parameters. Electron and optical microscopy studies would be of great use in determining the crystal habit and in understanding the nucleation and growth processes of crystallization.

The phase transition in sPS is also observed to be induced by drawing. A study of the orientation and conformation change upon deformation would be useful in understanding the mechanism of structural transition. Polarized infrared spectroscopy coupled with mechanical measurements of stress and strain would provide a molecular as well as a macroscopic description of the process of transformation during deformation. It would be useful to know if a critical stress must be reached for transformation, and also how the thermal history affects the deformation induced transition behavior. Stress-strain measurements are valuable as virtually no information on the mechanical properties of sPS have been reported. Due to the high degree of orientation induced by coextrusion, the tensile strength of drawn fibers is expected to be quite large.

References

1. Tashiro, K.; Takano, K.; Kobayashi, M.; Chatani, Y.; Tadokoro, H. *Ferroelectrics* **1984**, *57*, 297.
2. Furukawa, T.; Date, M.; Ohuchi, M.; Chiba, A. *J. Appl. Phys.* **1984**, *56*, 1481.
3. Dvey-Aharon, H.; Sluckin, T. J.; Taylor, P. L.; Hopfinger, A. J. *Physical Review B* **1980**, *21*, 3700.
4. Reneker, D. H.; Mazur, J. *Polymer* **1985**, *26*, 821.
5. Tashiro, K.; Kobayashi, M. *Polymer* **1986**, *27*, 667.
6. Furukawa, T.; Date, M.; Ohuchi, M.; Chiba, A. *J. Appl. Phys.* **1984**, *56*, 1481.
7. Mopsik, F. I.; DeReggi, A. S. *Appl. Phys. Lett.* **1984**, *44*, 65.
8. Sussner, H.; Dransfeld, K. *J. Polym. Sci., Polym. Phys. Ed.* **1978**, *16*, 529.
9. Marcus, M. A. *Ferroelectrics* **1981**, *32*, 149.
10. Tanaka, H.; Lovinger, A. J. *Macromolecules* **1987**, *20*, 2638.
11. Hsu, S. L.; Lu, F. J.; Waldman, D. A.; Muthukumar, M. *Macromolecules* **1985**, *18*, 2583.
12. Kobayashi, M.; Tashiro, K.; Tadokoro, H. *Macromolecules* **1975**, *8*, 158.
13. Vittoria, V.; Russo, R.; De Candia, F. *J. Macromol. Sci.-Phys.* **1989**, *B28*, 419.
14. Guerra, G.; Vitagliano, V. M.; De Rosa, C.; Petraccone, V.; Corradini, P. *Macromolecules* **1990**, *23*, 1539.



